**The Dissertation Committee for Louise Zhiying Wang Certifies that this is the approved version of the following dissertation:**

# Kinetic Analysis of HIV-1 Reverse Transcriptase in the presence of Non-nucleosides

**Committee:**

Kenneth A. Johnson, Supervisor

Andrew Ellington

David W. Hoffman

Jon D. Robertus

Christian Whitman

# Kinetic Analysis of HIV-1 Reverse Transcriptase in the presence of non-nucleoside inhibitors

**by**

**Louise Zhiying Wang, B.A.**

**Dissertation**

Presented to the Faculty of the Graduate School of

The University of Texas at Austin

in Partial Fulfillment

of the Requirements

for the Degree of

**Doctor of Philosophy**

**The University of Texas at Austin**

**May, 2004**

# Dedication

To my parents and grandparents

## Acknowledgements

With utmost respect to my advisor, Ken Johnson, who taught and helped me for the last five years with his endless patience. My gratitude to JoAnn whose kindness and support especially enriched my life.

Also to my committee members for sharing their time, experience and knowledge: Andy Ellington, Christian Whitman, Jon Robertus, and Dave Hoffman.

And to the Johnson lab members whose expertise and invaluable assistance/discussions strengthened my understanding of my project -- Vi Dougherty, Jarle Lillemoen, Harold Lee, and especially Jeremiah Hanes. Special thanks to YuChih Tsai for always rushing over to solve my computer problems and to Jeff Bartron for constantly showering me with words of encouragement when I get frustrated. I am truly fortunate to work with you all.

Last, but far from least, to my future husband, David Humphrey, who deserves my heartfelt gratitude for supporting me every step of the way. Words are not enough to express how much you have done for me. I owe you a lifetime of B&J's.

# Kinetic Analysis of HIV-1 Reverse Transcriptase in the presence of non-nucleoside inhibitors

Publication No._____

Louise Zhiying Wang, Ph.D.
The University of Texas at Austin, 2004

Supervisor: Kenneth A. Johnson

Current treatment for human immunodeficiency virus (HIV) infection or acquired immunodeficiency syndrome (AIDS) delays the conversion of infected helper T cells to monoclonal malignant cells but does not eradicate HIV. A novel non-nucleoside inhibitor, CZ-1 (2-naphthalenesulfonic acid, 4-hydroxy-7-[[[[5-hydroxy-6-[(4-cinnamylphenyl)azo]-7-sulfo-2-naphthalenyl]amino]carbonyl]amino]-3-[(4-cinnamylphenyl)azo], disodium salt), was designed to bind at an unconventional site on HIV type 1 reverse transcriptase (RT) (1). I examined the effect of CZ-1 on the kinetic parameters governing the single nucleotide polymerization. CZ-1 decreased the amplitude of the reaction as previously shown for other non-nucleoside inhibitors due to the slow equilibration of the inhibitor with RT. CZ-1 also weakened the apparent DNA binding affinity. Likewise, DNA weakened the apparent CZ-1 binding affinity. In contrast, CZ-1

did not affect the $K_d$ and the maximum incorporation rate of the incoming nucleotide. We therefore conclude that CZ-1 represents a new class of NNRTIs distinct from Nevirapine and related NNRTIs. CZ-1 can bind to RT in both the absence and presence of DNA. In the ternary enzyme-DNA-CZ-1 complex, the binding of DNA is weakened and incorporation of the next nucleotide onto the primer is inhibited. A possible mode of inhibition for CZ-1 is the distortion of RT conformation and the consequent misalignment of DNA at the active site. Unexpectedly, CZ-1 also inhibited human mitochondrial DNA polymerase (*pol γ*), although I did not see evidence of nonspecific inhibition via self-aggregation or intercalation with DNA.

The second part of my project aimed to characterize a non-nucleoside drug-resistant mutant form of HIV-1 RT, containing a single amino acid substitution at position 103 from lysine to asparagine. Three non-nucleoside RT inhibitors, CZ-1, HBY 097, and α-APA, exhibited similar inhibition kinetics on this mutant as on the wild type RT.

The third part of my project determined that HIV RT exhibited similar polymerization kinetics whether utilizing an RNA template or DNA template. This validation suggests that the measured kinetic parameters were similar for RNA-directed minus-strand DNA synthesis and DNA-directed plus-strand DNA synthesis.

# Table of Contents

# List of Tables

# List of Figures

# List of Illustrations

# CHAPTER 1: Overview of HIV-1 Reverse Transcriptase and Non-nucleoside Inhibitors

## 1. INTRODUCTION

After human immunodeficiency virus (HIV) was first associated to the development of acquired immunodeficiency syndrome (AIDS) in 1983 (2), on-going research has been focusing on the key enzymes in the viral replication process, the reverse transcriptase (RT), integrase and protease. They are the primary targets for current drug design. Our lab has been studying the inhibition mechanism of RT.

Retroviral reverse transcriptases (RT) were discovered in 1970 by Baltimore (3) and Temin (4). RTs are biochemically distinct from other DNA polymerases in two aspects. First, RTs copy a single-strand viral RNA genome into double-strand pro-viral DNA using both RNA and DNA as a template, unlike other DNA polymerases, which can only copy DNA templates to synthesize new DNA strands. The RT active site can accommodate both DNA and RNA substrates to fulfill the requisite primer/template alignment during different stages of reverse transcription. Unlike replicative DNA polymerases, RTs lack the 3' to 5' exonuclease activity (5) that is responsible for proofreading and correcting mismatched nucleotides. Therefore, the fidelity of DNA synthesis is substantially lower for RTs, in comparison to the fidelity of most replicative DNA polymerases. Essentially, low fidelity polymerization accounts for the characteristic

hypermutability of human immunodeficiency viruses (HIV), the etiological agent of the acquired immunodeficiency syndrome (AIDS) (6). Rapid mutation facilitates HIV evolution, which allows HIV to evade the immune system, confers drug resistance, and is a major obstacle in AIDS treatment.

According to the Joint United Nations Programme on HIV/AIDS, as of December, 2003, 40 million people are estimated to be living with HIV/AIDS. In 2003 alone, 5 million people acquired HIV and 3 million died from AIDS. Despite of the antiretroviral therapy, we still need better regimens and more powerful drugs to thwart this worldwide epidemic.

## 2. REPLICATION OF HIV-1

In 1983, HIV was first discovered in Luc Montagnier's laboratory (2,7) at the Louis Pasteur Institute. In the same year, several independent isolates of HIV were identified in Robert C. Gallo's laboratory (8,9) at the National Cancer Institute. HIV was initially named as human T-cell leukemia virus type 3 (HTLV-III) or adult T-cell leukemia virus (ATLV) until it was confirmed to be the cause of AIDS (6).

HIV is a plus-strand RNA retrovirus. Like other retroviruses, HIV replicates through a DNA intermediate. HIV replicates by going through cycles of infection of susceptible host cells, $CD4^+$ helper T cells of the immune system (Fig. 1). The fusion of the virus with the host cell happens when HIV binds to the CD4

receptor and another co-receptor on the membrane. Upon entry into the host cell, HIV undergoes reverse transcription to copy its genetic material, RNA, into DNA. The conversion of single-stranded viral RNA into double-stranded pro-viral DNA is catalyzed by RT. The product DNA is integrated into the host genome inside the nucleus. While some viruses remain latent, others become activated and transcribe the viral DNA into messenger RNA, which is then translated into viral proteins. The viral proteins and RNA assemble at the cell membrane to form a new virus. The life cycle of HIV is completed by maturation associated with cleavage by HIV protease (10), budding from the cell membrane, and release from the host cell to infect another host cell.

*De novo* mutations are generated by inherently promiscuous reverse transcription during the viral life cycle (Fig. 1), thus introducing base substitutions, frame shifts, genetic rearrangements and hypermutations (11,12). HIV has been shown to contain a high level of genetic variation (13,14). Each single nucleotide variant on a branch in the HIV phylogenetic tree is deemed a unique and viable virus (15). There are 296 drug-resistant mutations that have been recorded in the HIV database from Los Alamos National Laboratory (http://hiv-web.lanl.gov). HIV RT replicates DNA and RNA with an error frequency of 1 in $10^4$ leading to one mutation per genome per replication cycle (15), the hypermutation of HIV is the "Achilles' heel" of anti-AIDS therapy.

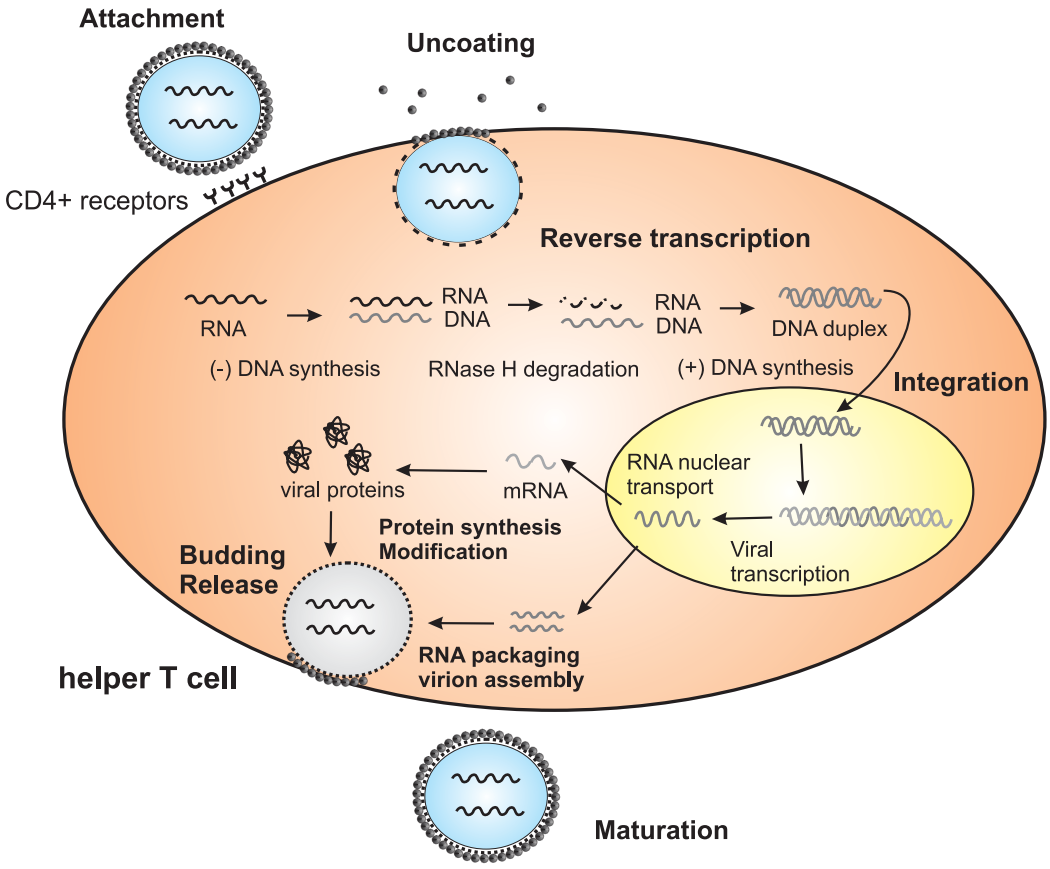


Figure 1. HIV-1 life cycle. HIV infects $CD4^+$ helper T cells of the immune system. After being engulfed by the host cells, the viral single-stranded RNA is copied into double-stranded DNA by HIV RT. The proviral DNA is integrated into the host genome by the HIV integrase. The host cellular polymerases transcribe the proviral DNA into viral RNA, which is subsequently translated into proteins by cellular translational machinery. Virions are assembled and bud from the cell membrane to infect other host cells. Modified from *www.niaid.nih.gov/daids/dtpdb/virpage1.htm*.

Drug-resistant strains appear in a matter of weeks after the treatment begins (16).

## 3. STRUCTURE OF HIV-1 REVERSE TRANSCRIPTASE

The first moderately high resolution (3.5 Å) crystal structure of RT was reported by Kohlstaedt et al.(17). HIV-1 RT is a heterodimer of two tightly associated polypeptides, 66 kDa (p66) and 51 kDa (p51).

### 3.1 p66 subunit

The p66 subunit consists of a polymerase (*pol*) domain and an RNase H domain (Fig. 2). The *pol* domain in turn is comprised of four subdomains, fingers (residue 1-88 and 121-146), thumb (residue 243-311), palm (residue 89-120 and 147-242), and connection (residue 312-425) (17). Encoded by the N-terminal 425 amino acid residues, the *pol* domain is a member of the *pol* A family and is structurally similar to the DNA polymerase I Klenow fragment from *E. coli* with the shape of a right hand. The DNA binding cleft is formed primarily by the p66 fingers, palm, and thumb domains. The polymerase active site, located at the base of the DNA binding cleft in the hairpin between β9 and β10 loop, contains three conserved aspartic acid residues, two of which are part of the characteristic YXDD motif of polymerase structures (17,18). The fifth domain of p66 subunit is

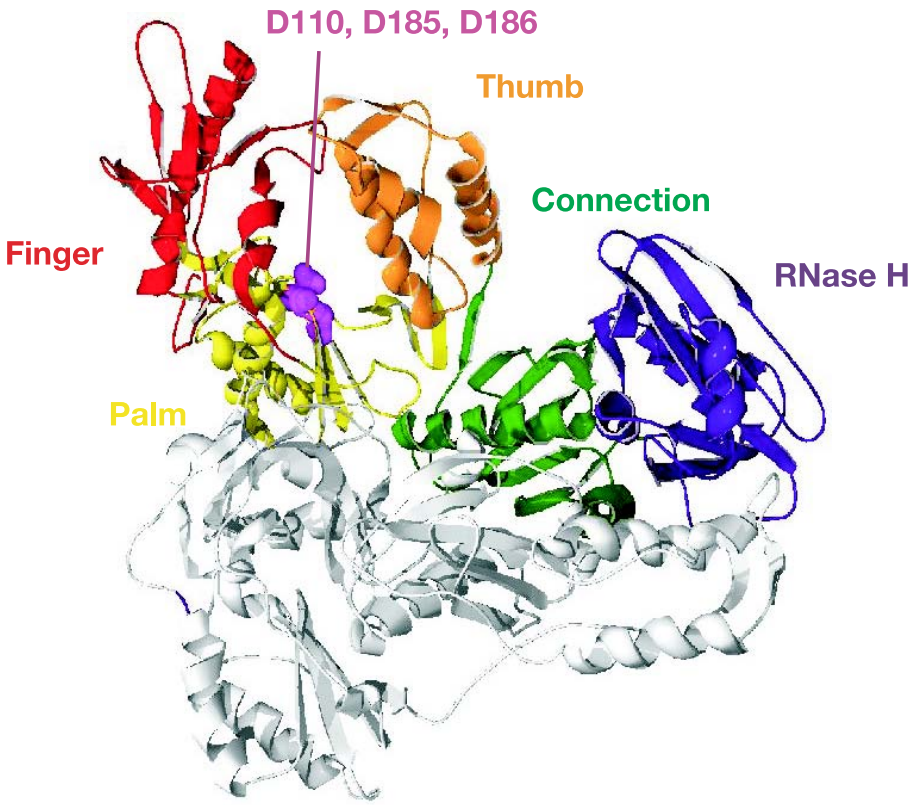


Figure 2. Structure of an unliganded HIV-1 RT heterodimer. The five domains of the p66 subunit are labeled and colored on the figure, while the p51 subunit is in gray color. The polymerase active site is highlighted by its conserved residues, D110, D185, and D186, in space-filled model. This image was generated with *1DLO.pdb* (19) using Swiss PDB viewer, POV-Ray, and Corel DRAW.

the Ribonuclease H (RNase H) domain, comprised of the 135 C-terminal amino acid residues. RNase H cleaves the RNA template in an RNA-DNA duplex, after it is copied by the RT DNA polymerase. The "RNase H primer grip" consists of amino acids that interact with the DNA primer strand. This grip may control the interactions between the RNA template and the RNase H active site, depending on the sequence and structure of the nucleic acid (20). The catalytic triad (E478, D443, D498) bind divalent cations ($Mg^{2+}$) within the RNase H active site. $Mg^{2+}$ ions neutralize the negative charges of key residues in both the polymerase (21) and RNase H active site, stabilizing the association of RT with primer/template (22).

### 3.2. p51 subunit

The p51 subunit is formed by proteolytic cleavage of the 120 C-terminal amino acids of the p66 subunit by HIV protease (23) and hence contains the four domains of the polymerase core while lacking the RNase H domain. The two subunits have identical N-terminal sequences. Although the secondary structures are similar, the orientations of the domains are different in the p66 and p51 subunits such that only the p66 subunit possesses a functional polymerase active site in its palm domain. In the p51 subunit, the connection domain lies between its palm and thumb to block its DNA polymerase active site (17), thus rendering the site inactive (24). Both the thumb domain of p51 and the RNase H domain of p66

go through conformational changes to form the primer/template-binding site and the tRNA-binding site in the active form of HIV RT (25).

### 3.3. Nucleic acid substrate binding

HIV-1 RT has nonrestrictive substrate specificity in that it catalyzes the polymerization of four different combinations of primer/template duplexes: RNA/RNA, DNA/RNA, RNA/DNA, and DNA/DNA (26). The majority of the protein contacts located in the primer/template binding cleft are common among RT-tRNA/RNA, RT-DNA/DNA, and RT-DNA/RNA complexes, except for a few contacts between the p66 fingers domain and the viral tRNA/RNA that are not detected with RT-DNA/DNA (27).

Crystallographic studies of RT-DNA complexes reveal conformational changes during DNA binding and nucleotide binding (Fig. 3). In the RT-DNA binary complex, DNA binding along a groove stretching from the polymerase active site to the RNase H active site (28) increases the flexibility of RT (29) and causes a rotation of the thumb domain of p66 (30) towards the primer/template, in concert with conformational changes in the YMDD motif (31). The DNA primer terminus is in the vicinity of the catalytic aspartic triad in the palm domain of p66. Hydrophobic interactions and possible hydrogen bonds help stabilize the polymerase-DNA complex (32). DNA base pairs close to the active site are A-form in structure with a widened minor groove, similar to what has been observed with other DNA polymerases (33). Six to seven base pairs away from the

polymerase active site, the bound DNA exhibits a 40˚ bend (18), and transitions to B-form DNA structure. However, the functional significance of the transition from B to A-DNA is not understood.

### 3.4. Ternary complex formation

The formation of the ternary RT-DNA-dNTP complex resembles ternary complexes of other DNA polymerases. A binding pocket is formed by a closure of the fingers domain towards the palm and thumb domains to accommodate the 3'-hydroxyl group of an incoming nucleotide. The distal portion of the finger domain bends inward to the palm domain and the polymerase active site (Fig. 3), inducing a repositioning of the primer 3'-terminus with respect to the rest of the polymerase active site. The palm domain itself shifts slightly to rearrange the side chains of the active site residues. The incoming nucleotide also brings in two divalent metal ions. One metal ion facilitates the formation of catalytic RT complex. The other metal ion coordinates the incoming nucleotide with the oxygen ions of the triphosphate of the nucleotide, the side chains of strictly conserved Asp185 and Asp110, and the backbone carbonyl oxygen of Val111. The metal ions are positioned closely to the 3'-hydroxyl group of the primer terminus. The conformational change induced upon nucleotide binding specifically positions Asp110 for metal chelation. The nucleotide base stacks against the primer terminus and residues Arg72 and Gln151. The triphosphate

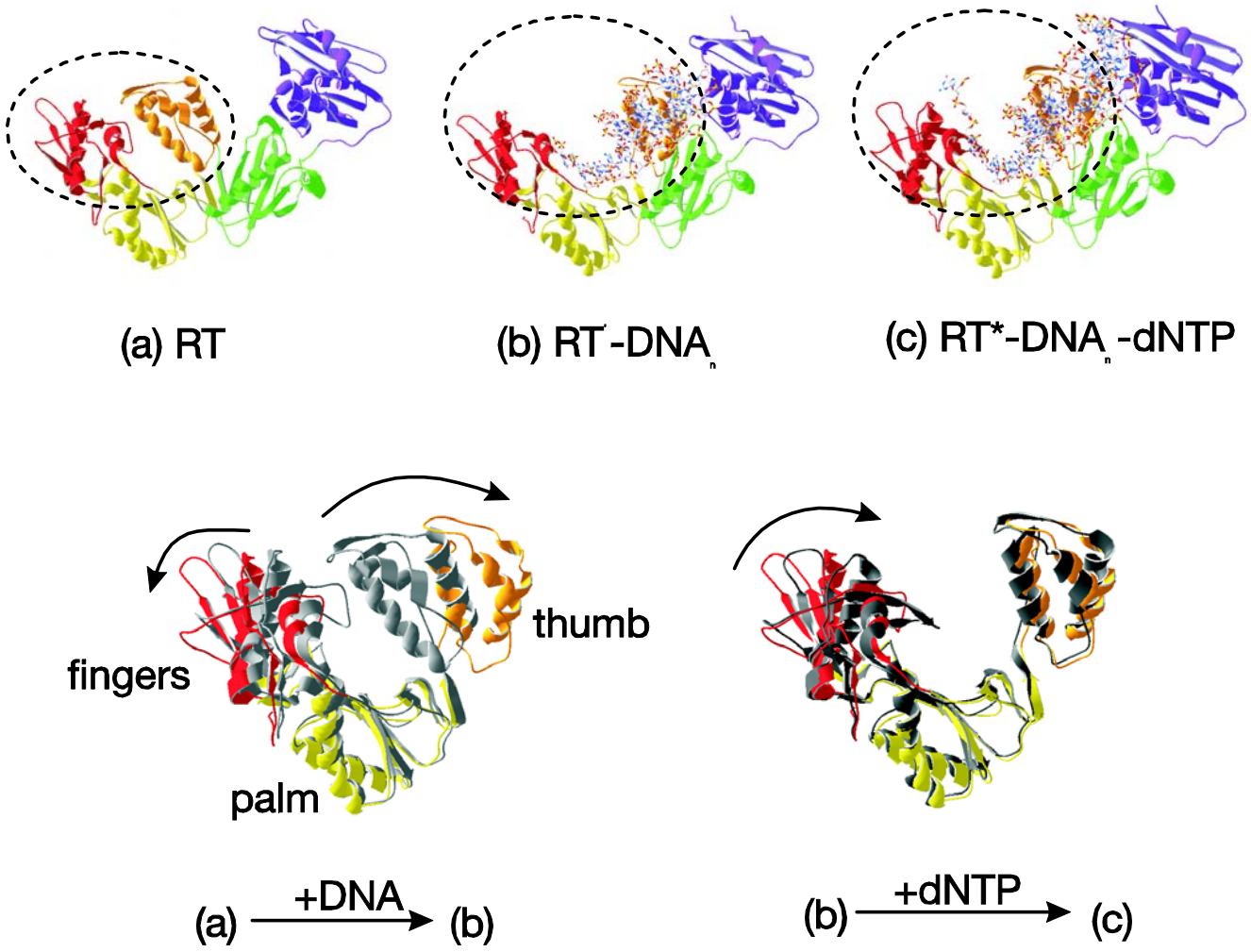
(a) RT
(b) RT-DNAn
(c) RT*-DNAn-dNTP
fingers
thumb
palm
(a) +DNA (b)
(b) +dNTP (c)

Figure 3. Conformational changes inside HIV-1 RT p66 subunit during DNA polymerization. (a) unliganded form of RT; (b) binary complex RT'/$DNA_n$; (c) ternary complex RT*/$DNA_n$/dNTP; (a→b) rotation of the p66 thumb domain away from the fingers domain induced by DNA binding (see the arrow); (b→c) hinge movement of the fingers domain to close down to the polymerase active site at the floor of the palm domain induced by nucleotide binding (see the arrow). The thumb domain in a→b is in light grey in the absence of DNA, and in orange color in the presence of DNA. The fingers domain in b→c is in red color in absence of dNTP, and dark gray in presence of dNTP. RT' denotes the enzyme form after the conformational change induced by DNA binding. RT* represents the enzyme form after the conformational change induced by nucleotide binding. Both the protein and DNA backbones are shown in ribbon diagrams. The DNA template and primer are in ball-and-stick model.

portion is contacted by Lys65 (γ phosphate), Arg72 (α phosphate), two main-chain NH groups, and two metal ions (34-36).

### 3.5. Nucleotide binding pocket

Several amino acids - Asp113, Tyr115, Phe116, and Gln151- form a binding pocket for the 3'-hydroxyl group of a nucleotide (Fig. 4). The 3'-hydroxyl group forms a hydrogen bond with the Tyr115 main-chain-NH. Tyr115 contacts 2' position modifications and prevents ribonucleoside incorporation by interference with a 2'-hydroxyl (28,33). Another requirement for the stabilization of the ternary complex is a positive charge conferred from residue 154. Lys154 is the only positively charged residue in the VLPQGWK motif on the β8-αE loop at the junction of the fingers and palm domains of HIV-1 RT. Lys154 assumes different orientations in the binary and ternary complexes. Lys154 also interacts with and stabilizes the side chains of Glu89 and Asp86.

### 3.6. Translocation

The aromatic residues in the vicinity of the polymerase active site are thought to be involved in transitions between different stages of the catalytic process. During DNA polymerization and translocation, conformational changes occur at the "primer grip" (the β12-β13 hairpin of p66 palm domain).

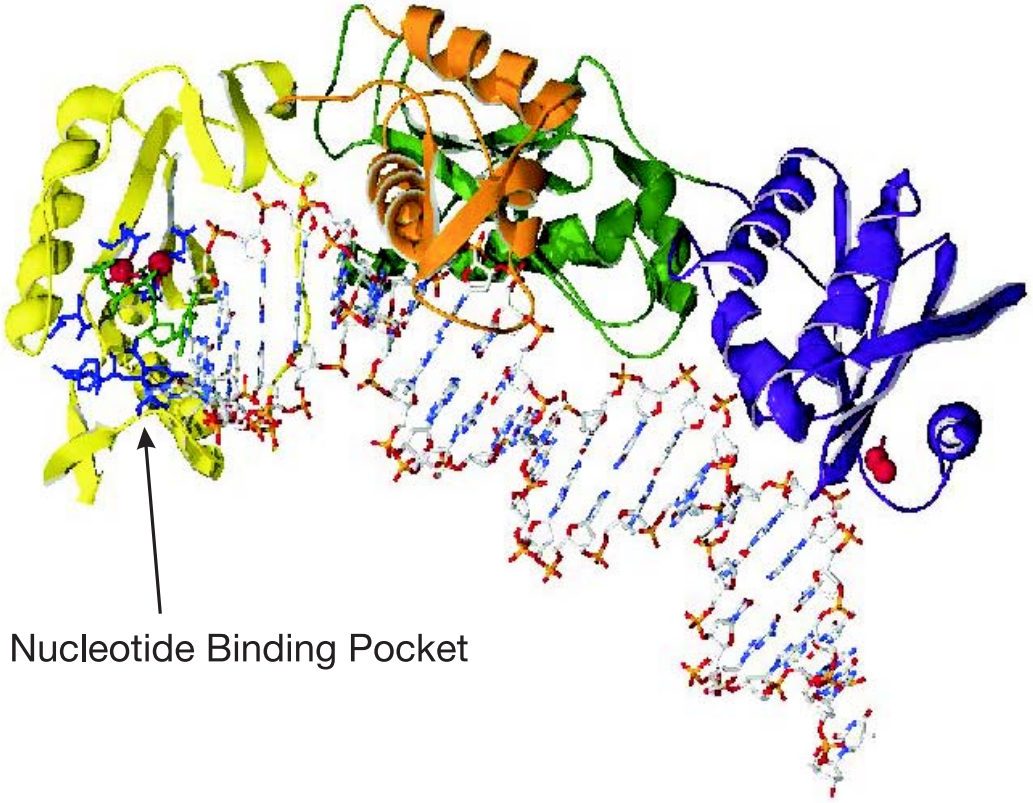


Figure 4. Nucleotide binding region. Only the palm (yellow), thumb (orange), connection (green) subdomain, and RNase H domain (blue) are shown here. The residues lining the nucleotide binding pocket are colored in blue. A TTP (colored in green) is bound at the active site. A DNA duplex is shown in a ball-and-stick model. Magnesium ions are colored in pink.

Translocation refers to the process in which elongated primer/template DNA is relocated from the nucleotide-binding site (pre-translocation complex N) to the priming site (post-translocation complex P) (37). Structural elements that help move nucleic acid and protein along the translocation track during polymerization include the primer grip, template grip, and helices αH and αI of the p66 thumb (31). Two antiparallel α-helices (H and I) of the thumb domain interact in the region of DNA bend. Whereas α-helix I interacts with the sugar-phosphate backbone of the template strand, α-helix H is partially embedded in the widened DNA minor groove and interacts primarily with the primer strand.

## 4. FUNCTIONS OF REVERSE TRANSCRIPTASE

HIV-1 RT replicates viral RNA into pro-viral DNA by catalyzing three consecutive catalytic activities (38,39). First, it synthesizes a minus-strand DNA by RNA-dependent DNA polymerization, which is initiated by a host tRNA primer. Second, the RNase H domain of reverse transcriptase degrades the RNA template from the RNA-DNA heteroduplex (40) in a reaction occurring in tandem as minus-strand DNA synthesis proceeds. Finally, it synthesizes a plus-strand DNA by DNA-dependent DNA polymerization using a DNA primer (41-43).

### 4.1. Reverse Transcription of HIV RNA Genome

The complete process of reverse transcription catalyzed by HIV-1 RT is described in ten steps (Fig. 5) according to the model proposed by Hottiger and Hubscher (44). In the first step, synthesis of minus-strand (-) DNA initiates from the 3' end of a host $tRNA^{LYS,3}$ primer partially annealed to the primer binding site (PBS) region near the 5' end of the plus-strand (+) viral RNA template. HIV nucleocapsid protein could help initiation by facilitating RT to unwind the first 18 basepairs of the 3' end of $tRNA^{LYS,3}$ (45,46). In the second step, DNA synthesis continues and produces the strong-stop DNA intermediate. DNA synthesis stops when RT encounters the 7-methyl-guanine cap of the RNA. In the third step, the 5' end of the viral genomic RNA is degraded by the RNase H activity of RT to leave a single-stranded (-) strong-stop DNA. The fourth step involves the first strand transfer: (-) strong-stop DNA is translocated from 5' to 3' end of the same (intermolecularly) or a second genomic RNA template (intramolecularly) that is complementary to the 3' end of (-) strong-stop DNA. This DNA translocation is also referred to as the first jump. Intramolecular first jump is possible because there are two identical copies of single-stranded RNA of the inverted repeats in each HIV. In the fifth step, the (-) strong-stop DNA synthesis resumes into the primer binding site (PBS) region while RNase H activity hydrolyzes the entire viral RNA template except the polypurine tract (PPT) fragment, which serves as

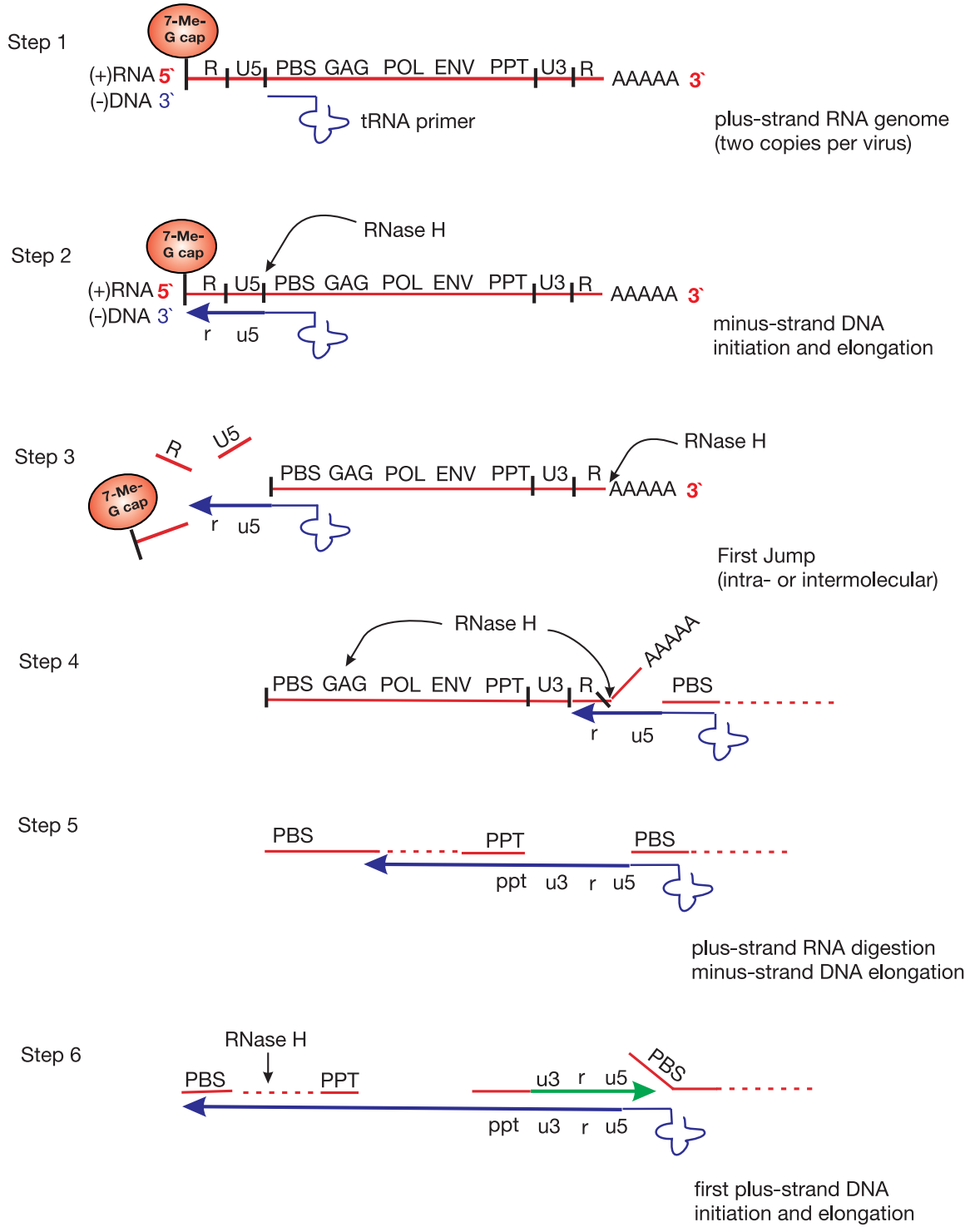
Step 1
7-Me-
G cap
(+)RNA 5`
(-)DNA 3`
R U5 PBS GAG POL ENV PPT U3 R AAAAA 3`
tRNA primer
plus-strand RNA genome
(two copies per virus)
Step 2
RNase H
7-Me-
G cap
(+)RNA 5`
(-)DNA 3`
R U5 PBS GAG POL ENV PPT U3 R AAAAA 3`
r u5
minus-strand DNA
initiation and elongation
Step 3
R
U5
7-Me-
G cap
PBS GAG POL ENV PPT U3 R
AAAAA 3`
RNase H
r u5
First Jump
(intra- or intermolecular)
Step 4
RNase H
AAAAA
PBS GAG POL ENV PPT U3 R
PBS
r u5
Step 5
PBS
PPT
PBS
ppt u3 r u5
plus-strand RNA digestion
minus-strand DNA elongation
Step 6
RNase H
PBS
PPT
u3 r u5
PBS
ppt u3 r u5
first plus-strand DNA
initiation and elongation

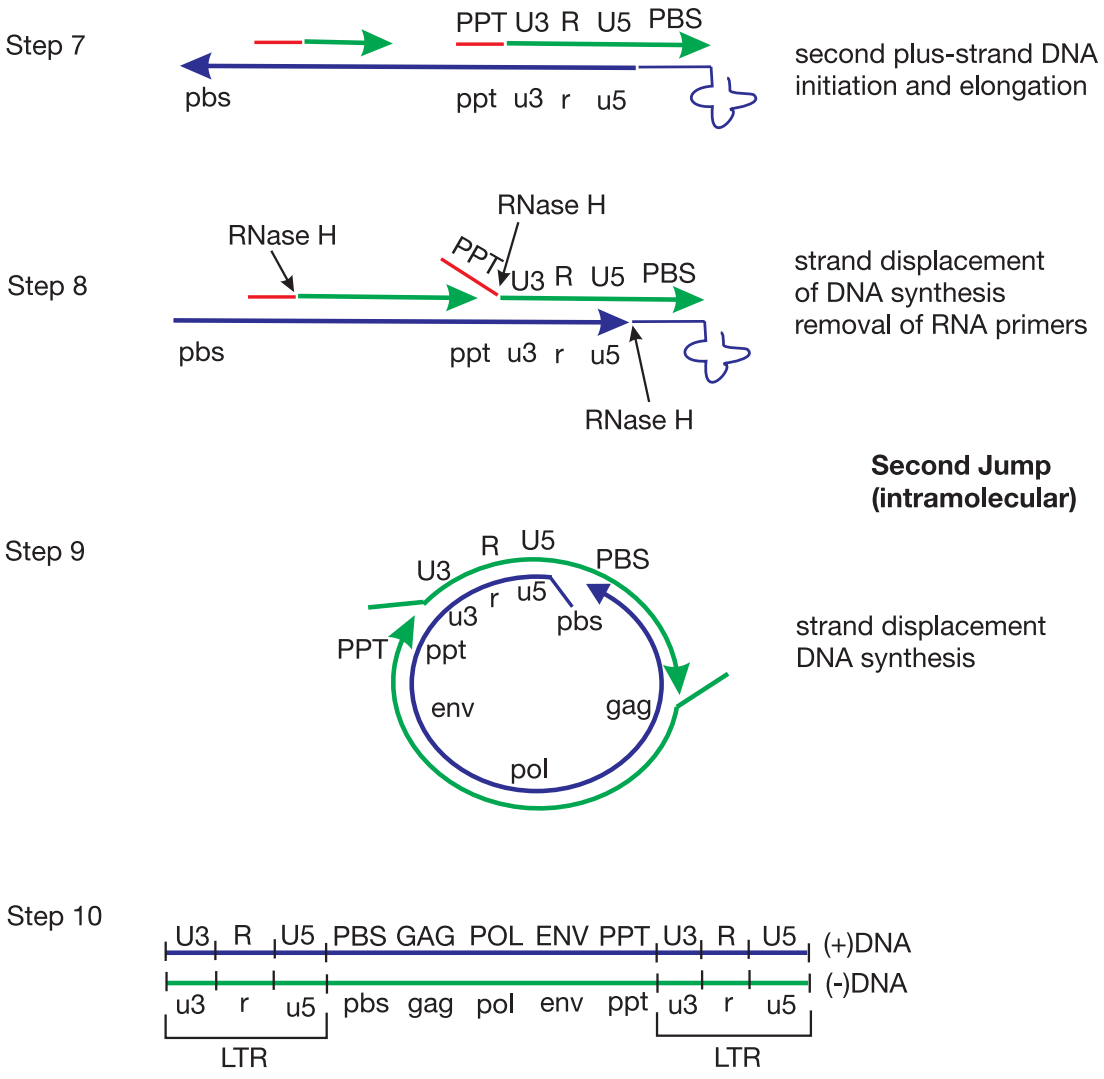


Figure 5. The Reverse Transcription Process. Uppercase letters indicate plus-strand regions while lowercase letters indicate minus-strand regions. Redrawn from Hottiger and Hubscher (41), 1996.

the primer to initiate (+) DNA synthesis in the sixth step. The HIV-1 genome has a second PPT in the *pol* region. The PPT may be the origin for the second (+) DNA synthesis in the seventh step, which yields two discrete (+) strands of unintegrated linear DNA. This second PPT region facilitates replication although it seems not to be mandatory. In the eighth step, the tRNA primer is removed by RNase H from the 5' (-) DNA as soon as the 3' (+) DNA extends past it. The ninth step involves the second strand transfer: the complementary copies of PBS sequences at the 3' ends of (+) strong-stop DNA and the nascent (-) DNA base pair. This intramolecular second jump circularizes the DNA strands. In the last step, (-) and (+) DNA synthesis continues to complete the synthesis of the double-stranded pre-integrative DNA (47). The end product of reverse transcription is called pro-viral DNA and is longer at both ends than the original viral RNA template. The entire process takes place in cytoplasm of host immune cells, CD4, within the first six hours of infection. After synthesis, pro-viral DNA is transported to the nucleus of host cells as a nucleoprotein complex (44), followed by integration into host DNA, catalyzed by HIV integrase (48).

### 4.2. RNase H cleavage/hydrolysis

The polymerase and RNase H active sites of HIV-1 RT are separated by nineteen to twenty base pairs of DNA/RNA heteroduplex when the template does not contain a secondary structure (17,18,49-53). The primer/template can be

productively bound to RNase H while non-productively bound to the polymerase. RNase H activity is not required for RT to read through the secondary structure of the RNA template (49), although the polymerase and RNase H activities in HIV-1 RT are coupled by the movement of the enzyme along the template during the polymerization process. This correlation is evident by examination of the overlap of RNA cleavage sites and pause sites for primer elongation through an RNA hairpin on the template (49).

RNase H cleavage shows some sequence dependence. During retrovirus replication, the RNase H domain of RT carries out nonspecific hydrolysis that removes RNA from the DNA/RNA replication intermediate, making nascent DNA available for a second round of synthesis (54). Specific RNase cleavage is required in the following steps: (1) release of the cognate tRNA primer from (-) DNA prior to second strand transfer (55,56), (2) excision of the 3' end polypurine tract (PPT) of the RNA genome from the replication intermediate and subsequent use of PPT to prime (+) strand DNA synthesis, and (3) removal of the PPT primer from (+) strand DNA by a precise cleavage at the PPT/U3 junction, generating a correct viral DNA end for subsequent integration (57). The PPT is resistant to RNase H cleavage. The PPT-selective processing is induced by inherent structural distortions resulting from the PPT sequence itself (58).

The specificity of RNase H cleavage is governed by the structure and the proper positioning of the DNA/RNA primer/template duplex in the p66 subunit,

relative to the RNase H active site (59). A series of HIV-1 RT p66 residues within the connection domain and RNase H domain interact with the DNA primer strand and may control the trajectory of the RNA template relative to the RNase H catalytic center. This region is referred to as the "RNase H primer grip" and is conserved between retroviral and bacterial RNase H (20). Substitution of the conserved residues in the RNase H primer grip region reduces the polymerization-independent cleavage activity significantly (60). Residues in the RNase H primer grip, the thumb domain, and particularly the minor groove binding track (61), are crucial for the unique interactions between RT and PPT, that create the correct positioning for precise RNase H cleavage.

## 5. KINETIC MECHANISM OF REVERSE TRANSCRIPTASE

The kinetic parameters of HIV-1 RT have been measured by transient state single nucleotide incorporation assays (21,62). Transient state, also known as pre-steady-state kinetic methods are preferred over steady-state kinetic analyses for dissection of reaction mechanisms as steady-state kinetic analyses can not address the individual steps of a reaction. The observed steady-state turnover rate, $k_{cat,}$ is usually dominated by the slow dissociation rate of DNA from a polymerase rather than the actual polymerization rate. Therefore, individual reaction steps such as the binding of DNA and an incoming nucleotide, the putative protein conformational change, the chemistry step, and the product dissociation step, can

only be resolved by pre-steady-state kinetic methods (63). These methods allow direct measurement of each elementary step in a reaction mechanism while the enzyme is examined as a stoichiometric reactant. Pre-steady-state kinetic studies using synthetic primer/template molecules and nucleotides have determined the polymerization mechanism of RT and the rate constants for the elementary steps in the reaction pathway (62).

The mechanistic pathway for RT polymerization (Fig. 6) is similar to other polymerases and involves the following steps: (1) tight binding of a primer/template duplex substrate to the polymerase heterodimer (E), which induces a conformational change of the enzyme (E'-$D_n$) (64,65), (2) binding of the next correct nucleotide (dNTP) and divalent metal ions required for catalysis to the enzyme/DNA binary complex (E'-$D_n$), which forms a ground-state "open" ternary complex of enzyme/DNA/nucleotide (E'-$D_n$-dNTP), a diffusion-limited initial association, (3) a rate-limiting conformational change, which is a relatively slow isomerization to a "closed" ternary complex (E'*-$D_n$-dNTP) that properly positions the nucleotide for catalysis (21), (4) a fast chemical incorporation step involving the formation of a phosphodiester bond between the 3'-hydroxyl primer terminus and the α-phosphate of the nucleotide (E'-$D_{n+1}$-PPi), followed by the release of pyrophosphate (PPi), and (5) processive synthesis whereby the elongated primer/template DNA is translocated from complex N to complex P (37,62,66-68) after which the enzyme either continues to polymerize; or

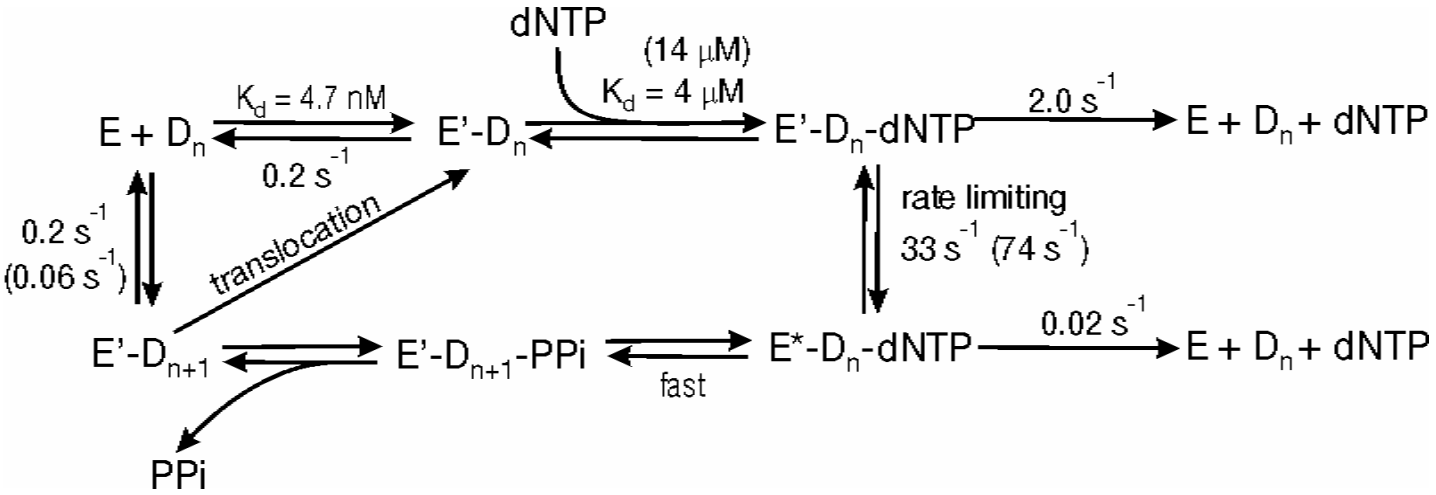


Figure 6. A scheme for the polymerization pathway of HIV-1 reverse transcriptase. Kinetic measurements using an RNA template are indicated in parentheses, all others are determined using a duplex DNA/DNA primer/template. E represents enzyme. $D_n$ represents substrate DNA. $D_{n+1}$ represents product DNA with an elongated primer. dNTP represents the incoming nucleotide. E' denotes the form of RT after a conformational change induced by DNA-binding. E'* denotes the transitional state of RT after the second conformational change upon nucleotide binding. PPi represents pyrophosphate. Data were reported by Kati *et al* (62)

alternatively exhibits distributive synthesis where the enzyme dissociates from the primer/template DNA. Following dissociation, the polymerization process restarts via the formation of the initial binary complex (E'-$D_n$).

The binding of RT to a primer/template DNA substrate can occur in two states – productive and nonproductive – due to the pause sites in the secondary structure of the template (69). Moreover, a nonproductive E-DNA complex is formed when DNA is bound at a site distal to the DNA-binding tract. However, the nonproductive complex can isomerize to a productive E'-DNA complex, which can successfully bind and incorporate an incoming nucleotide (70,71).

## 6. RNA- VERSUS DNA-DEPENDENT DNA POLYMERIZATION

RNA and DNA-dependent DNA polymerization are similar in the rate-limiting step – the conformational change following nucleotide binding (21,62,68,72). Nevertheless RNA-directed polymerization has been differentiated from DNA-directed polymerization by pre-steady-state kinetic analysis (62). At a faster polymerization rate (66 $s^{-1}$ compared to 20 $s^{-1}$) and a slower steady state rate (0.06 $s^{-1}$ compared to 0.18 $s^{-1}$) (73), RNA seems to be the preferred template for HIV-1 RT.

For DNA polymerases, the fidelity of replication during forward polymerization and exonuclease error correction is largely a function of the two-step reaction: a correct nucleotide binding to properly base-paired duplex DNA

followed by a conformational change (74). The fidelity of DNA synthesis by HIV-1 RT is 10 to 60-fold higher with an RNA template (73) than with a DNA template (62) (Table 1). With a DNA template, mismatched nucleotide incorporations opposite a template base thymine displayed a 250-fold increase of the equilibrium dissociation constant ($K_d$) and a 7 to 80-fold decrease of the maximum incorporation rate ($k_{pol}$), relative to the incorporation of matched deoxyadenosine 5'-triphosphate (dATP). In contrast, with an RNA template, the incorporation of dGTP, dCTP, and dTTP opposite a template uridine (rUTP) were 370- to 24,700-fold slower and had a 50- to 80-fold lower affinity than dATP (73). RNA-dependent DNA replication is much more selective for the maximum incorporation rates and binding affinities of incorrect nucleotides are substantially lower.

Several structural factors can be attributed to higher fidelity with an RNA template. Misaligned intermediates are formed less frequently with RNA templates than with DNA templates (75). Topology and thermodynamic stability of DNA/DNA and DNA/RNA duplexes vary in a sequence-dependent manner (76,77). In addition, the secondary structure of a template might affect the efficiency of nucleotide incorporation (49,69,78-80).

Table 1: Fidelity of HIV-1 RT with 25/45mer primer/template.

| | DNA template[1] | | | |
|---|---|---|---|---|
| dNTP | $K_d$ ($\mu$M) | $k_{pol}$ ($s^{-1}$) | $k_{pol}/K_d$ ($\mu M^{-1}s^{-1}$) | fidelity[3] |
| dATP | 4 | 33 | 8.25 | - |
| dGTP | 1010 | 4.8 | $4.75 \times 10^{-3}$ | 1740 |
| dCTP | 1240 | 0.52 | $4.19 \times 10^{-4}$ | 19700 |
| dTTP | 840 | 0.41 | $4.88 \times 10^{-4}$ | 16900 |
| | RNA template[2] | | | |
| dATP | 14 | 74 | 5.28 | - |
| dGTP | 1000 | 0.2 | $2.0 \times 10^{-4}$ | 26000 |
| dCTP | 1100 | 0.03 | $3.0 \times 10^{-5}$ | 176000 |
| dTTP | 700 | 0.003 | $4.9 \times 10^{-6}$ | 1100000 |

[1] Kati et.al., 1992 (62).

[2] Kerr and Anderson, 1997 (73).

[3] Calculated as $[(k_{pol}/K_d)_{correct} + (k_{pol}/K_d)_{incorrect}]/(k_{pol}/K_d)_{incorrect}$.

## 7. RNA SECONDARY STRUCTURE SWITCHING

The secondary structure of an RNA or DNA template causes RT to stall during polymerization (49,69,78-80). The DNA/RNA and DNA/DNA substrates predominantly bind at the polymerase active site of RT in a nonproductive state at strong pause sites and in a productive state at non-pause sites. Pause sites are segments of templates where secondary structures such as hairpin stems prevent the DNA substrate from binding productively to RT consequently stalling the polymerization process. Suo and Johnson proposed a model for the motion of RT progressing through the RNA secondary structure at 37$^{o}$C (49). While remaining associated with RT, it is postulated that the non-productively bound DNA/RNA is slowly converted to a productive state upon melting of the next stem base pair, followed by fast nucleotide incorporation. Interestingly, the hairpins in RNA secondary structure can disassemble and reform when HIV-1 RT reads through the stem region of the first hairpin structure. Moreover, HIV-1 RT facilitates such RNA secondary structure switching by inducing unwinding of the secondary structure in the template strand near the 3' end of the primer (49,69,78,79). This model demonstrates a dynamic RNA or DNA template secondary structure during DNA polymerization catalyzed by RT.

## 8. NON-NUCLEOSIDE REVERSE TRANSCRIPTASE INHIBITORS

Current treatment of HIV-infected or AIDS patients enlists four types of drugs: nucleoside analog reverse transcriptase inhibitors (NRTIs), nonnucleoside reverse transcriptase inhibitors (NNRTIs), fusion/entry inhibitors, and protease inhibitors (PIs), which are often used either in a monotherapy or a combination therapy. These inhibitors can only retard the conversion of infected T cells to monoclonal malignant cells. In spite of the development of drug-resistant mutant strains, HIV-1 RT remains as one of the main targets for antiretroviral therapies used in the treatment of AIDS.

### 8.1. NNRTIs vs. NRTIs

NNRTIs differ from NRTIs in their chemical structures (Fig. 7 and Fig. 8), binding sites (Fig. 9), and inhibition mechanisms (Fig. 10). NRTIs are structural derivatives of nucleosides or nucleotides with modified functional groups whereas NNRTIs are highly hydrophobic aromatic compounds. The 5'-triphosphates of NRTIs bind at the nucleotide binding sites on HIV-1 RT, directly competing with incoming nucleotides. As a result, several cellular DNA polymerases, in particular, the human mitochondrial DNA polymerase (*pol* γ), are also inhibited by NRTIs, causing severe side effects (81). Unlike NRTIs, NNRTIs enter a hydrophobic pocket adjacent to the active site, inducing a conformational change

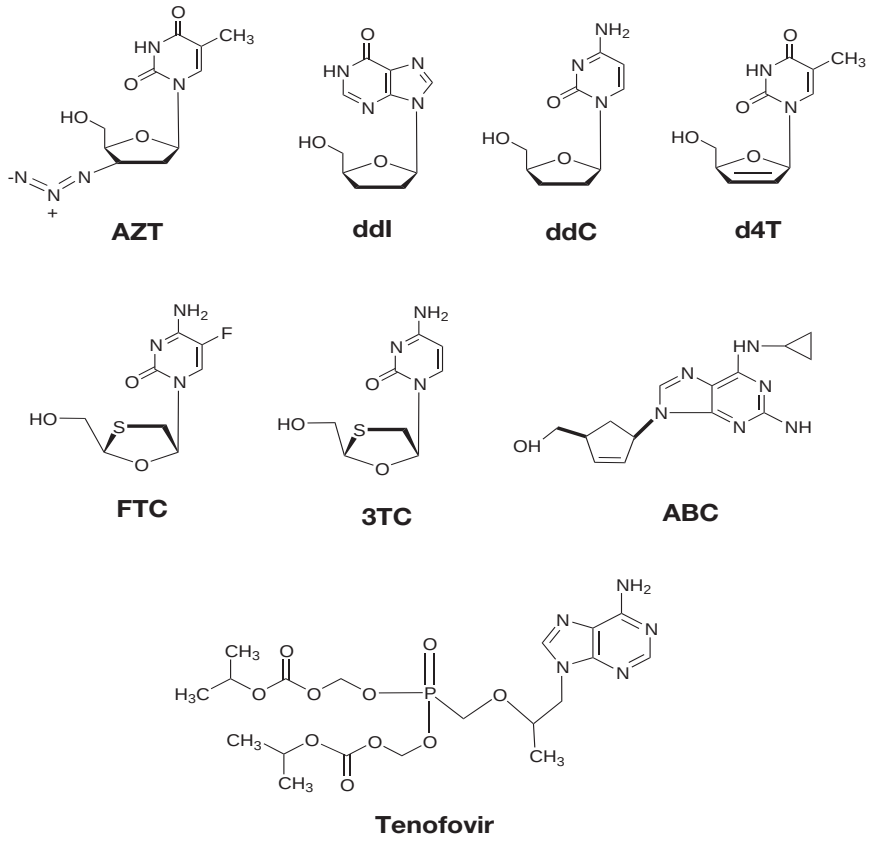


Figure 7. Structures of NRTIs approved by the FDA.

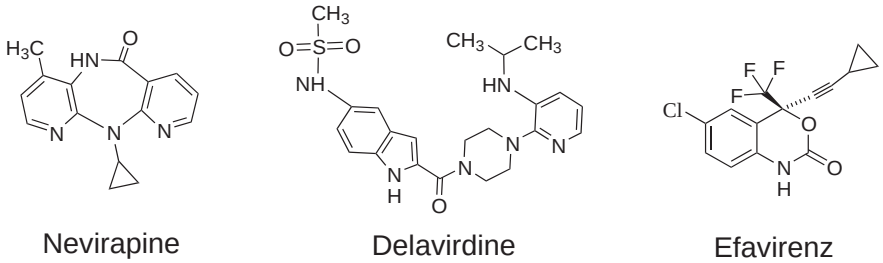


Figure 8. Structures of NNRTIs approved by the FDA.

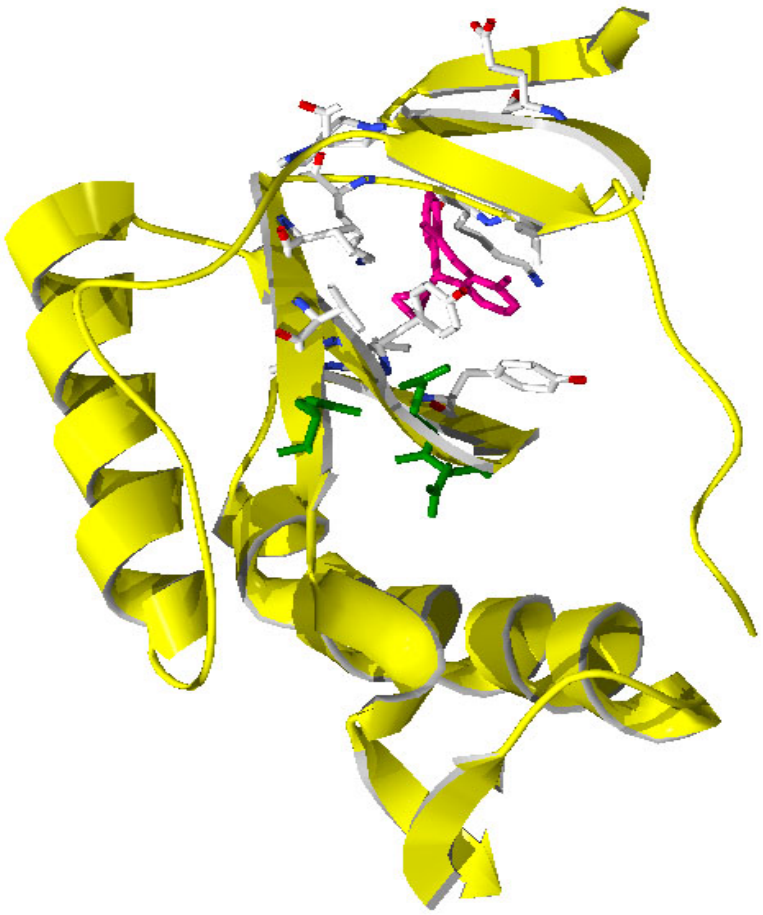

Figure 9. NNRTI versus NRTI Binding Sites. Nevirapine is in a pink-colored ball-and-stick model. The side chains of the residues inside the NNRTI binding pocket are in ball-and-stick models. The *pol* active site is outlined by the key residues, the aspartic triad, in green-colored ball-and-stick model. NRTIs bind directly at the active site onto the 3'-end of the primer.

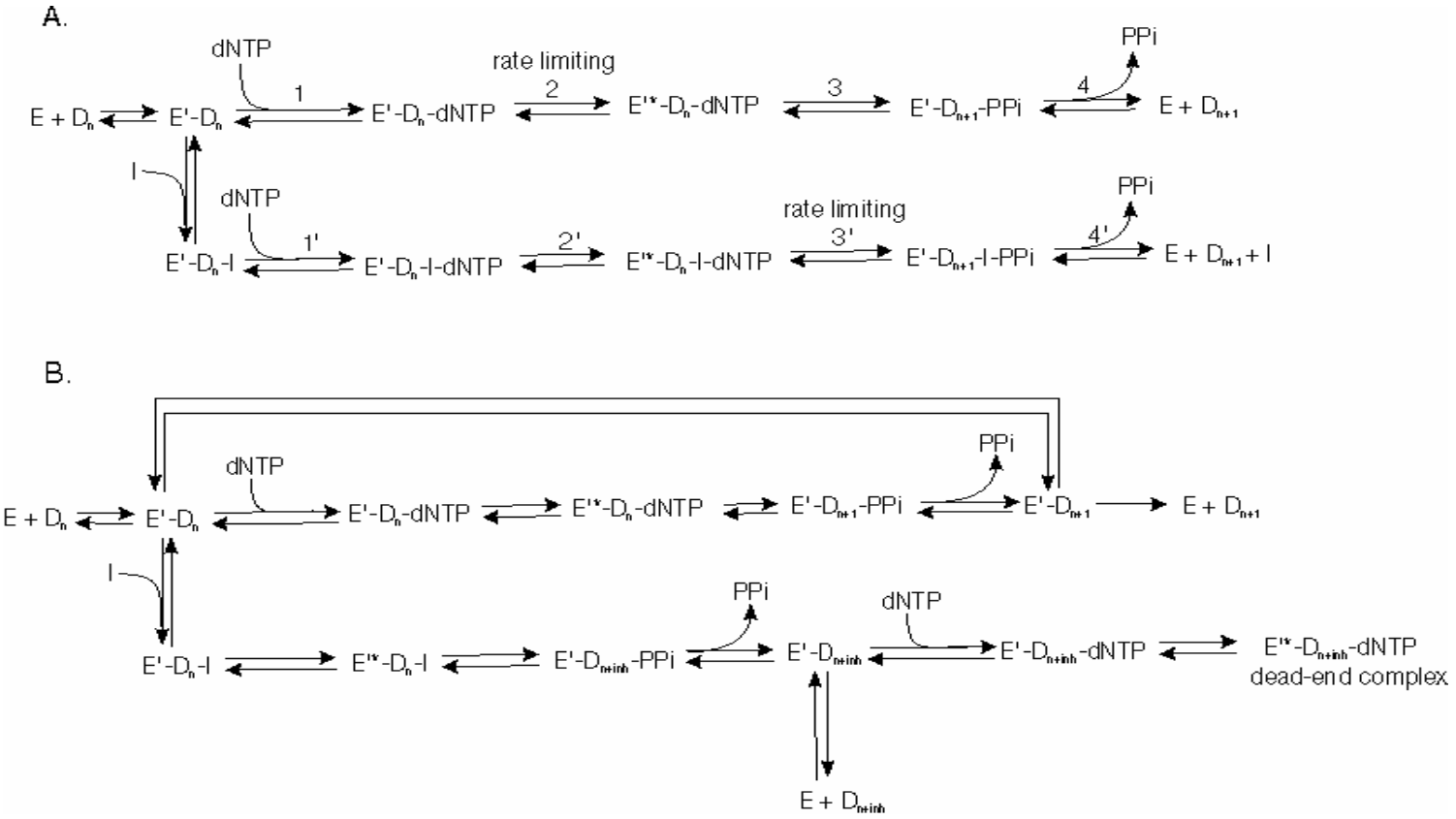


Figure 10. Inhibition mechanisms of NNRTI (panel A) and NRTI (panel B)

that locks RT into an inactive state by perturbing the position of catalytic residue. NRTIs bind to RT-DNA complexes at the ground-state binding step, but the DNA chain elongation ends after an NRTI is incorporated due to the lack of a 3'-hydroxyl group (Fig. 10A). NNRTIs can bind to RT-DNA complexes before dNTP and inhibit the chemistry step (Fig. 10B). NNRTIs are structurally diverse compounds that bind to a hydrophobic region near the polymerase active site in the palm domain of the p66 subunit of HIV-1 RT (82). The NNRTIs currently approved for use in antiretroviral therapy include nevirapine (83), delavirdine (84), and efavirenz (85). Although NNRTIs are less toxic than NRTIs, they elicit allergic responses, disturb metabolic functions, and appear to be toxic to the liver and central nervous system (86). Moreover, because they bind to nonessential residues, resistance is readily achieved by mutation of amino acids surrounding the NNRTI binding pocket.

### 8.2. Structural and Conformational Effects of NNRTI binding

In unliganded RT, the thumb domain contacts the finger domain, somewhat covering the substrate-binding cleft. The NNRTI binding alters the flexibility of the domains which correlate motions with the binding pocket (29). The effects include domain shifts relative to the enzyme core (30) and the misalignment of the conserved residues of the polymerase active site (Asp110, Asp185, and Asp186) relative to the catalytically required $Mg^{2+}$ ions (21).

Rotation and stiffening of the p66 thumb domain skew the orientation of the primer/template with respect to the polymerase and RNase H active sites of RT (87). Esnouf et al suggests that NNRTIs inhibit RT by locking the polymerase active site into an inactive conformation, reminiscent of the conformation observed in the inactive p51 subunit (88). However, kinetic measurement showed that NNRTIs do not block the nucleotide induced hinge movement of the finger domain, but inhibit the rate of the chemical reaction of the polymerization (21).

### 8.3. Inhibition mechanism of NNRTIs

First generation NNRTIs such as nevirapine and TIBO do not compete with either primer/template or nucleotide substrates for binding to the enzyme. Pre-steady state kinetic studies revealed that NNRTIs inhibit HIV-1 RT by slowing down the chemical reaction (step 3', Fig. 10A), without affecting the nucleotide binding and the consequent conformational change (step 2', Fig. 10A) (21). In a single turnover experiment, the observed fast product formation is catalyzed by uninhibited HIV-1 RT because the equilibration of the inhibitor with the E-D complex is slow relative to the rate of the polymerization reaction. Spence *et al*. postulated that the binding of the NNRTIs switches the positions of the carboxyl groups of the conserved aspartic acid residues and resultantly reduces the rate of the $Mg^{2+}$-dependent chemical reaction (21), and the chemical

reaction of the enzyme-DNA-inhibitor-nucleotide complex becomes the rate limiting step in the polymerization pathway.

The structural distortions caused by the NNRTI binding also reduce the affinity of HIV-1 RT for the primer/template as well as the specificity of RNase H cleavage (89). Aside from the chemical reaction at the active site, other reverse transcription events such as strand transfer, strand displacement, and recognition of tRNA primer in the initiation of reverse transcription (19) could also be affected by this class of inhibitors.

### 8.4. Effect of mutations on the structure to develop resistance to NNRTIs

HIV adapts to NNRTIs by evolving in the vicinity of NNRTI binding pocket in HIV-1 RT. Single amino acid substitutions include L74I/V, V75I/L, A98G, L100I, K101E/I/Q, K103N/Q/R/T, V106A/I, V108I, E138K, T139I, G141E, V179D/E, Y181C/I, Y188C/H/L, V189I, G190E/Q, P225H, P236L, and V233E (90-101). Switched amino acids can cause rearrangement of residues inside the NNRTI binding pocket and hence repositioning of NNRTIs (102,103), or alter the interaction(s) of the NNRTI and the binding pocket as in the case of K103N.

Residue 103 is not located inside the hydrophobic NNRTI binding pocket but near the entrance to the pocket (Fig. 11). The most clinically prevalent K103N causes resistance to most of the NNRTIs. In unliganded RT, K103N

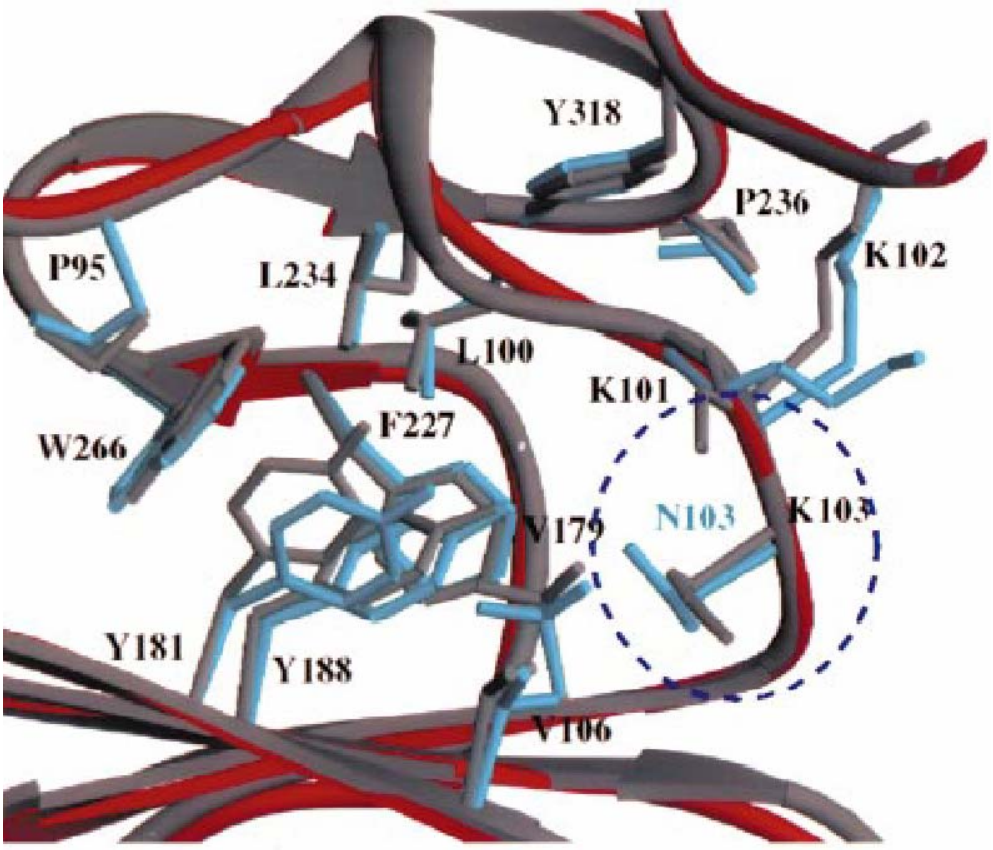


Figure 11. K103N resistance mechanism. Position 103 (highlighted by the blue dotted circle) is at the entrance to the NNRTI binding pocket for wild type RT (gray ribbons) and the K103N mutant (red ribbons). Hsiou *et al.* proposed a direct interaction (3.3 angstroms) between the OH of Y188 and the $NH_2$ of N103. Duplicated from Hsiou *et al.*, 2001 (104).

creates an extra hydrogen bond with its $NH_2$ group and the OH group of Y188 (104). Instead of distorting the structure of complex between HIV-1 RT and NNRTIs, K103N is thought to prevent NNRTIs from contacting the binding pocket.

The side chains of mutated amino acid residues prevent RT from accepting the inhibitors as substrates by two mechanisms. Mutations can alter the structure of the binding site and impose steric hindrance for inhibitors to enter the binding pocket. Mutations can also destabilize the hydrophobic and electrostatic interactions between the enzyme and NNRTI. These mutational factors contribute to weaker binding of NNRTIs to HIV RT, which leads to drug resistance.

## 8.5. Novel Class of NNRTIs

Computational structure-biased design identified some naphthyl urea compounds as a novel class of NNRTIs (1). According to the molecular docking program, they do not bind to the conventional NRTI or NNRTI binding site. They inhibit not only the wild type but also drug-resistant HIV-1 RT. They did not appear to inhibit T4 DNA polymerase, T7 DNA polymerase, and the Klenow fragment in a previous study (1). Further investigation into their inhibition

mechanism is performed as part of this thesis in order to assess their efficacy and mechanism of action.

## 9. SUMMARY

In this chapter I have presented an updated review of research results pertaining to HIV-1 RT. Current understanding of this enzyme can be divided into the following aspects: structure-function relationship, fidelity of polymerization, and development of drug-resistant through mutation. The focus of my dissertation project is on the last aspect. In the following chapters, I will describe the efficacy of a novel class of NNRTIs as well as the characterization of a mutant HIV. Three different NNRTIs with a range of size and shape were chosen to determine their effectiveness. Polymerization mechanisms of wild type HIV-1 RT and K103N mutant in the presence of CZ-1, α-APA, and HBY097 were investigated. HBY097 and α-APA are the conventional NNRTIs that are known to bind at the hydrophobic pocket adjacent to the active site, while CZ-1 does not. The kinetic parameters were compared to gain insights into the drug resistance mechanism of K103N. The inhibition mechanism of CZ-1 was delineated to facilitate the design of future RT inhibitors.

# CHAPTER 2: Experimental Methods and Materials

## 1. MATERIALS

All chemicals were purchased from Sigma Aldrich (St. Louis, MO) unless otherwise noted. Bacterial cell lines, dATP, T4 polynucleotide kinase, and kinase buffer were purchased from Invitrogen Corp. (Carlsbad, California). [$\gamma$-$^{32}$P] ATP (3000 Ci/mmol) was purchased from NEN life science products, Inc. (Boston, MA). The P-11 resin for the phosphocellulose column and filter paper and discs were purchased from Whatman (Chilton, NJ). The sepharose resin was purchased from Amersham Biosciences (Piscataway, NJ). Micro-Bio-Spin-6 columns and electrophoresis apparatuses were obtained from BioRad Laboratories, Inc. (Hercules, CA). RNAse-free reagents were obtained from Ambion Inc. (Austin, TX). Microfuge tubes were purchased from Phenix Research (Hayward, CA). Glassware and forceps were autoclaved.

### 1.1. RT, p66 (K103N) and p51 (K103N) construction

Plasmids pKK322 of the HIV-1 reverse transcriptase subunits p66 (WT) and p51 (WT) were generously provided by Roger Goody (105). Since the p51 subunit has been postulated to be a proteolytic cleavage product of the p66

subunit (23), both p66 and p51 subunits should contain the K103N mutation in the physiological form of HIV-1 RT heterodimer. The two plasmids encoding the p66 and p51 subunit with K103N mutation, respectively, were created by site-directed mutagenesis. The process was carried out using the QuikChange® Site-Directed Mutagenesis Kit from Stratagene, (La Jolla, CA). A pair of forward and reverse primers containing the genetic change from AAA to AAC was designed. The pKK322-B plasmid and the primers were mixed in a PCR reaction catalyzed by pfu Turbo DNA polymerase. The new constructs, containing the one base substitution, were transformed into DH5α competent cells (Invitrogen, CA) for amplification. After the presence of the mutation was confirmed by sequencing, the extracted plasmid DNA from DH5α cells was transformed into Tuner competent cells (Novagen / EMD Biosciences, San Diego, CA) for protein expression.

### 1.2. Protein expression and Purification of HIV-1 Reverse Transcriptase.

Transformed *E. coli* cells expressing the p66 and p51 subunits were grown separately in Lennox L broth supplemented with ampicillin (0.1 mg/mL) at 37$^{o}$C. The optical density of the bacterial culture was measured at 600 nm with a spectrophotometer, Beckman Coulter DU640 (Fullerton, CA). When the optical density reached 0.6, protein expression was induced by adding 0.5 mM isopropyl

β-D-thiogalactopyranoside. The cells were then grown for 16 hours at 37°C and harvested by centrifugation at 4000x *g* for 10 min. The crude cell lysates were analyzed by SDS-PAGE stained with Coomassie Blue. Based upon the gel-staining intensities of the bands corresponding to the p66 and the p51 subunits, the cell pellets were combined in a ratio of 3.9 to 1 by weight for the large and small subunit, respectively, in order to achieve a ratio of 1.25 to 1 at the end of the purification process (Fig. 12).

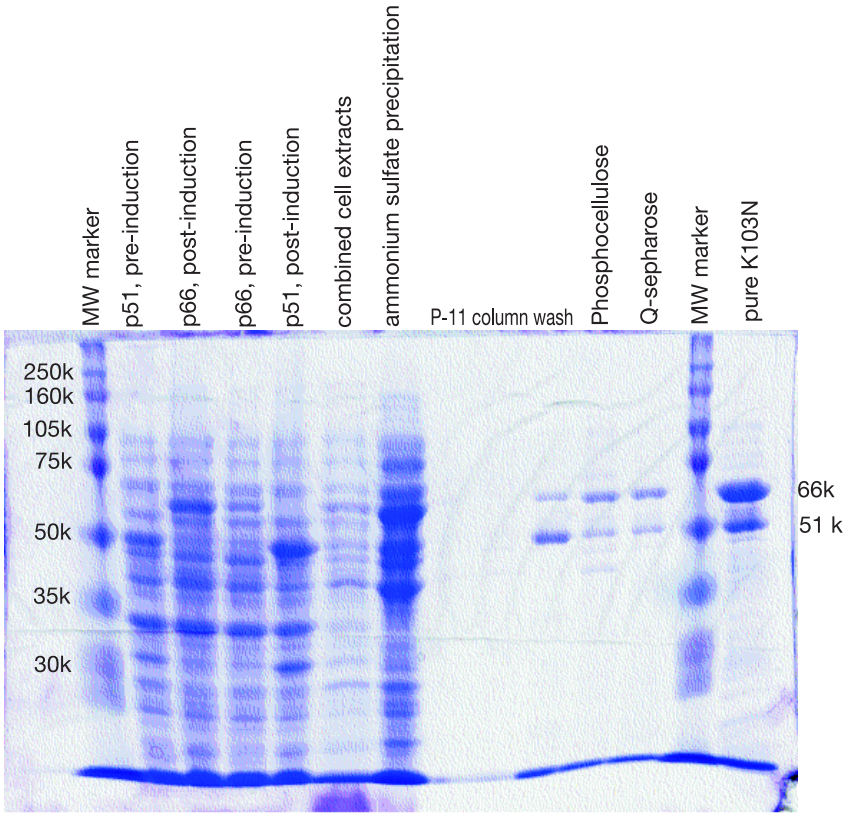


Figure 12. Gel of the K103N purification procedure.

The procedures for purification of wild type RT were modified from previously described by Kati *et al.* (62,106) and were performed at 4$^{o}$C as follows. The cells (24.5 g) were resuspended in buffer A (50 mM Tris-HCl, pH 7.9 (at 4$^{o}$C, or pH 7.5 at room temperature), 500 mM NaCl, 2 mM EDTA, 1 mM phenylmethanesulfonyl fluoride, 10 % glycerol, 0.01 % Triton-X, and 1 mM dithiothreitol) to a final volume of 125 ml. The suspension was homogenized in a dounce. Lysozyme was added to 0.75 mg/ml. The bacterial cells were further broken down with a Branson Sonifier 450 (VWR) at 50% duty cycle, total output 30 Watts (control 8). The suspension was sonicated three times for 30 sec with 2-min lapses in between. Cell extract was centrifuged at 75,500*g* for 1 hour. The viscosity of the solution was decreased when the nucleic acid was removed by adding 0.4% polyethylenimine drop-wise and incubated for 15 min. Nucleic acid precipitate was then separated by centrifugation (10,000 x *g* for 20 minutes) and discarded. Protein in the supernatant was precipitated by 60 g ammonium sulfate / 100 ml and separated by centrifugation (18,000 x *g* for 20 minutes). Protein pellets were resuspended in and dialyzed against buffer A overnight. After spinning out the sediment (75,000 x *g* for 20 minutes), the protein solution was loaded onto a 20 ml phosphocellulose column pre-equilibrated with buffer A, washed with 10 column volumes of buffer A, and eluted with a 0.05 to 1 M sodium chloride gradient (300x300 ml). Pure protein fractions determined by SDS-PAGE were pooled together and dialyzed for 4 hour with buffer A.

Dialysate was loaded onto a 10 ml Q-sepharose column equilibrated with buffer A. Flow through and the first 15 ml fraction from washing with buffer A were collected and concentrated with Amicon Centriprep YM-50 (Fisher Scientific) at 3000xg for 2 hour. Concentration of RT was determined by UV spectroscopy absorbance at 280 nm with an extinction coefficient of 260,450 $M^{-1}cm^{-1}$. Reaction amplitude of the preparation showed approximately 0.5 to 0.7 active sites per p66/p51 heterodimer. The enzyme concentration was calibrated for the fraction of active protein (see Active Site Titration).

### 1.3. Synthetic DNA Oligonucleotides

All experiments in Chapters 3 and 4 were performed with the same DNA duplex 25/45-mer (Fig. 13A) as described by Kati et. al (62) in which the next base coded for incorporation was dATP. Oligonucleotides were synthesized by Integrated DNA Technologies, Inc. (Coralville, IA) and purified by denaturing polyacrylamide gel electrophoresis (PAGE). Each DNA pellet was resuspended in 1 ml distilled water for at least 2 hours at room temperature before running on a 15% denaturing polyacrylamide gel. Each DNA band was visualized by a short wavelength (254 nm) UV lamp and eluted with 3 to 5 ml TE buffer, pH 8.0. Gel solution was frozen for 30 minutes at -80$^{o}$C and thawed rapidly in a glass beaker of boiling water. DNA was eluted from the gel by shaking the solution in a 37$^{o}$C incubator overnight. Gel debris was spun down in a table-top centrifuge for 2

minutes at ~ 1000 x *g*. The supernatant was filtered through 0.22 μm discs and subsequently concentrated by butanol extraction. Greater than 4 volumes of N-butanol was added to the filtered supernantant and centrifuged for 2 min at setting 4 (~ 1000 x *g*), following by removing the organic upper layer containing butanol. This step was repeated until the aqueous phase, containing DNA, was less than 0.5 ml. Concentrated DNA solution was added 0.3 M sodium acetate, pH 5.2, and then 2 volumes of chilled 100 % ethanol to precipitate DNA. This solution was chilled for at least 20 min. at -20$^{o}$C and centrifuged for 10 min. at 4$^{o}$C and 13,000 rpm. DNA pellet was air-dried and resuspended in 50 to 100 μl of sterile water.

A. 25D/45D:

5 -GCCTCGCAGCCGTCCAACCAACTCA- 3
3 -CGGAGCGTCGGCAGGTTGGTTGAGTTGGAGCTAGGTTACGCGGCAGG-5

B. 25D/45R:

5 -GCC TCGCAGCCGT CCAACC AACTCA- 3
3 -CGGAGCGUCGGCAGGUUGGUUGAGUUGGAGCUAGGUUACGCGGCAGG-5

C. PCR primers for producing T7 promoter - 45mer template

5'-TAATACGACTCACTATA GGACGGCATTGGATCGAGGTTGAGTTGG-3'
3'-GCCGTAACCTAGCTCCAACTCAACCAACCTGCCGACGCTCCG-5'

Figure 13. Synthetic 25mer primer and 45mer template.

Concentrations of the oligonucleotides were determined by UV absorbance at 260 nm using a spectrophotometer DU640 (Beckman Coulter Inc., Fullerton, CA). Equimolar amount of 25-mer and 45-mer were annealed by placing the solution in a heating block at 95$^{o}$C and then cooling the heating block containing the solution on the bench for 2 hours to overnight.

### 1.4. RNA 45-mer Template.

The 45-mer RNA template (Fig. 13B) was synthesized by *in vitro* transcription using the T7 MEGAscript *In Vitro* Transcription Kit (Ambion Inc., Austin, TX) or Ampliscribe T7 High Yield Transcription Kit (Epicentre Technologies, Madison, WI). DNA containing the 17-mer T7 promoter sequence in front of the 45-mer template was synthesized by PCR. Forward and reverse PCR primers (Fig. 13C) were synthesized by Integrated DNA Technologies, Inc. (Coralville, IA). The PCR product, T7 promoter-template DNA 62-mer (Fig. 13C), was concentrated by ethanol precipitation before it was added into the reaction mixture to initiate the 6 hr. *in vitro* transcription. The 45-mer RNA was purified by 10% denaturing PAGE, and visualized under short wavelength UV. RNA was eluted from excised gel with TE buffer, pH 8.0, followed by precipitation with 0.3 M sodium acetate and 100% ethanol. RNA pellet was washed with 70% ethanol, air-dried, and finally, resuspended in water. RNA concentration was determined by measuring the absorbance at 260 nm.

RNAse*Zap*® and RNAse*Zap* Wipe® (Ambion, Inc., Austin, TX) were used to clean working areas, pipettors and gloved hands throughout the preparation to prevent contamination of the solutions or degradation of the RNA template by RNases.

### 1.5. Non-nucleoside inhibitors

The naphthalene sulfonic acid compounds were synthesized as described previously (1) and provided by our collaborator, Dr. George Kenyon. HBY097 and α-APA were courteously provided by Dr. Edward Arnold. The non-nucleoside inhibitors were dissolved and stored in dimethylsulfoxide (DMSO) at -20$^{o}$C and diluted by at least 700-fold to a stock solution with water. Control experiments showed that the final concentrations of DMSO were low enough that they did not affect the measured kinetics.

### 1.6. Buffers

All experiments were carried out at 37$^{o}$C. RT was incubated with DNA in a reaction buffer containing 50 mM Tris-acetate pH 7.5, 100 mM potassium acetate, 0.1 mM EDTA and 0.1 mg/ml BSA. dATP was diluted into the same buffer with 4 mM magnesium acetate. PAGE loading buffer contains 0.5 M EDTA, 0.1% bromophenol blue, 0.5 % xylene cyanol in 100% formamide. The

denaturing PAGE polymerization solution contains 15% polyacrylamide, 0.8% bis-acrylamide, 7M Urea, and 1X TBE.

## 2. METHODS

### 2.1. 5'-$^{32}$P Labeling of DNA Primer

Before annealing, the primer was 5'-radiolabeled with [$\gamma$-$^{32}$P] ATP by T4 polynucleotide kinase for 1 hour at 37$^{o}$C. The kinase was denatured by placing the reaction at 95$^{o}$C for 5 min. Un-reacted and contaminating nucleotides were removed from the labeled primer using a Micro Bio-Spin-6 column. The final concentration of labeled 25-mer after column separation was determined by thin layer chromatography. 1 μl samples of the labeling solution taken before and after the micro-centrifugation were spotted on a PEI cellulose plate (EM Science, Gibbstown, NJ). The mobile phase was 0.3 M $KH_2PO_4$, pH 3.4. The free nucleotide migrated to the top of the plate while the DNA remained at the starting point. The PEI cellulose plate was exposed to a phosphor screen, which was in turn scanned in a phosphorimager. The intensity signals were analyzed with the software ImageQuant to determine the ratio of counts of labeled DNA before and after Bio-Spin column purification to estimate the yield. The final concentration was calculated as the initial 25-mer concentration multiplied by the ratio.

## 2.2. Rapid Quench Experiments

Experiments were carried out at 37$^{o}$C in a rapid quench flow system RQF-3 designed by Dr. K.A. Johnson (107) and built by KinTek Corporation (www.kintek-corp.com, Austin, TX). The experiments were initiated by mixing a pre-equilibrated complex of enzyme with primer/template, in the absence or presence of inhibitor, with an excess of dATP in 2 mM $MgCl_2$ (15 μl each), for time periods ranging from 0.01 to 20 seconds, and quenched with 80 μl of 0.5 M EDTA, pH 8.0. The reaction sample was then expelled into a microcentrifuge tube containing 30 μl of polyacrylamide gel loading buffer (0.05% bromophenol blue, 0.005% xylene, and 20 mM EDTA pH 8.0 in formamide). The concentrations of all the reagents were the final concentrations after 1 to 1 mixing of the reactants.

## 2.3. Product Analysis

During each time course, the formation of 26-bp product was quantitated by monitoring the extension of 5'-labeled 25-mer to 26-mer. The products were resolved on a denaturing gel and the dried gel was exposed to a phosphor-screen, which was scanned with a PhosphorImager Storm 860 (Amersham Biosciences, Piscataway, NJ). Intensity of the DNA bands was calculated with the ImageQuant 5.0 software (Amersham Biosciences, Piscataway, NJ). The final

product concentration was determined by multiplying the final reaction concentration of 25-mer primer by the ratio of the signal intensity (I), $\frac{I_{26mer}}{I_{25mer} + I_{26mer}}$.

## 2.4. Data Analysis

The concentration of the 26-mer product was plotted again time for each burst experiment as shown in Figure 14. Data were fit by nonlinear regression using the program GraFit 5.0.1 (Erithacus Software). Data points from a pre-steady-state burst experiment were fit to the burst equation, $y = A \cdot (1 - e^{-kt}) + m \cdot t$, where $y$ represents the concentration of the 26-mer product, $A$ the burst amplitude, $k$ the observed burst rate, $m$ the slope of the linear steady state phase, and $t$ the reaction time. The steady state rate was calculated by dividing the slope by the concentration of active enzyme. The observed burst rates were plotted against nucleotide (dATP) concentration and fit with a hyperbolic equation, $y = \frac{k_{\max} \cdot S}{K_d + S}$, where $k_{max}$ represents the maximum incorporation rate, $K_d$ the apparent equilibrium dissociation constant for the nucleotide, and $S$ the concentration of nucleotide. For single nucleotide incorporation experiments done in the presence of increasing concentrations of the inhibitor, the plot of the amplitude of each time course as a function of inhibitor concentration was fit with a hyperbolic

equation, $y = E - \frac{E \cdot I}{K_d + I} + B$, where $y$ represents the amplitude of the enzyme-DNA (E•D) complex, $E$ the total enzyme concentration, $I$ the total inhibitor concentration, $B$ the background signal, and $K_d$ the apparent equilibrium dissociation constant for the non-nucleoside inhibitor.

The standard deviation listed for each rate, rate constant, and equilibrium constant value was obtained from the fit of the data by nonlinear regression.

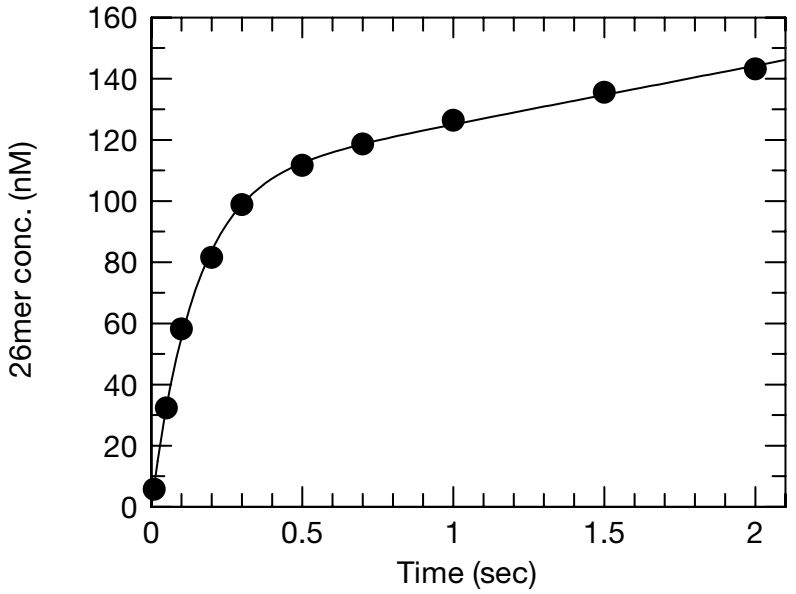


Figure 14. Time dependence of primer elongation. The time course of 26-mer formation typically shows two phases. The first exponential phase corresponds to the nucleotide incorporation. The second linear phase corresponds to the slower steady-state release of the 26-mer product from the enzyme.

Repetitive and duplicative experiments with sufficient number of data points ensured the accuracy of the error estimates and the reproducibility of our conclusions.

## 2.5. Titration of active enzyme with DNA

The concentration of active enzyme, as well as the $K_d$ for DNA in the presence of different concentrations of the inhibitor, were determined by an active site titration experiment as previously described (62). Freshly thawed RT was added to increasing concentrations of 5'-$^{32}$P-labeled 25/45-mer DNA, in the presence or absence of inhibitor and incubated for 5 min. Each sample of E•D or E•D•I complex was mixed with equal volume of dATP for 0.5 sec. and quenched with 0.5 M EDTA, pH 8. The amplitudes were obtained by fitting each time course to the burst equation. The amplitudes were then plotted as a function of DNA concentration. The results from experiments done in absence of the inhibitor were fit with a quadratic equation, $A = \frac{(K_d + E + D*F) - \sqrt{(K_d + E + D*F)^2 - 4*E*D*F}}{2}$, where $A$ is the amplitude, $E$ is the total enzyme concentration, $D$ the total DNA concentration, $K_d$ the equilibrium dissociation constant for DNA, and $F$ the binding factor. The binding factor is the fraction of E•D complexes in which the DNA is productively bound. It corrects for the actual concentration of DNA in productive E•D

complexes because the data from DNA titration experiments showed that both inactive and active enzymes were bound to DNA. The nonproductive E•D complexes tie up a percentage of DNA molecules, resulting in a lower apparent concentration of DNA for reaction. The maximum amplitude obtained was 49% (for WT RT) or 69% (for K103N RT) of the protein concentration determined by the $UV_{280}$ absorbance measurements. All enzyme concentrations reported here are calibrated via active site titration.

## 2.6. Determination of the inhibitor equilibrium dissociation constant

Wild type RT (100 nM) was preincubated with saturating concentration (200 nM) of 5'-$^{32}$P-labeled 25/45-mer DNA and a range of concentrations of inhibitor for 15-20 minutes at 37$^{o}$C in reaction buffer. Concentrations of inhibitor were included in the initial solution where the equilibrium between E•D and E•D•I complexes was established. The partially saturated E•D complex was diluted by half when mixed rapidly with an equal volume of 150 μM dATP (in 10 mM $MgCl_2$) and allowed to react for 0.01 to 3 seconds. The reactions were quenched with 0.5 M EDTA at the indicated time points. The individual time course of primer extension at each inhibitor concentration was fit to the burst equation, $y = A \cdot (1 - e^{-k \cdot t}) + m \cdot t$, to yield the amplitude for each burst curve. The amplitudes of the burst phases were plotted against the inhibitor concentrations.

The data were fit to either a quadratic equation, $y = E - \frac{(K_d + E + I) - \sqrt{(K_d + E + I)^2 - 4 * E * I}}{2} + B$, or a hyperbolic equation, $y = E - \frac{E * I}{K_d + I} + B$, where $y$ represents the amplitude, $E$ the total active enzyme concentration, $I$ the total inhibitor concentration, $B$ the baseline, and $K_d$ the equilibrium dissociation constant for the inhibitor from E•D•I complex.

## 2.7. Determination of Other Equilibrium Dissociation Constants in the Reaction Pathway

Data were simulated using the software TK Solver 4.0 (Universal Technical Systems, Inc.) in order to estimate the equilibrium dissociation constant for CZ-1 binding to E•D complex and free enzyme, respectively. Estimated numerical values were entered into the program to solve for seven equations simultaneously. The $K_d$'s calculated by TK Solver were used to simulate data, which were compared by overlaying the simulated data with the experimental data. When the simulated data can be superimposed perfectly with experimental data, the $K_d$ values were finalized.

## 2.8. Determination of the DNA Equilibrium Dissociation Constant

The conditions and method are the same as active site titration experiments except that the enzyme concentration, as corrected by active site titration, is a constant value. The results from DNA titration experiments done in the presence of the inhibitor were fit with a hyperbolic equation, $y = E - \frac{E * D}{K_d + D} + B$, where $y$ represents the amplitude, $E$ the total active enzyme concentration, $D$ the total DNA concentration, $B$ the baseline, and $K_d$ the equilibrium dissociation constant for DNA from the enzyme.

## 2.9. Determination of the Inhibitor Binding Rate Constant

The apparent binding rates of the non-nucleoside inhibitors to the E•D complex were determined by a rapid quench-glow method consisting of two sequential mixing steps. First, CZ-1 was mixed with a solution of E•D complex and allowed to react from 0.1 to 30 seconds. Then dATPMg$^{2+}$ was added to initiate the reaction. Polymerization was allowed to take place for 0.2 seconds, which is approximately one single turnover as determined by the burst curves from the first experiment. The reactions were terminated by mixing with 0.5 M EDTA, pH 8.0. The product concentration was normalized by dividing by the maximum amount of turnover detected in 0.2 seconds in the absence of the inhibitor. When calculating the apparent binding rate of CZ-1, each data set of

normalized product formation as a function of time was fit to an exponential decay equation, where $[P]_{normalized} = A * e^{-k_{obs} * t} + C$. $A$ represents the amplitude, $k_{obs}$ the apparent binding rate constant, $t$ the time, and $C$ the background signal. Association and dissociation rates for formation of the E•D•I complex were obtained by analysis of the CZ-1 concentration dependence of the observed rate of binding as in the function, $k_{obs} = k_{on} * [I] + k_{off}$. Direct estimate of $k_{off}$ was not possible due to the large errors in the extrapolated intercept, therefore the binding rate was calculated by fitting the data to the equation, $K_d = \frac{k_{off}}{k_{on}}$ and $k_{obs} = k_{on} * ([I] + K_d)$, such that $k_{off}$ was constrained to agree with both the $K_d$ value and the observed binding rate.

## 2.10. Measurement of Nucleotide Equilibrium Dissociation Constant and Maximum Catalytic Rate of dATP incorporation

RT and primer/template were mixed, followed by addition of increasing concentrations of inhibitor. The mixture was preincubated for 10 minutes. Each reaction was initiated by mixing equal volumes of dATP over a range of concentrations in $Mg^{2+}$ containing reaction buffer with the E•D•I complex solutions, and was quenched with 0.5 M EDTA, pH 8.0. Each time course was fit to a burst equation to yield the burst amplitude and rate. The plot of the single

turnover rates against increasing concentrations of dATP at each concentration of inhibitor was fit to a hyperbolic equation, $y = \frac{k_{\max} \times S}{K_d + S}$, where $y$ represents the single turnover rate from each burst curve, $k_{max}$ represents the maximum catalytic rate of polymerization, $K_d$ represents the equilibrium dissociation constant, and $S$ represents the concentration of the substrate, which is dATP in this case.

## 2.11. Static Light Scattering

Inhibitor stocks at 14mM in DMSO were diluted with 50 mM potassium phosphate buffer. The buffer was pre-filtered with 0.02 μm Anodisc 47. Samples were analyzed with the miniDAWN® triple-angle light scattering detector for ambient HPLC from Wyatt Technology Corporation (Santa Barbara, CA) using a neon helium ion laser at 632 nm. The laser power and integration times were comparable for all experiments. The detector angle was 90°. Each sample was measured three or more times at room temperature.

## 2.12. Fluorescence Spectroscopy and Fluorescence Polarization Anisotropy

Stock solutions of DNA and CZ-1 were diluted in the reaction buffer: 50 mM Tris-acetate pH 7.5, 100 mM potassium acetate, 0.1 mM EDTA. CZ-1 is naturally fluorescent. The fluorescence intensities were measured with a

QuantaMaster (QM-1) basic pulsed spectrofluorometer from Photon Technology International (Lawrenceville, NJ). Each sample volume was 100 μl. Emission wavelength scan was obtained by examining excitation at 352 nm and scanning emission from 365 to 650 nm. Excitation wavelength scan was obtained by examining emission at 440 nm, scanning excitation from 250 to 425 nm. The polarization angles for both the excitation and emission filters were set at 0 and 90 degree to obtain four sets of fluorescence intensity data. The signals from horizontal and vertical polarization were respectively denoted as $I_{vv}$ ($0^o$ exicitation; $0^o$ emission), $I_{vh}$ ($0^o$ exicitation; $90^o$ emission), $I_{hh}$ ($90^o$ exicitation; $90^o$ emission), $I_{hv}$ ($90^o$ exicitation; $0^o$ emission). The anisotropy (r) value was calculated as $r = \frac{I_{vv} * I_{hh} - I_{hv} * I_{vh}}{I_{vv} * I_{hh} + 2 * I_{hv} * I_{vh}}$ (108). The anisotropy value was plotted against DNA concentration to check for signs of interaction.

## 2.13. Transmission Electron Microscopy

Solutions were prepared to final concentrations of 20, 50, 250, and 500 μM CZ-1 in double-distilled water. At room temperature, 5 μl of each solution was dropped onto a carbon-coated grid from Electron Microscopy Sciences (Fort Washington, PA) for 30 seconds. The grid was then blotted on filter paper to remove excess solution, washed three times with water, and negatively stained with 2% aqueous uranyl acetate for 10 seconds. Images were obtained with a

transmission electron microscope, Philips TEM 208, at 80 kV. Micrographs were recorded at 44000x magnification.

# CHAPTER 3: Mechanism of Inhibition of HIV-1 Reverse Transcriptase by Naphthyl Urea Compounds

## 1. INTRODUCTION

Since the introduction of antiretroviral therapy, the life span of HIV-infected or acquired immunodeficiency syndrome (AIDS) patients has been extended (109). However, the rate of infection is still on the rise (110) and current antiviral drugs cannot eradicate HIV. Rapid evolution of RT introduces new strains of HIV that can evade the effects of the drugs (111). Current treatments call for frequent screening to look for increases in viral load, indicating new drug-resistant forms of the virus, which must be countered by a new combination of drugs. The current strategy for drug design is to address the changes in HIV by new drugs with a different resistance pattern. The purpose of this study is to investigate the properties of a new series of compounds. I evaluated the drug potency quantitatively and examined the mechanism of inhibition of HIV-1 RT.

Current AIDS therapeutics approved by the Food and Drug Administration include seven nucleoside analogs, one nucleotide analog, eight protease inhibitors, one entry/fusion inhibitor, and three non-nucleoside analogs. RT is responsible for replication of single-stranded viral RNA into double-stranded DNA. The proviral DNA is later integrated into the host cellular DNA

during the course of viral infection (41). Two types of anti-AIDS or anti-HIV drugs target RT: the nucleoside analog reverse transcriptase inhibitors (NRTIs) and non-nucleoside analog reverse transcriptase inhibitors (NNRTIs). NRTIs, such as 3'-azido-3'-deoxythymidine (AZT) (112) and 2',3'-dideoxycytidine (ddC) (113), become phosphorylated by cellular enzymes to their triphosphate form and subsequently are incorporated by HIV RT. NRTIs prevent the last nucleotide on the primer from forming a 3'-phosphodiester bond with the next nucleotide and thereby terminate elongation. To varying degrees they also block cellular DNA polymerases, in particular the mitochondrial DNA polymerase (Pol γ) (114), which has been shown to lead to severe toxic side effects (115,116).

NNRTIs are structurally diverse hydrophobic compounds that show little toxic side effects, but they are predominantly effective toward HIV-1 RT and not HIV-2 RT (117). NNRTIs bind in hydrophobic pocket approximately 10 angstroms away from the RT polymerase active site (118) in the palm domain of the p66 subunit (17), distorting the positions of key residues that comprise the aspartic triad (D110, D185, and D186) (21,119). It has been shown by Spence *et al.* (21) that the first generation NNRTIs, Nevirapine and TIBO, are slow-tight binding inhibitors that reduce the rate of the chemical reaction and increase the affinity of nucleotide binding to RT in complex with the inhibitor and DNA (E•D•I complex). As a result of slower chemical reaction, the two steps of nucleotide binding, entailing the initial ground-state binding and the subsequent

conformational change, reach equilibrium leading to tighter, albeit non-productive nucleotide binding. However, current NNRTIs are not effective towards all mutant forms of HIV RT (120).

The biggest barrier in the battle against AIDS is mutation, which confers resistance to RT inhibitors. RT can go through genetic mutation during replication to evolve a form of RT that obstructs the binding of the drug (121,122), disarranges the template/primer (59,123,124), or facilitates the removal of chain terminators (125). Due to the lack of exonuclease proofreading activity and a high frequency of mutation, RT is continuously generating new drug-resistant HIV strains (15,126). In patient plasma, drug-resistant mutations of HIV-1 RT have been detected in the presence of all RT inhibitors (127), including the most recent NNRTI, Efavirenz (128). As a result of cross-resistance, the combination drug regimen exacerbated the problematic mutations in HIV RT (129,130). Therefore, new distinct drugs are required to counter the rapid RT evolution.

In this chapter, I report the kinetic analysis of a new class of NNRTIs identified by computational structure-based design (Fig. 15) (1). These compounds are naphthalene sulfonic acids. They do not bind to the conventional NRTI or NNRTI binding site. They inhibit not only the wild type enzyme but also NRTI- and NNRTI-resistant HIV-1 RT mutants. They did not appear to inhibit

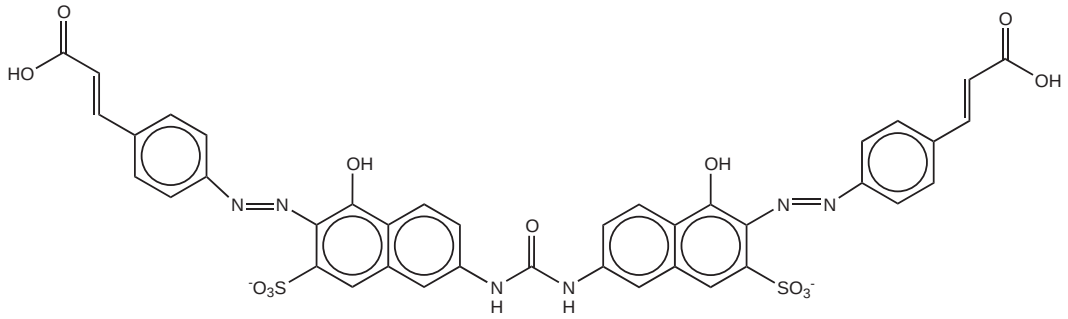


CZ-1

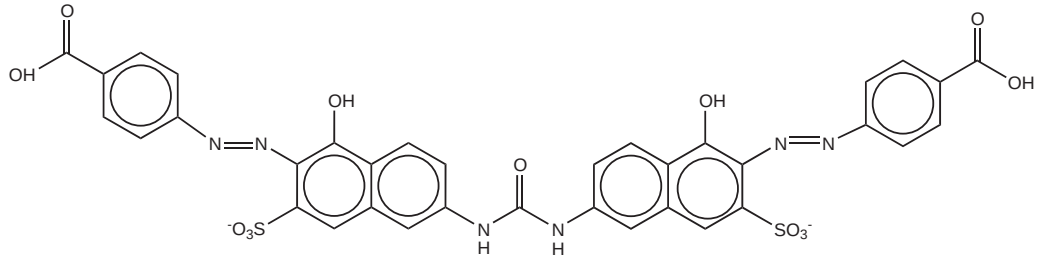


EDC11

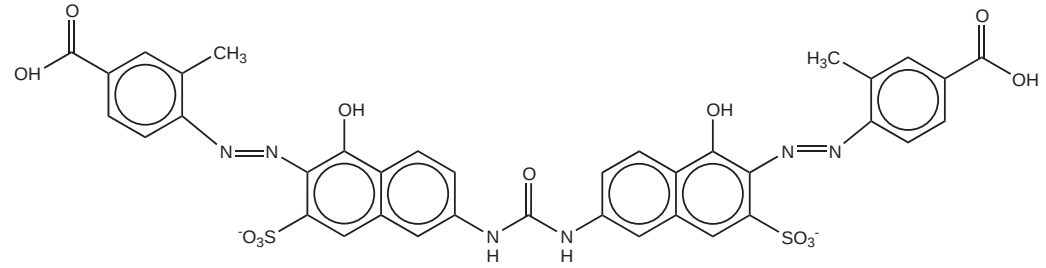


EDC12

Figure 15. Structures of the inhibitor compounds CZ-1, EDC 11, and EDC 12.

T4 DNA polymerase, T7 DNA polymerase, and the Klenow fragment in a previous study (1). In comparison to two other derivatives with modified terminal moieties, CZ-1 was predicted to be the most potent and the least toxic by results from cell culture screening and preliminary activity assays (1). Further investigation into the inhibition mechanism by CZ-1 is essential for the assessment potential as a new class of inhibitors of HIV RT.

Our data revealed that CZ-1, unlike other NNRTIs, interfered with template-primer binding. We propose that CZ-1 binds to RT with or without DNA and induces conformational changes at the polymerase active site, which consequently slow or prevent nucleotide incorporation. CZ-1 is similar to other NNRITs in that each appears to slow the rate of catalysis in the EDI complex by binding to a site adjacent to the catalytic site. However, it also weakens the binding of DNA, while conventional NNRITs strengthen DNA binding by slowing the dissociation rate (21) in the presence of the correct nucleotide.

## 2. RESULTS

### 2.1. Inhibition of Single Nucleotide Incorporation by CZ-1

We first examined the effect of CZ-1 on the pre-steady state burst of single nucleotide incorporation catalyzed by HIV RT with a defined primer/template. In this experiment, the rate of the burst provides a direct

measurement of the rate of polymerization at the active site and the amplitude defines the concentration of reactive enzyme-DNA (E•D) complexes and steady state turnover is limited by the release of product from enzyme (62,74,131). We incubated the E•D complex with 0 to 20 μM of inhibitor before mixing with dATP·$Mg^{2+}$ to start the reaction and obtained results shown in Figure 16A, in which an initial burst of polymerization was followed by a slow steady state turnover. In the absence of CZ-1, the burst amplitude for dATP incorporation catalyzed by 50 nM RT was 49 ± 3 nM with 100 nM DNA, the burst rate was 7.3 ± 0.9 $s^{-1}$ and the steady state rate was 0.13 $s^{-1}$. Increasing the inhibitor concentration reduced the amplitude of the burst phase as well as the rate of the linear steady state phase to almost zero (Fig. 16*A* and Fig. 17*A*) but did not affect the burst rates. Reduction in the amplitude is presumably caused by the binding of CZ-1 to E•D. These results infer that both the equilibration of CZ-1 with E•D and the dissociation of primer-template from the enzyme-DNA-inhibitor (E•D•I) complex are slow relative to the rate of nucleotide incorporation (21). The reduction in the burst amplitude but not rate is consistent with the slow equilibration of the inhibitor so that the observed amplitude reflects reaction by uninhibited enzyme (21). Accordingly, plotting the amplitude of the burst as a function of inhibitor concentration provides a direct titration to quantitate inhibitor binding as shown in Figure 16B. Fitting the curve to a hyperbolic

function defines an apparent $K_d$ of 1.3 ± 0.2 μM for the binding of inhibitor to E•D.

Similar effects on the burst amplitude and steady state rates observed with EDC 11 and EDC 12 suggest identical inhibition mechanisms as CZ-1. The modified moieties in EDC 11 and 12 (Fig. 15) only slightly affected the binding affinities to HIV-1 RT slightly. The hyperbolic function of amplitude versus inhibitor concentration defined the equilibrium dissociation constants for EDC11 and EDC12 to be 1.9 ± 0.4, and 1.5 ± 0.6 μM, respectively (data not shown).

After obtaining the equilibrium dissociation constant for CZ-1 at 100 nM (50 nM excess) DNA concentration, we repeated the experiment with 150 nM (100 nM excess) DNA to observe the effect of DNA on CZ-1 binding. Increasing the total DNA concentration from 100 nM to 150 nM effectively doubles the concentration of free DNA in the presence of 50 nM enzyme. The results showing the dependence of the burst kinetics on CZ-1 concentration at 150 nM DNA concentration are shown in Figure 16. Doubling the concentration of free DNA twofold leads to a corresponding increase in the apparent $K_{d,CZ\text{-}1}$ from 1.3 ± 0.2 μM (Fig. 16*B*) to 3.4 ± 1.0 μM (Fig. 17*B*). The correlation between the increase in DNA concentration and the increase in the apparent $K_{d,CZ\text{-}1}$ implies competition between the inhibitor and DNA, which can be related mathematically

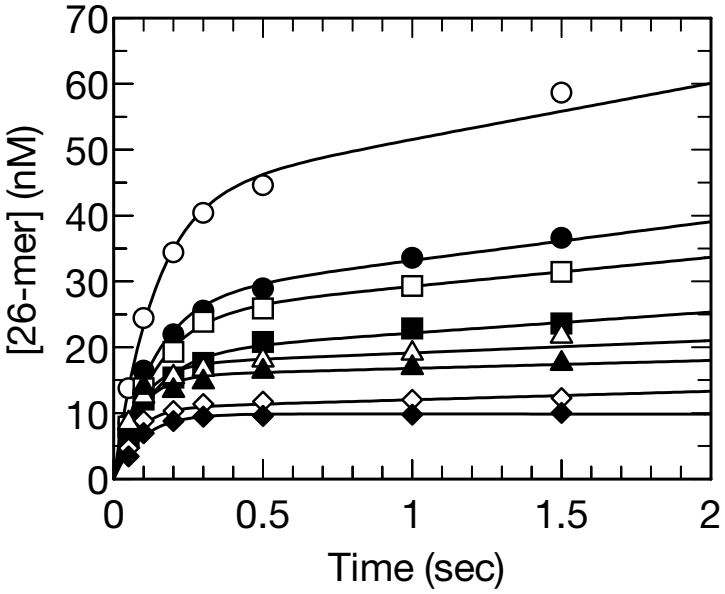
70
60
50
40
30
20
10
0
[26-mer] (nM)
0
0.5
1
1.5
2
Time (sec)

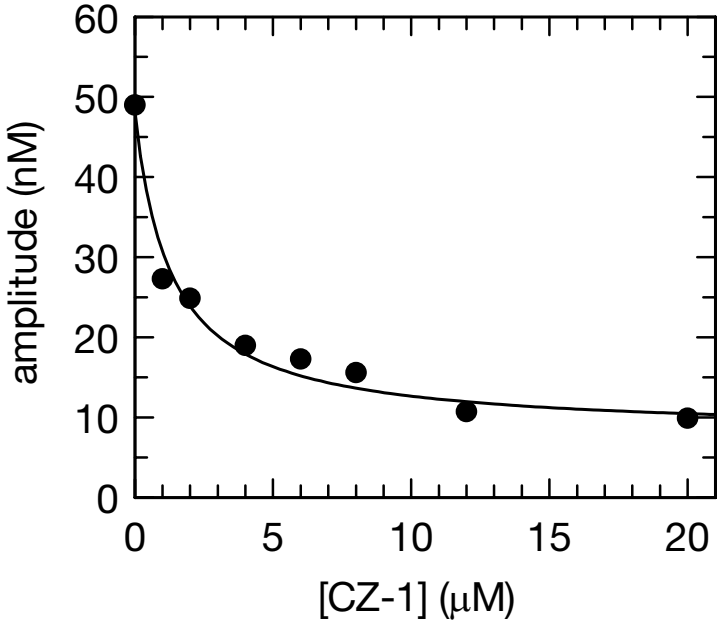
60
50
40
30
20
10
0
amplitude (nM)
0
5
10
15
20
[CZ-1] (μM)

Figure 16. DNA-directed single nucleotide incorporation in the presence of CZ-1 with a ratio of RT to DNA concentration at 1:2. (Upper panel) Wild type RT (100 nM), 5'-$^{32}$P-25/45-mer DNA (200nM), and various concentrations of CZ-1 were pre-incubated for 15-20 min at 37$^{o}$C in reaction buffer (see materials and methods). Concentrations of 0 (○), 1(●), 2(□), 4(■), 6(△), 8(▲), 12(◇), and 20 (◆) μM of CZ-1 were included in the initial solution where the equilibrium between E•D and E•D•I complexes was established. The E•D complex was diluted by ½ when mixed rapidly with an equal volume of 150 μM dATP (in 10 mM $MgCl_2$) and allowed to react for 0.01 to 5 sec. The reactions were quenched with EDTA at the indicated time points. The individual time course of primer extension at each CZ-1 concentration was fit to the burst equation, $y = A \cdot (1 - e^{-k \cdot t}) + m \cdot t$, to yield the maximum amplitude for each burst curve. (Lower panel) The amplitudes of the burst phases were plotted against the CZ-1 concentrations. The data were fit to a hyperbolic equation, $y = E - \frac{E \cdot I}{K_d + I} + B$, that defined an apparent $K_d$ value of 1.3 ± 0.2 μM.

**A.**

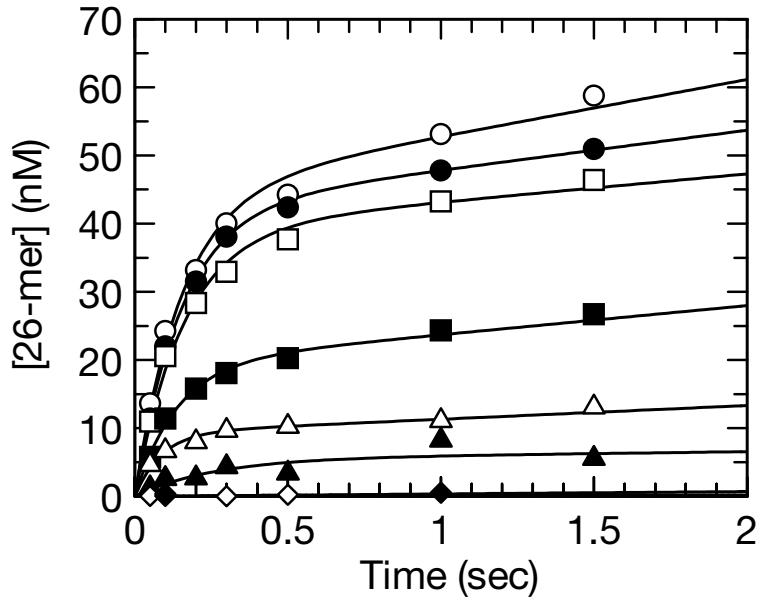
70
60
50
40
30
20
10
0
[26-mer] (nM)
0
0.5
1
1.5
2
Time (sec)

**B.**

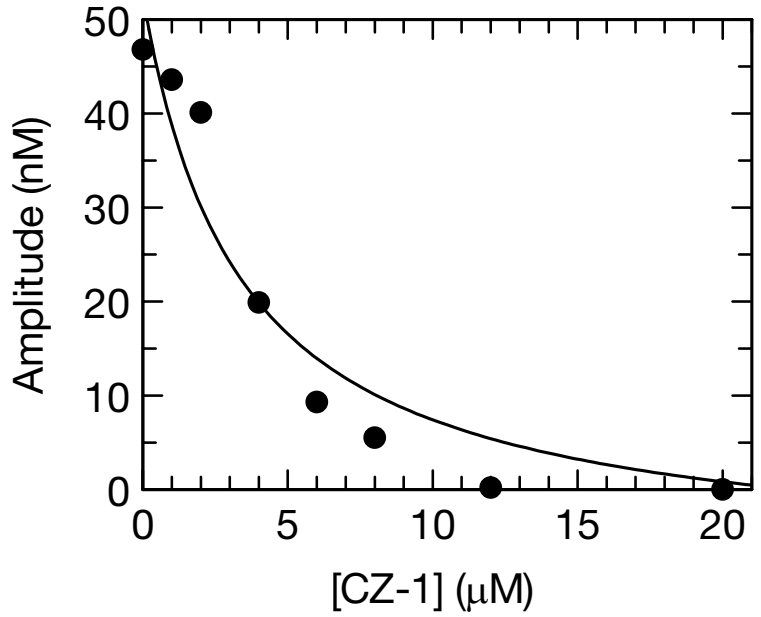
50
40
30
20
10
0
Amplitude (nM)
0
5
10
15
20
[CZ-1] (μM)

Figure 17. DNA-directed single nucleotide incorporation in the presence of CZ-1 with a ratio of RT to DNA concentration at 1:3. (A) Wild type RT (100 nM), 5'-$^{32}$P-25/45-mer DNA (300nM), and various concentrations of CZ-1 were pre-incubated for 15-20 min at 37$^{o}$C in reaction buffer (see materials and methods). Concentrations of 0 (○), 1(●), 2(□), 4(■), 6(△), 8(▲), 12(◇), and 20 (◆) μM of CZ-1 were included in the initial solution where the equilibrium between E•D and E•D•I complexes was established. The E•D complex was diluted by ½ when mixed rapidly with an equal volume of 150 μM dATP (in 10 mM $MgCl_2$) and allowed to react for 0.01 to 5 sec. The reactions were quenched with EDTA at the indicated time points. The individual time course of primer extension at each CZ-1 concentration was fit to the burst equation, $y = A \cdot (1 - e^{-k \cdot t}) + m \cdot t$, to yield the maximum amplitude for each burst curve. (b) The amplitudes of the burst phases were plotted against the CZ-1 concentrations. The data were fit to a hyperbolic equation, $y = E - \frac{E \cdot I}{K_d + I} + B$, that defined an apparent $K_d$ value of 3.4 ± 1.0 μM.

by the equation, $K_{d,CZ-1}^{app} = K_{d,CZ-1}(1 + \frac{[I]}{K_{d,DNA}})$. The slope of the DNA concentration dependence suggests that the ratio of $K_{d,CZ-1}/K_{d,DNA}$ is approximately 42. We further explored this competition by examining the effect of CZ-1 on the apparent $K_d$ for DNA binding.

## 2.2. DNA Dissociation Constant Dependence on CZ-1 Concentration

The possible competition between CZ-1 and DNA was checked by measuring the apparent $K_{d,DNA}$ for DNA binding in the presence of various concentrations of CZ-1. The apparent $K_{d,DNA}$ was obtained by measuring the DNA concentration dependence of the burst amplitude as described previously (62) at various concentrations of CZ-1 (0, 2, 5, or 10 μM) (Fig. 18). In each sample, DNA and CZ-1 were combined immediately before adding 200 nM RT and allowed to equilibrate for 15 to 30 minutes at 37°C before initiating the polymerization reaction. The reactions were initiated by adding dATP•$Mg^{2+}$ to pre-incubated mixtures of RT and DNA with or without CZ-1. The burst amplitude was plotted as a function of DNA concentration at each CZ-1 concentration. In the absence of CZ-1, DNA binds HIV-1 RT tightly and the titration curve was fit to a quadratic equation. As the concentration of CZ-1 was increased, the titration curves deviated away from the infinitely tight binding

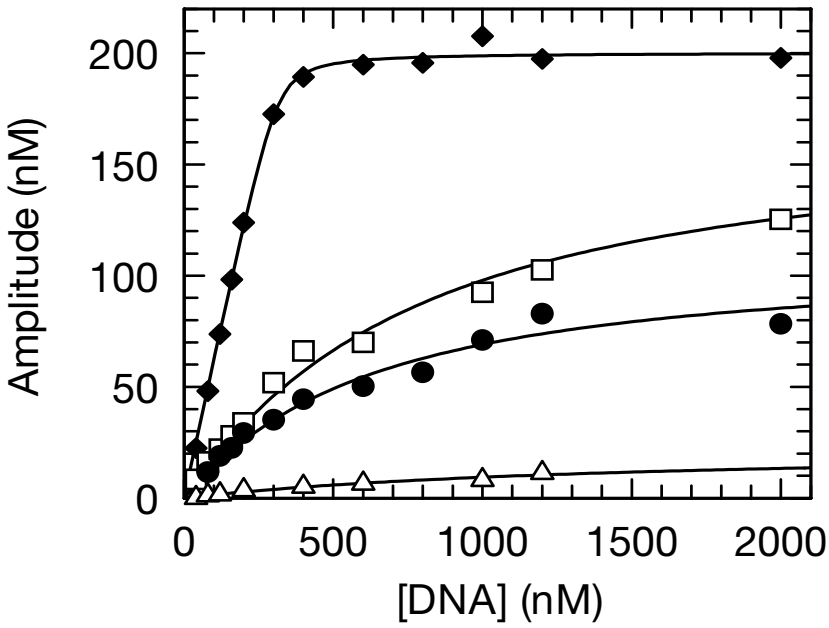
Amplitude (nM)
200
150
100
50
0
0
500
1000
1500
2000
[DNA] (nM)

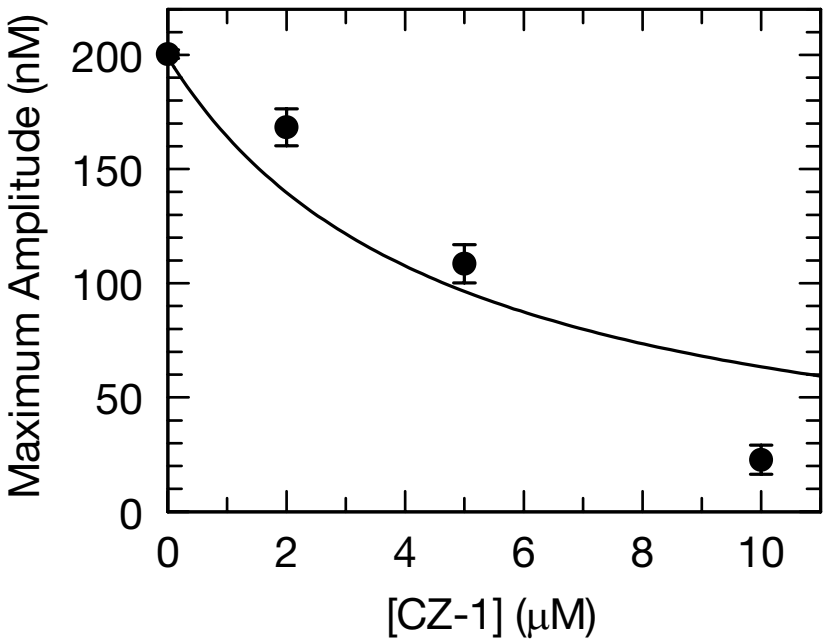
Maximum Amplitude (nM)
200
150
100
50
0
0
2
4
6
8
10
[CZ-1] (μM)

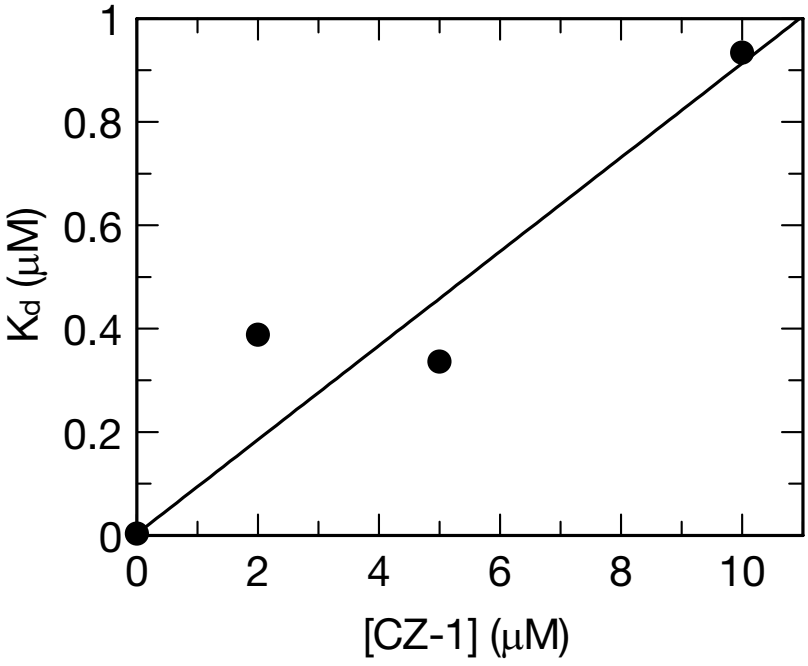


Figure 18. Dependence of CZ-1 concentration on the DNA dissociation constant. (Upper panel) Active site titration of wild type RT with 25/45-mer duplex DNA was done in the presence of different concentrations of CZ-1. For the initial experiment without CZ-1 (◆), RT (200 nM active concentration determined by the amplitude from the titration) and increasing concentrations of 5'-$^{32}$P-25/45-mer DNA were incubated on ice for less than 5 min in reaction buffer. The titration curve was fit to a quadratic equation. For each titration experiment with 2 (□), 5(●), or 10 (△) μM of CZ-1, the inhibitor was combined with increasing concentrations of DNA at 37$^{o}$C before RT was added. The E•D or E•D•I complex was rapidly mixed for 0.5 sec with an equal volume of 100 μM dATP in the reaction buffer containing 2 mM $MgCl_2$. For each CZ-1 concentration, the

amplitudes were plotted as a function of the DNA concentrations. Each titration curve was fit to a hyperbolic equation (Chapter 2) to obtain the amplitudes and apparent $K_{d,DNA}$. (Middle Panel) The amplitude was plotted against the concentration of CZ-1. The curve was fit to the hyperbolic equation to obtain the apparent $K_d$ of CZ-1 binding to E•D complex, 4.7 ± 1.8 μM. (Lower Panel) The values of apparent $K_{d,\,DNA}$ were plotted against the CZ-1 concentrations. The plot was fit to the equation, $_{app}K_{d,DNA} = K_{d,DNA} \cdot (1 + \frac{I}{K_i})$, to yield a true $K_{d,DNA}$ value of 0.003 ± 0.001 μM and a $K_i$ value of 0.035 ± 0.016 μM, which is equivalent to the $K_{d,CZ\text{-}1}$ for binding to the free enzyme .

asymptotes and hence the curve was fit to a hyperbolic equation to obtain the apparent $K_d$ for DNA binding (Fig. 18*A*). The apparent $K_d$ for DNA binding was reduced at increasing concentrations of CZ-1 (Fig. 18*B*), indicating that CZ-1 interfered with E•D complex formation. If CZ-1 was directly competitive with DNA such that CZ-1 could not bind in the presence of DNA then high concentrations of DNA should overcome the inhibition. However, the maximum amplitudes of the burst reaction were reduced at 0, 2, 5, and 10 μM of CZ-1 (200, 168, 108, and 23 nM, respectively) indicating that CZ-1 is still capable of binding to the enzyme as the DNA concentration is extrapolated towards infinity.

The amplitude in presence of CZ-1 was never restored to the uninhibited level, even when the DNA concentration was raised to ten-times in excess of enzyme concentration. These results suggest that there is no absolute competition between DNA and CZ-1 binding to RT and hence additional DNA cannot reverse inhibition by CZ-1, i.e. additional DNA cannot cause CZ-1 to dissociate from E•D•I complexes and restore active E•D complexes. Accordingly, we propose that CZ-1 and DNA do not share the same binding site in its entirety, although CZ-1 and DNA interfere with each other to bind to HIV-1 RT and the sites may overlap. This model was illustrated in Scheme 1.

According to Scheme 1, we can interpret the results as that the binding of CZ-1 weakens the binding of DNA and vice versa, meanwhile when CZ-1 is bound to the E•D complex, it inhibits the rate of nucleotide incorporation. Direct

competition between CZ-1 and DNA would represent one extreme of the model shown in Scheme 1 where the ternary E•D•I complex was extremely weak or could not form at all. In the present case, all four species in the thermodynamic box contribute to the observed inhibition and the only equilibrium constant that can be measured directly is that for forming the E•D complex in the absence of inhibitor. All other measurements in the presence of both DNA and inhibitor are complicated by the presence of an equilibrium mixture of E•D, E•I and E•D•I leading to the observed apparent $K_d$ for either CZ-1 or DNA.

Details of CZ-1 interference with DNA-RT binding were learned by observing the effect of CZ-1 on the *apparent* $K_{d,DNA}$. Uninhibited wild type RT binds a 25/45-mer DNA duplex tightly with an apparent $K_d$ of 3 ± 1 nM while the *apparent* $K_{d,DNA}$ was increased to 388 ± 18 nM, 336 ± 23 nM, and 934 ± 63 nM at 2 μM, 5 μM, and 10 μM of CZ-1, respectively (Fig. 18*C*). If one assumes

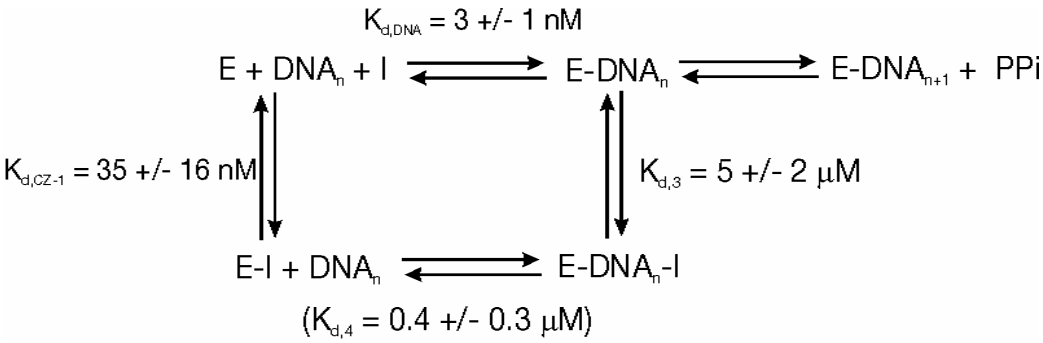


Scheme 1: Inhibition mechanism of CZ-1. Only $K_{d,DNA}$ was directly measured in the experiment. The other three $K_d$ values were approximations.

that a model for simple competition applies, then the apparent $K_{d,DNA}$ should follow a function of $K_{d,DNA}^{app} = K_{d,DNA}(1+[I]/K_I)$, where $K_I$ represents the $K_d$ for CZ-1 binding to free enzyme. The function of the apparent $K_{d,DNA}$ to inhibitor concentration was fit by this linear regression to yield a true $K_{d,DNA}$ value of 3.2 ± 1.4 nM for the dissociation of DNA from E•D complex, and the $K_{d,CZ\text{-}1}$ of 35 ± 16 nM (Fig. 18C) for binding to free enzyme.

If the $K_{d,CZ\text{-}1}$ for binding to free enzyme is 33 nM, then can we account for the *apparent* $K_d$ of 1.3 μM for the CZ-1 concentration dependence of inhibition of the burst amplitude? The results suggest that both DNA and CZ-1 bind tightly to free enzyme and each greatly weakens the binding for the other. However, as described above, the competition is not absolute. As shown in Figure 18B, extrapolation to infinite DNA concentration yields a fractional burst amplitude dependent upon CZ-1 concentration. If we assume that this data represents the condition where DNA saturates enzyme in both CZ-1-bound and free states, then this curve represents the binding constant for CZ-1 binding to E•D complex ($E \bullet D + I \Leftrightarrow E \bullet D \bullet I$), such that the fractional amplitude for uninhibited enzyme follows the equation, $y = E - \frac{K_d}{K_d + [I]} + B$. The fitted line shown in Figure 18B defines a $K_d$ = 4.7 ± 1.8 μM for the binding of inhibitor to the E•D complex.

The CZ-1 inhibition pathway with kinetic parameters is summarized in Scheme 1. The $K_d$ for DNA binding to E•I complex could be calculated since the $K_d$ for the three other steps in the thermodynamic box were determined. Using the relationship, $\frac{K_{d,DNA} \times K_{d,3}}{K_{d,CZ-1} \times K_{d,4}}$, the equilibrium dissociation constant of DNA with E•I complex, $K_{d,4}$, was estimated to be 0.43 ± 0.32 μM. The hundred fold difference between $K_{d,DNA}$ (3 ± 1 nM) and $K_{d,4}$ (0.4 ± 0.3 μM) suggests that CZ-1 binding to HIV-1 RT before DNA decreases the DNA binding affinity by approximately hundreds of times, conforming to our theory of DNA displacement by CZ-1. Because $K_{d,CZ-1}$ for CZ-1 binding to the free enzyme (35 ± 16 nM) is about 1000x fold greater than $K_{d,4}$ for CZ-1 binding to E•D complex (4.7 ± 1.8 μM), we conclude that the primary mode of action for CZ-1 is to bind the ligand-free HIV-1 RT and displaces DNA from the active site, rather than the conventional action of inhibition of binding to and interfering with the chemical reaction inside the E•D complex, as nevirapine does.

The software TK solver was also used to simultaneously solve the $K_d$ of CZ-1 dissociation from E•D•I complex, the $K_d$ of CZ-1 dissociation from E•I complex, and the $K_d$ of DNA dissociation from E•D•I complex. Refering to Scheme 1, steps 1 to 4 in the inhibited reaction pathway were dissected into seven equations:

$K_{d,1} = E * I / EI$

$K_{d,2} = E * D / ED$

$K_{d,3} = ED * I / EDI$

$K_{d,4} = EI * D / EDI$

$D = D_o - ED - EDI$

$E = E_o - ED - EDI - EI$

$I = I_o - EI - EDI$

*E* represents the equilibrium enzyme concentration, $E_o$ the initial enzyme concentration, *D* the equilibrium DNA concentration, $D_o$ the initial DNA concentration, *ED* the concentration of E•D complexes, *EDI* the concentration of E•D•I complexes, and *EI* the concentration of E•I complexes. $K_{d,1}$ was determined in this experiment (see above and Fig. 18). $E_o$, $D_o$, and $I_o$ were known from the reaction conditions. Estimates were inserted into the equations along with the known values. The solved $K_d$ values (shown in Scheme 2) were used to simulate the data for the DNA titration experiments. The simulations were superimposed with real data to check the accuracy of the calculations. $K_{d,CZ-1}$ for the E•D•I complex is 8 μM, $K_{d,CZ-1}$ for the E•I complex is 9.6 nM, and $K_{d,DNA}$ for the E•D•I complex is 2.5 μM. The $K_d$ values calculated by TK Solver agreed with the experimental data. The association between DNA and RT is three fold tighter than the association of CZ-1 with RT, verifying that CZ-1 is not competitively inhibiting DNA binding. Since the dissociation constant for E•I complexes is almost three magnitudes smaller than that for E•D•I complexes, CZ-1 appears to

bind unliganded RT predominantly. CZ-1 can bind E•D complex with a 1000-fold less affinity than with free enzyme. Comparably, DNA can bind E•I complex with a 1000-fold less affinity than with free enzyme.

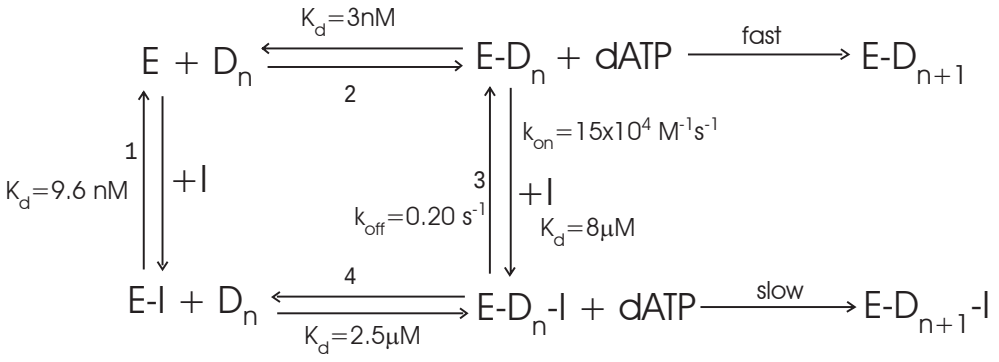


Scheme 2: Inhibition mechanism of CZ-1 to HIV-1 RT with simulated Kd values

### 2.3. dATP concentration dependence of the nucleotide incorporation rate in the presence of different amounts of CZ-1

We proceeded to examine the next steps in the polymerization pathway, the two-step binding of nucleotide (21,72) followed by the chemical step (62,68). We examined the kinetics of dATP binding and incorporation. In this experiment, we measured the maximum incorporation rate ($k_{pol}$) and the dissociation constant of dATP ($K_{d,dATP}$) from the uninhibited fraction of catalytic E•D complexes. 0 to 5 μM of CZ-1 was added to the equilibrated E•D complexes. During the quench

flow operation, equal volumes of the pre-incubated mixture (consisting of RT, DNA, and CZ-1) and dATP•$Mg^{2+}$ were rapidly mixed into the reaction loop and quenched after various times. Product concentration was plotted against time to reveal the burst and steady state phase for each reaction (Fig. 19*A*) and fit to a burst equation to calculate the burst rate. Burst rate was plotted against dATP concentration (Fig. 19*B*) and fit to a hyperbola to obtain $k_{pol}$ (Fig. 19*C*) and $K_{d,dATP}$ (Fig. 19*D*). The $k_{pol}$ was approximately constant with values of 4.3 ± 0.3 $s^{-1}$ (without CZ-1), 4.4 ± 0.3 $s^{-1}$ (1 μM CZ-1), 3.7 ± 0.2 $s^{-1}$ (2 μM CZ-1), and 4.8 ± 0.5 $s^{-1}$ (5 μM CZ-1). Similarly, the $K_{d,dATP}$ remained in the low μM range: 0.5 ± 0.2, 0.5 ± 0.2, 0.2 ± 0.1, and 0.4 ± 0.2 μM at 0, 1, 2, and 5 μM, respectively. The independence of $K_{d,dATP}$ and $k_{pol}$ from CZ-1 concentration indicates that CZ-1 does not affect the nucleotide binding and the chemistry step. These observations were consistent with the conclusion that the observed product formation is catalyzed only by uninhibited E•D complex.

**A.**

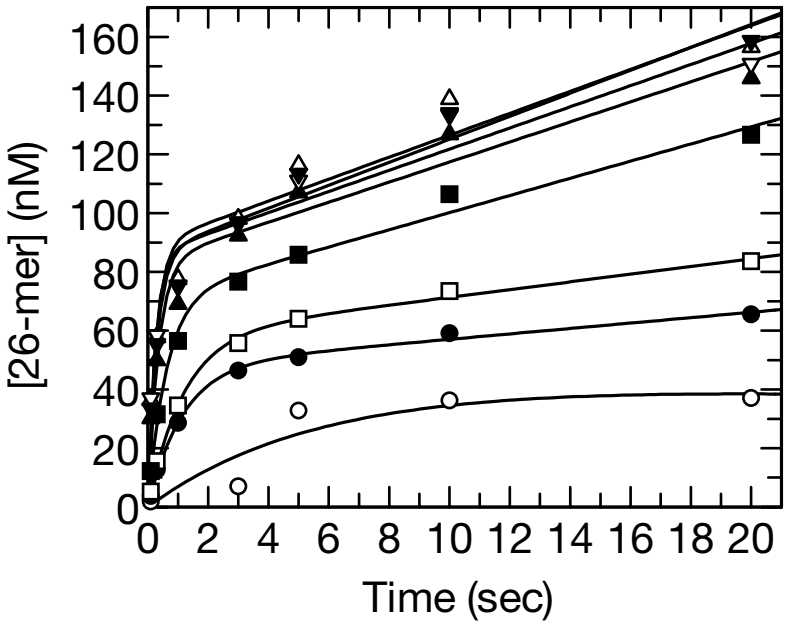
[26-mer] (nM)
Time (sec)
0
20
40
60
80
100
120
140
160
0 2 4 6 8 10 12 14 16 18 20

**B.**

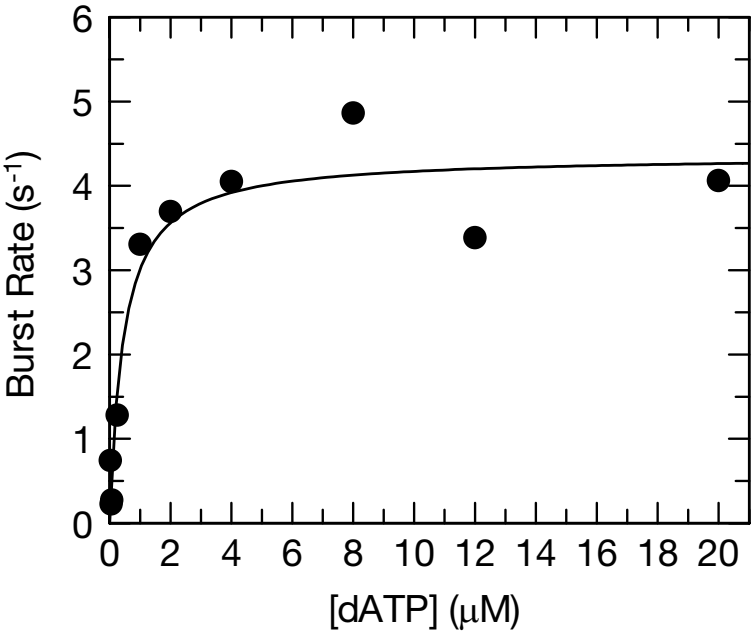
Burst Rate ($s^{-1}$)
[dATP] (μM)
0
1
2
3
4
5
6
0 2 4 6 8 10 12 14 16 18 20

**C.**

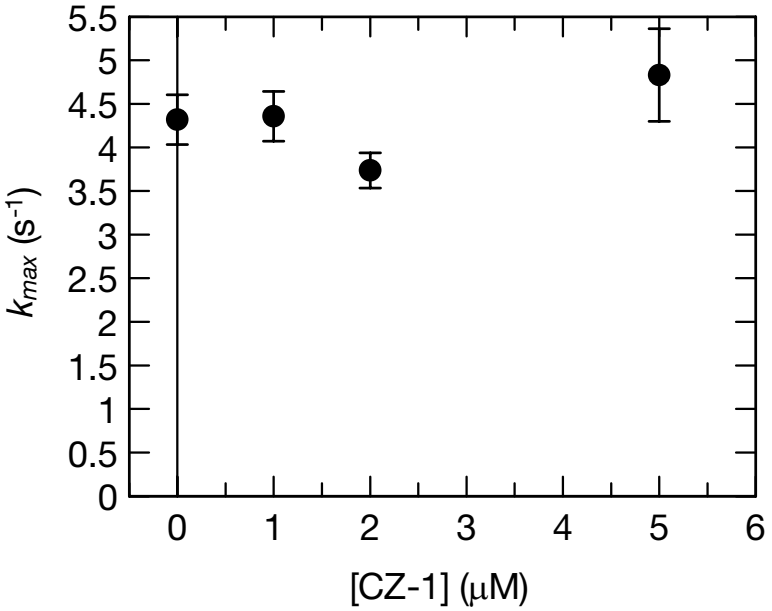
5.5
5
4.5
4
3.5
3
2.5
2
1.5
1
0.5
0
$k_{max}$ ($s^{-1}$)
0
1
2
3
4
5
6
[CZ-1] (μM)

**D.**

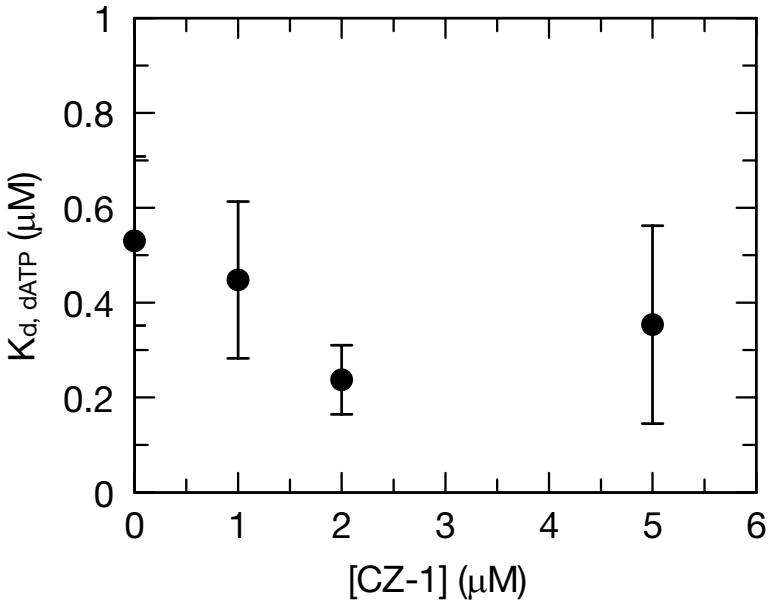
1
0.8
0.6
0.4
0.2
0
$K_{d, dATP}$ (μM)
0
1
2
3
4
5
6
[CZ-1] (μM)

Figure 19. dATP concentration dependence of the nucleotide incorporation rate in the presence of different amounts of CZ-1. (A) A solution of RT (200 nM) and [5'-$^{32}$P]-labeled duplex DNA (400 nM) mixed with 0, 1, 2, and 5 μM CZ-1, respectively, was incubated at 37$^{o}$C for 10 to 15 minutes. The reaction was initiated by mixing equal volumes of Mg•dATP and E•DNA•CZ-1 complex solutions, and was quenched with 0.5 M EDTA, pH 8.0. The dATP concentrations were 0.025(○), 0.05(●), 0.075(□), 0.25(■), 1(△), 2(▲), 4(◇), 8(◆), 12(▽), and 20 (▼) μM. Each of the time courses was fit to a burst equation, $y = A \cdot (1 - e^{-k \cdot t}) + m \cdot t$. Shown here is a plot of time courses of product formation in the presence of 2 μM CZ-1. (B) The single nucleotide incorporation rates were plotted out as a function of the dATP concentration. The plot of the single turnover rates against increasing concentrations of dATP at 1 μM CZ-1 shown here is representative of the trends seen at other concentrations of CZ-1. The curves were fit to hyperbolas that yielded (C) the maximum incorporation rates and (D) the apparent $K_{d,dATP}$ values, which were plotted against the CZ-1 concentrations.

## 2.4. CZ-1 binding rates

Our data indicated that the equilibration of inhibitor with the E•D•I complex is slow relative to the rate of polymerization. We measured the rates of CZ-1 binding by a rapid quench-flow method consisting of two sequential mixing steps. First, CZ-1 was mixed with a solution of E•D complex and allowed to react from 0.1 sec to 30 sec. Then dATP•$Mg^{2+}$ was added to initiate the reaction. Polymerization was allowed to take place for 0.2 sec, which is sufficient for approximately one single turnover as determined by the burst curves from the first experiment. The reactions were terminated by mixing with EDTA. The product concentration was normalized by dividing by the maximum amount of turnover detected in 0.2 sec without the inhibitor. The fraction of product formation was plotted as a function of time allowed for the incubation of CZ-1 with E•D (Fig. 20*A*). Four CZ-1 concentrations were tested: 5, 10, 15 and 20 μM. Each curve of the product formation was fit to a single exponential decay function to calculate the values of the observed binding rates, $k_{obs}$, which were in turn linearly dependent on the CZ-1 concentration to define the values for the association and dissociation rate constants. The observed binding rates were 0.09 ± 0.01 $s^{-1}$, 0.51± 0.02 $s^{-1}$, 1.6 ± 0.2 $s^{-1}$, 1.7 ± 0.1 $s^{-1}$, respectively. Unexpectedly, the observed binding rates at 15 and 20 μM CZ-1 were a lot higher and did not seem to fit the

linear relationship established at the lower CZ-1 concentrations. Since the latter two concentrations are too far beyond the inhibition concentration range

A

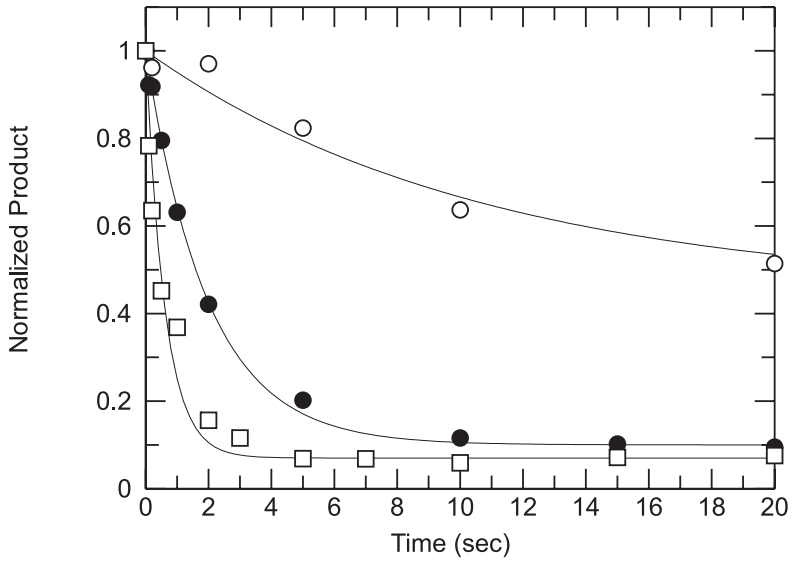


B

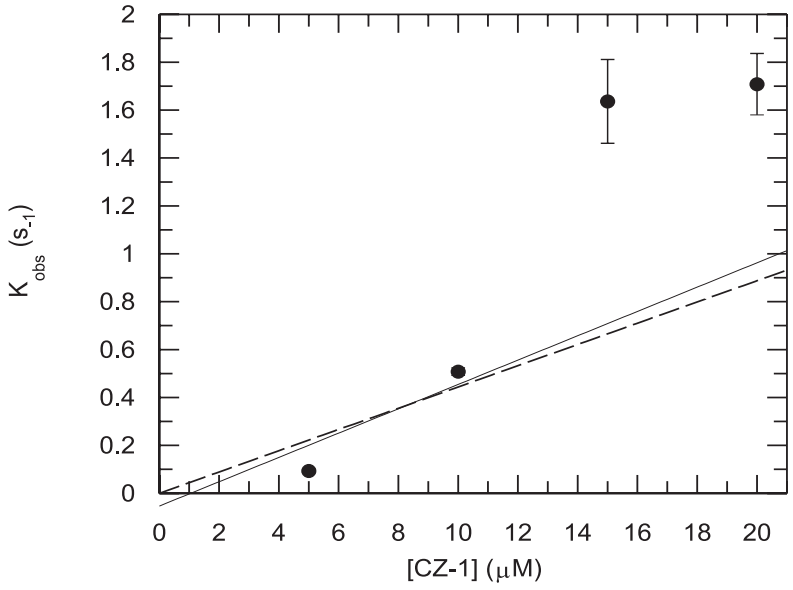

Figure 20. The apparent binding rate of CZ-1. RT (100 nM) was pre-incubated with 5'-$^{32}$P-DNA (100 nM). (A) The E•DNA solution was half diluted when mixed with 5 (○), 10 (●), 15 (□), or 20 μM of CZ-1 for indicated times. Next, the E•D•I solution was half diluted again when mixed dATP (100 μM) for 200 ms. Fitting the curves to single exponential decays rendered apparent binding rates of 0.093 ± 0.009, 0.51 ± 0.02, 1.6 ± 0.2, and 1.7 ± 0.2 $s^{-1}$ for 5, 10, 15, and 20 μM CZ-1, respectively. (B) Association and dissociation rate constants for the E•D•I complex were obtained by analysis of the CZ-1 concentration dependence of the observed binding rate constant, where $k_{obs} = k_{on} * [I] + k_{off}$ and $K_d = \frac{k_{off}}{k_{on}}$, such that $k_{off}$ was constrained to agree with both the $K_d$ value and the observed binding rate. Only the first two data points at 5 and 10 μM CZ-1 were utilized in the linear fit because the two latter data points were far beyond the $K_d$. A linear fit with a floating initial $k_{obs}$ value rendered a negative intercept and a slope of 0.05 (solid line). The best estimate would be a linear fit with the intercept fixed to zero, which rendered a slope of 0.04 ± 0.01 (dashed line), so the $k_{on}$ rate was (4 ± 1) x $10^4$ $M^{-1}s^{-1}$ and $k_{off}$ rate was 0.06 ± 0.01 $s^{-1}$.

observed in prior experiments and the $K_d$ value, we used only the first two concentrations to estimate the binding rates.

Compared to Nevirapine, with a $k_{on}$ of 9.9 x $10^4$ $M^{-1}s^{-1}$ and a $k_{off}$ of 0.0019 $s^{-1}$(21), CZ-1 displayed a similar $k_{on}$ of 4 x $10^4$ $M^{-1}s^{-1}$ and $k_{off}$ of 0.06 $s^{-1}$. The differences in the association and dissociation rate are not surprising since the $K_{d,CZ\text{-}1}$ (1.3 μM) is about 100-fold greater than $K_{d,Nevirapine}$ (0.019 μM). In short, CZ-1 displayed binding rates in the same order of magnitude as Nevirapine and TIBO within the range of inhibition concentrations. However, this simple analysis may not be entirely valid for CZ-1 since the inhibition appears to be a function of dissociation of the E•D complex. For example, it is possible that the faster inhibition observed at higher CZ-1 concentrations may reflect a direct stimulation of the DNA dissociation following formation of an E•D•I ternary complex. Since the rates exceed the rate of DNA dissociation the observed reaction inhibition is not due to the binding only to free enzyme, which would be rate-limited by the release of DNA.

### 2.5. CZ-1 specificity

Recent reports on nonspecific inhibition by drugs due to aggregation of the compounds (132-135) raised our concerns about the efficacy and specificity of CZ-1. Shortly after Skillman *et al.* discovered CZ-1 by computerized structure-based design (1), Shoichet *et al.* reported promiscuous inhibition by aggregation

of small molecules discovered by high throughput screening or molecular docking (132-135). These ligands typically display three properties: (1) they innately bind to many targets; (2) they chemically react with proteins; (3) they aggregate in solution at low micromolar concentrations. One of the first generation NNRTIs, Delavirdine, displayed indiscriminate and aggregation-based inhibition of non-targeted enzymes (135). Since CZ-1 was selected from the chemical database as a docking hit (1) and consists of many aromatic rings which are stereotypical for aggregating inhibitors, we used three approaches to ascertain the specificity of CZ-1. First, we examined the structures of CZ-1 at 5, 50, 250, and 500 μM by electron microscopy. In comparison to the electron microscopy images published by McGovern et al. (133), The data showed that the apparent particle size was small (about 28 nm, as compared to about 52 nm as observed by McGovern *et al.* (132)) and remained constant for all concentration (Fig. 21). Second, I examined aggregation by classic light scattering. No change in particle size was detected in the samples of CZ-1 at any concentration. Finally, I tested the sensitivity of the inhibition by CZ-1 to nonionic detergent (132) by repeating the DNA-directed single nucleotide incorporation experiments with the addition of 0.1% Triton X-100 (Fig. 22). Triton X-100 was found to reverse nonspecific inhibition by disrupting aggregates so that they could not interact with any surface residues on an enzyme (132). The presence of Triton X-100 did not change the inhibition mechanism of CZ-1. The burst amplitude and the steady state rate decreased

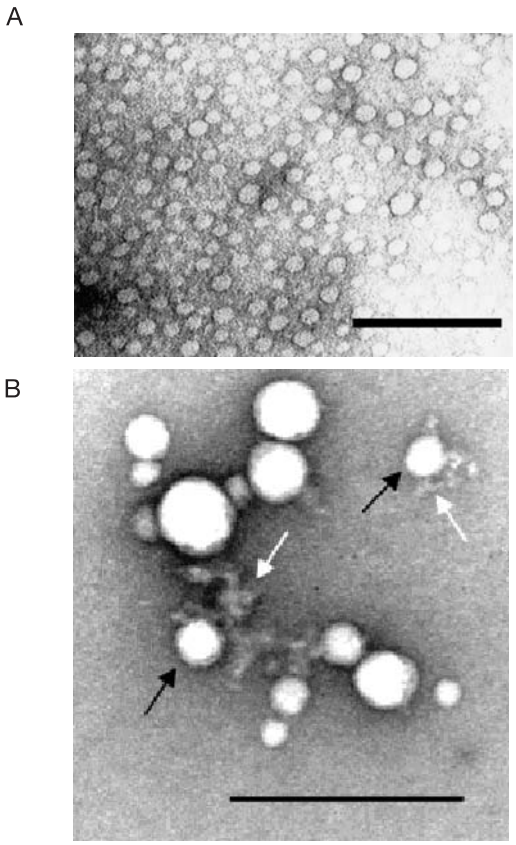


Figure 21. Visualization of CZ-1 by TEM under 44x magnification. (A) 500 μM CZ-1; (B) 100 μM I4PTH with 0.1 mg/mL β-galactosidase, reproduced from McGovern *et al.* (132). The size bar represents 200 nm.

A

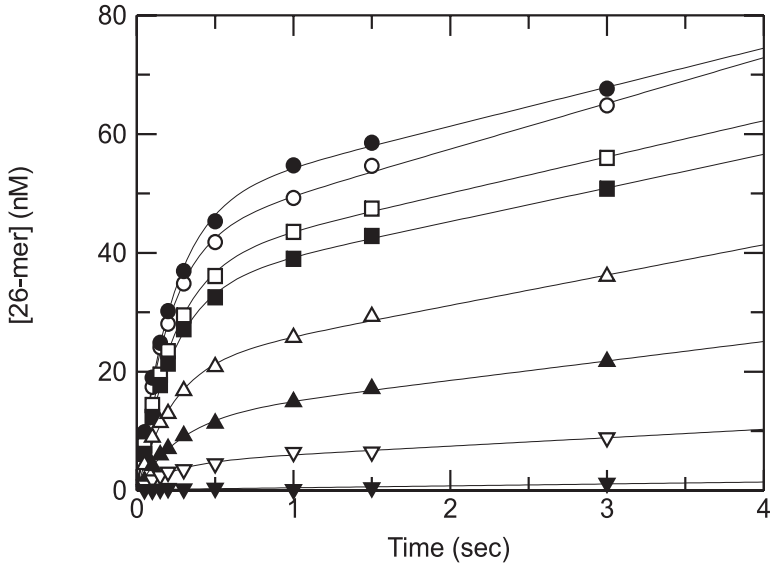
80
60
40
20
0
[26-mer] (nM)
0
1
2
3
4
Time (sec)

B

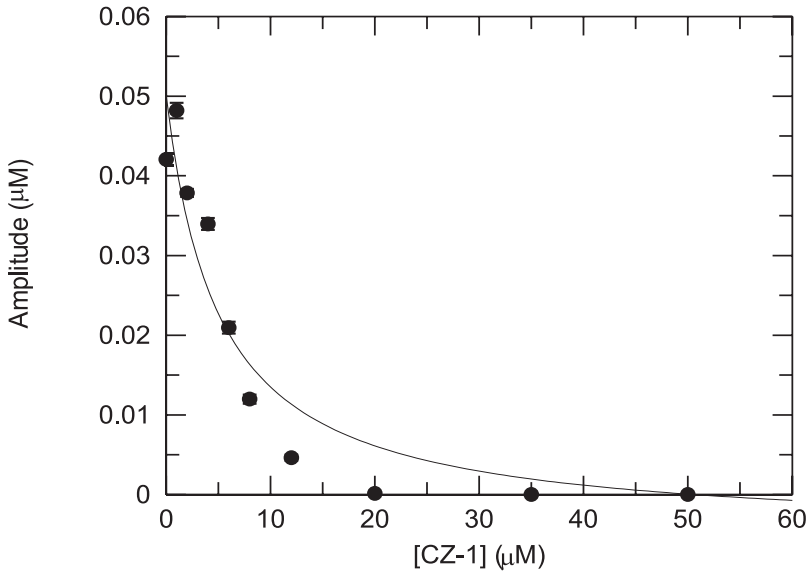
0.06
0.05
0.04
0.03
0.02
0.01
0
Amplitude (μM)
0
10
20
30
40
50
60
[CZ-1] (μM)

Figure 22. The presence of 0.1 % Triton X-100 slightly attenuates the efficacy of CZ-1. DNA-directed single nucleotide incorporation in the presence of CZ-1 and 0.1% triton-X. (A) Wild type RT (100 nM), 5'-$^{32}$P-labeled 25/45-mer DNA (200 nM), and various concentrations of CZ-1 were preincubated for 15-20 min at 37$^{o}$C in reaction buffer (see materials and methods). Concentrations of 0 (○), 1(●), 2(□), 4(■), 6(△), 8(▲), 12(▽), and 20 (▼) μM of CZ-1 were included in the initial solution where the equilibrium between E•D and E•D•I complexes was established. The E•D complex was diluted by half when mixed rapidly with an equal volume of 150 μM dATP (in 10 mM $MgCl_2$) and allowed to react for 0.01 to 3 sec. The reactions were quenched with EDTA at the indicated time points. The individual time course of primer extension at each CZ-1 concentration was fit to the burst equation, $y = A \cdot (1 - e^{-k \cdot t}) + m \cdot t$, to yield the maximum amplitude for each burst curve. (b) The amplitudes of the burst phases were plotted against the CZ-1 concentrations. The data were fit to a hyperbolic equation, $y = E - \frac{E \cdot I}{K_d + I} + B$, that defined a $K_d$ value of 5.2 ± 1.4 μM.

whereas the burst rate remained the same in response to the increase in CZ-1 concentration. However, the apparent $K_{d,CZ-1}$ was raised by four-fold, from 1.3 μM to 5.2 μM. A similar effect was observed when we repeated the experiment with an RNA template of the same sequence: the apparent $K_{d,CZ-1}$ was increased from 3.1 ± 1.3 to 13 ± 3 μM (data not shown). This suggests that Triton X-100 weakened some of the CZ-1 RT binding although it did not eliminate the inhibitory effect of CZ-1. These data argue against a model in which the aggregation of CZ-1 was responsible for the observed inhibition.

Aside from the likelihood of aggregation, the aromatic structure of CZ-1 also allows for possible intercalation with DNA. CZ-1 resembles chemotherapeutic drugs such as daunomycin and nogalamycin which inhibit cell replication by inserting themselves between two planar or stacked aromatic rings such as adjacent bases in a genetic sequence. The interaction results in a distortion of DNA helix structure. I scanned the emission spectra of three mixtures of 10 μM CZ-1 with 0 nM, 100 nM, 150 nM, and 200 nM DNA, respectively, by fluorescence spectroscopy (Fig. 23). When the excitation and emission peaks of CZ-1 with the four concentrations were overlaid, we did not observe any change in the peak intensity.

I also used fluorescence polarization anisotropy to titrate CZ-1 with a high concentration of 25/45mer DNA duplex (Fig. 24) and linearized DNA plasmid

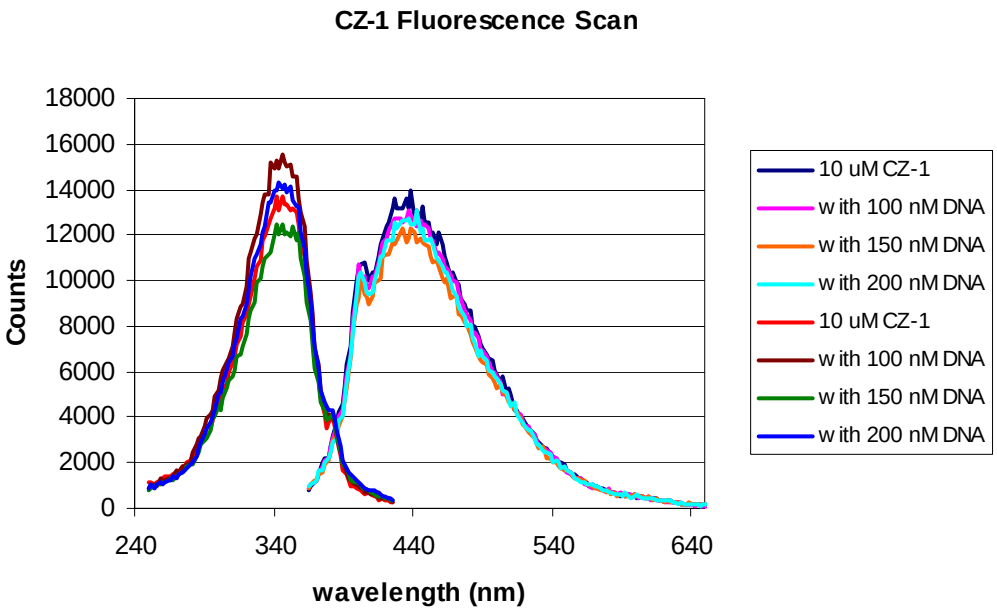


Figure 23. Fluorescence spectra of CZ-1. The inhibitor was combined with a range of DNA 25/45mer duplex concentration. Excitation wavelength was 352 nm and emission wavelength was 440 nm.

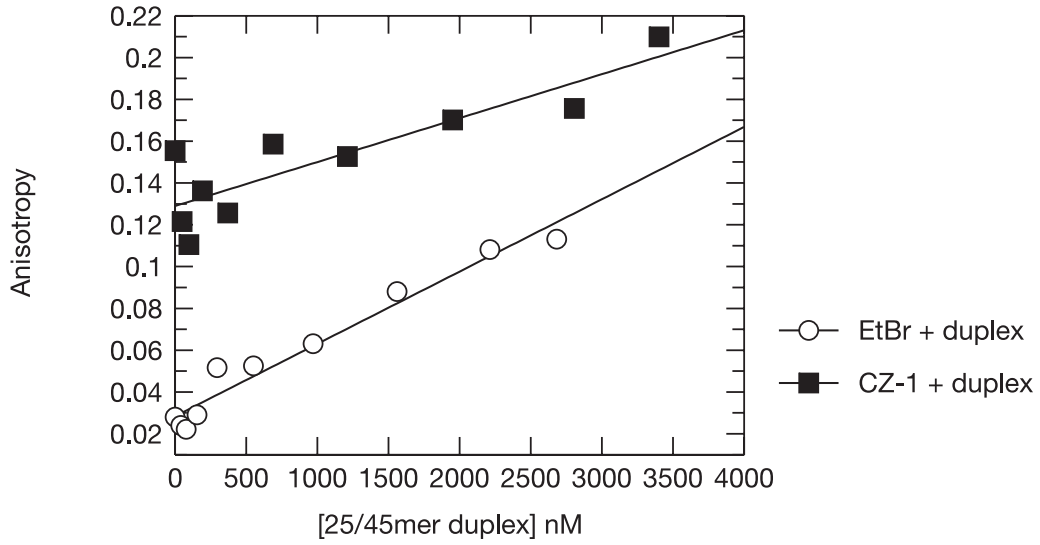


Figure 24. Fluorescence polarization anisotropy experiment of CZ-1 with synthetic DNA duplex. Titration of 2 μM CZ-1 with 25/45mer DNA at a range of concentrations

pUC18 (Fig. 25). As shown in Figure 24, adding 25/45mer duplex DNA to either CZ-1 or ethidium bromide did not create enough signals for data interpretation, so I added pUC18, which is 2686 bp, to enhance the fluorescence signals emitted by the drugs. I observed a significant change in anisotropy as 2 μM ethidium was titrated with pUC18. Prior to the fluorescence measurement, 100 μl of solution A and 200 μl of B were made. Solution A contained 2 μM drug alone, either CZ-1 or ethidium bromide. Solution B contained 2 μM drug and up to 4 μM DNA. Solution B was added to solution A by increments of microliters. An anisotropy measurement was taken after each addition. The anisotropy values were normalized by subtracting the initial values of the drug solutions from each successive value obtained as DNA was incrementally added into the drug solution. When analyzing the data, the anisotropy value was normalized by subtracting the initial value. Background signal from DNA yielded a hyperbolic curve of normalized anisotropy value of CZ-1 versus DNA concentration. The fluorescence signal intensity was the same as that of DNA solution without CZ-1. The normalized anisotropy of ethidium bromide, on the other hand, showed a linear relationship with DNA concentration. Ethidium bromide is known to intercalate with DNA. Since the normalized anisotropy value of CZ-1 did not display a linear relationship with DNA concentration, there is no obvious indication of any interaction that is slowing down the tumbling of the molecule. This result does not support the model that the observed inhibition of

polymerization by HIV RT under the conditions of the experiments reported here was due to nonspecific inhibition by aggregated CZ-1.

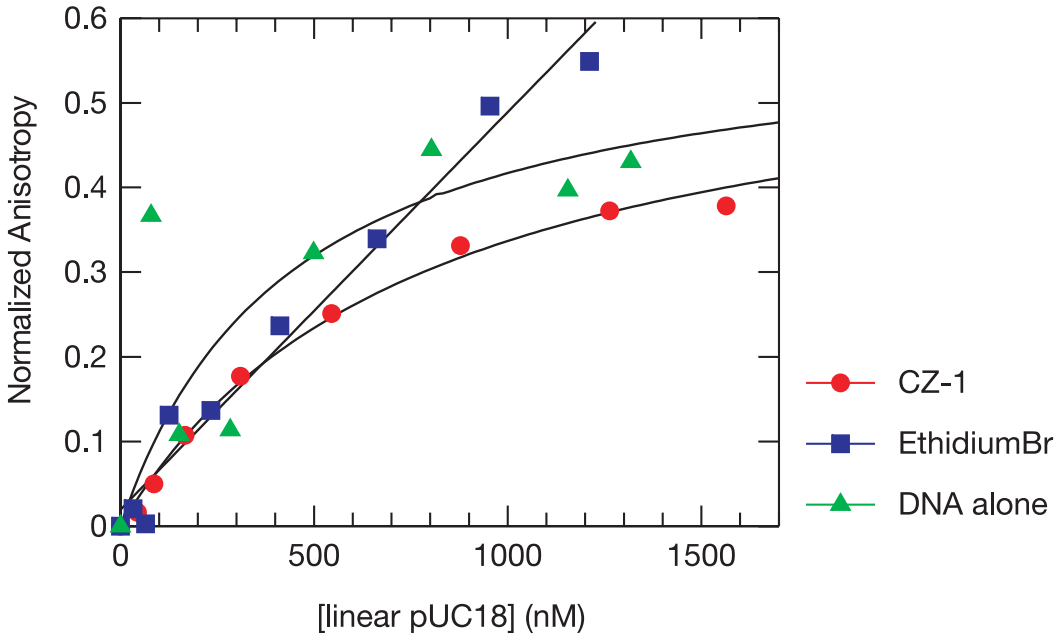


Figure 25. Fluorescence polarization anisotropy measurements of CZ-1 with DNA plasmids. (1) 2 mM CZ-1 mixed with increasing concentrations of DNA (●), (2) 2 μM ethidium bromide mixed with increasing concentrations of DNA (■), and (3) DNA alone (▲). The linear DNA plasmid was created by digesting a pUC18 plasmid with a restriction endonuclease, ScaI. The anisotropy value was normalized by subtracting the initial value, as there was no DNA in the drug solution, from each successive value, as DNA was being added into the drug solution.

### 2.6. CZ-1 SELECTIVITY: IT ALSO INHIBITS MITOCHONDRIAL DNA POLYMERASE.

Further testing of CZ-1 selectivity was carried out by inspecting its effect on Pol γ. Pol γ (200 nM large subunit was combined with 500 nM small subunit), 5'-$^{32}$P-25/45-mer DNA (300nM), and CZ-1 (0 to 30 μM) were incubated prior to reaction with dATP•$Mg^{2+}$. Individual curve of primer extension at each dose of CZ-1 was fit to the burst equation to determine the amplitude (Fig. 26*A*). The hyperbolic function of amplitude versus CZ-1 concentration provided the apparent dissociation constant of 2.2 ± 0.7 μM (Fig. 26*B*). As in the polymerization catalyzed by RT, the burst amplitude of polymerization catalyzed by *Pol* γ was dose-dependently reduced by CZ-1. Although CZ-1 did not inhibit prokaryotic DNA polymerases in the study reported by Skillman *et al*. (1), the data presented here demonstrates that CZ-1 effectively inhibits both *Pol* γ and RT.

## 3. DISCUSSION

I have characterized here a novel non-nucleoside inhibitor, CZ-1 by examining its effect on the pre-steady state kinetics of single nucleotide polymerization catalyzed by HIV RT. I examined the pre-steady state burst amplitude dependence on inhibitor and DNA concentration, as well as the burst rate dependence of the nucleotide concentration. The measurements afforded estimates of the equilibrium dissociation constants for CZ-1, DNA, and dATP

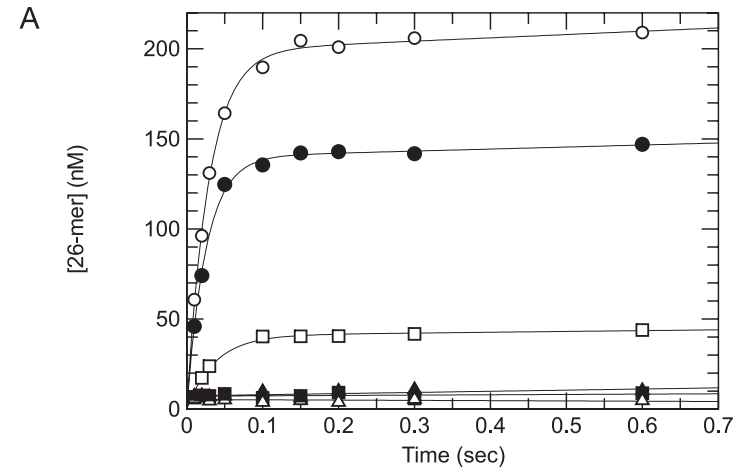
A
[26-mer] (nM)
200
150
100
50
0
0
0.1
0.2
0.3
0.4
0.5
0.6
0.7
Time (sec)

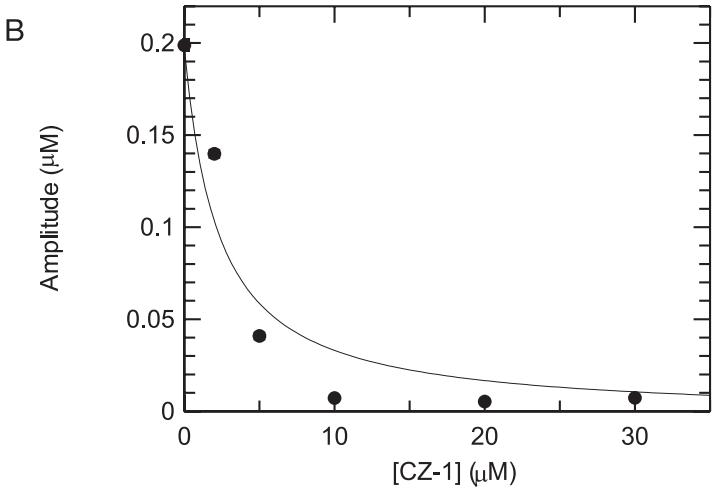
B
Amplitude (μM)
0.2
0.15
0.1
0.05
0
0
10
20
30
[CZ-1] (μM)

Figure 26. DNA-directed single nucleotide incorporation by mitochondrial DNA polymerase in the presence of CZ-1. (A) Mitochondrial DNA polymerase (400 nM large subunit combined with 1 μM small subunit), 5'-$^{32}$P-labeled 25/45-mer DNA (600 nM), and various concentrations of CZ-1 were pre-incubated for 15-20 min at 37$^{o}$C in reaction buffer (see materials and methods). Concentrations of 0 (○), 2(●), 5(□), 10(■), 20(△), and 30(▲)μM of CZ-1 were included in the initial solution where the equilibrium between E•D and E•D•I complexes was established. The E•D complex was diluted by 2-fold when mixed rapidly with an equal volume of 200 μM dATP (in 2.5 mM $MgCl_2$) and allowed to react for 0.01 to 0.6 sec. The reactions were quenched with 0.5 M EDTA (pH 8.0) at the indicated time points. The individual time course of primer extension at each CZ-1 concentration was fit to the burst equation to yield the maximal amplitude for each burst curve. (b) The amplitudes of the burst phases were plotted against the CZ-1 concentrations. The data were fit to a hyperbolic equation, $y = E - \frac{E \cdot I}{K_d + I} + B$, that defined an apparent $K_d$ value of 2.2 ± 0.7 μM.

binding to HIV RT. We observed mutual dose dependence of dissociation constants but not an absolute competition between CZ-1 and DNA in binding to RT. The independence of the dissociation constant for dATP from the concentration of CZ-1 implies that CZ-1 neither affects the nucleotide binding nor the chemistry step. Nevertheless, CZ-1 inhibits Pol γ and RT with similar levels of potency, even though there was no direct evidence of promiscuous inhibition via aggregation. The data reveal that the major source of inhibition is due to displacement of the DNA from the enzyme.

The amplitude of the burst phase represents the amount of uninhibited E•DNA complex available for fast nucleotide incorporation in a single turnover. Therefore, the reduction in the burst amplitude in the presence of the inhibitor is due to a reduction in the concentration of active E•D complex, as E•D•I and/or E•I complex are formed. The reduced burst amplitude and unchanged burst rate suggest that the rate of equilibration of CZ-1 with RT (dissociation and rebinding) is slower than the rate of polymerization catalyzed by uninhibited E•D complex in a single turnover. The unchanged burst rate of polymerization reflects the incorporation catalyzed by the uninhibited E•D complex.

Previously characterized non-nucleoside inhibitors form a ternary E•D•I complex that is still capable of nucleotide incorporation, but at a reduced rate (21). There is a slow but significant continuing reaction even at saturating concentrations of TIBO and Nevirapine. CZ-1, however, inhibits the

polymerization catalyzed by E•DNA complex to a greater extent because it abolishes the reaction seen during the steady state phase. This suggests that the E•D•I complex is not reactive, or at least is extremely slow relative to the rate seen in the presence of Nevirapine. In contrast to Nevirapine and TIBO, CZ-1 stalls dissociation of the E•D•I to favor the E•I complex. Although the E•D•I complex may form, as suggested by the observation that saturating DNA cannot completely overcome the inhibition, it appears to be non-reactive. It is reasonable to suppose that the binding sites for DNA and CZ-1 overlap substantially, but that the binding site for DNA is much larger. In the presence of a high concentration of CZ-1 and DNA they both may bind, but DNA may be dislodged from the catalytic site in such a way as to prevent nucleotide incorporation. Increasing DNA concentration cannot overcome the inhibition because the DNA site is already occupied.

Pre-incubation of CZ-1 with free enzyme before addition of DNA and Mg•dATP in the DNA titration experiments showed that DNA in ten-fold excess over RT concentration could not overcome inhibition by CZ-1. However, CZ-1 binds to RT and interferes with DNA binding, limiting the amount of uninhibited E•D complex available for dATP incorporation. Larger concentrations of CZ-1 increased the apparent equilibrium dissociation constant of DNA binding to RT, weakening RT-DNA binding and hence reducing the amplitude of the burst phase.

In summary, we conclude that CZ-1 binds to RT at a different site than that for the incoming nucleotide, based upon the result that $K_{d,dATP}$ is not affected by CZ-1 concentration,. Furthermore, the lack of effect on the observed tight binding of dATP and the rate of turnover supports the conclusion that CZ-1, like Nevirapine and TIBO (21), does not alter the conformational change that takes place after the ground-state nucleotide binding to RT.

A clear picture of CZ-1 selectivity awaits further experiments. Broader cellular toxicity assays are necessary since CZ-1 appeared to inhibit human mitochondrial DNA polymerase with a comparable (only two-fold weaker) binding affinity as with HIV-1 RT. The binding site on RT for CZ-1 remains unknown. Fluorescence scans did not detect any signs of interaction between CZ-1 and the DNA substrates. Images from electron microscopy and particle size distribution data from classic light scattering did not demonstrate aggregation of CZ-1 molecules. Nevertheless, Triton X-100 slightly perturbed the binding of CZ-1 and HIV-1 RT and the CZ-1 binding rate rose sharply at higher concentrations (Fig. 22*B*).

Kinetic evidence gathered through our work indicates that CZ-1 binds to RT both in the presence and absence of DNA to form E•I and ternary E•D•I complexes, to hinder the incorporation of the next correct nucleotide. Because the only observed reaction was due to the activity of the uninhibited E•D complex, we cannot ascertain whether CZ-1 blocks the nucleotide incorporation at the

binding step, conformational change or chemistry. In the case of previous analysis of inhibition by Nevirapine, analysis of the incorporation kinetics of the fully inhibited enzyme allowed us to establish that NNRTIs block chemistry without interfering with nucleotide binding or the conformational change step. A similar analysis is not possible with CZ-1 because no reaction is seen other than that in the uninhibited fraction of the enzyme.

It is likely that CZ-1 interferes with the proper alignment of DNA at the polymerase active site with its bulky shape. The characterization of this non-nucleoside inhibitor may help in the design of more effective drugs that are potent towards wild type, and drug-resistant strains of RT.

# **CHAPTER 4:** Kinetic Mechanism of Wild type and K103N Mutant HIV-1 Reverse Transcriptase in the Presence of HBY097, α-APA, and CZ-1

## 1. INTRODUCTION

For the past ten years, structural and biochemical research has been combined to render evidence for the relationship between structure and function of RT in the presence of NNRTIs. HIV-1 RT, an important therapeutic target in the treatment of AIDS, is effectively inhibited by the NNRTIs, while HIV-2 RT is not because it has different residues than the ones present in the NNRTI binding pocket on HIV-1 RT (136,137). Functional importance of drug-resistant mutation has been postulated qualitatively from crystal structures (104,138). This chapter presents quantitative examination of the effect of each NNRTI on RT mechanism. If the quantitative results agree with the qualitative ones from molecular structural studies and X-ray crystallography, the impact of certain mutations on the sensitivity of RT to the non-nucleoside inhibitors will be more clearly defined. This chapter describes a pre-steady state kinetic analysis of two forms of HIV-1 RT, the wild type and the drug-resistance mutant K103N, in the presence of three NNRTIs.

K103N is the most common mutation found in clinical trials and therapeutic uses (139). The K103N substitution was detected in majority of the patients with a rebound in plasma viral load, after being treated with nevirapine,

delavirdine, efavirenz (benzoxazinone, DMP266), α-APA (an α-anilinophenylacetamide derivative), or HBY 097 (a quinoxaline derivative) (140,141). Although it has not been reported whether K103N mutation directly contributes to the development of resistance to NNRTIs, it has been shown to decrease binding potency of the NNRTIs since it is usually the first mutation to appear in drug-resistant strains (142), as early as six weeks after beginning treatment with nevirapine (143). Located at the entrance to the NNRTI binding pocket (144), Lys103 forms an electrostatic interaction with the incoming NNRTI (145). Hsiou et al. proposed that Asn103 forms hydrogen bonds from its main chain nitrogen to the terminal oxygen on Tyr188 and water molecules in the pocket and adjacent to pocket residues (see Chapter 1). The interaction between Asn103 and Tyr 188 is likely to seal the entrance to the binding pocket (104). Ren et al. observed rearrangements of residues inside the NNRTI binding pocket as a consequence of K103N substitution (102). The resultant repositioning of the inhibitor and the conformational changes within the NNRTI binding pocket may cause the NNRTIs to bind more slowly to K103N (104). The purpose of my study was to test this theory and extend the level of understanding of the drug-resistance mechanism of this mutant.

Based on the studies of NNRTI resistance at the molecular structural level, I investigated at the kinetic level to help improve the design of anti-AIDS drugs. Comparing the kinetic parameters of the process with different NNRTIs provided

insight into the relationship between the chemical structure of the inhibitor and its effectiveness. General mechanisms for nucleotide incorporation by HIV-1 RT and for inhibition by NNRTIs (21,62) were previously established in our lab. I measured the kinetic parameters for the initial binding steps in the reaction pathway as well as the rates for the first turnover.

The nucleotide incorporation pathway described in Chapter 1 is the basic scheme for measuring kinetic parameters controlling the nucleotide incorporation catalyzed by HIV-1 RT. This biochemical approach was taken to build the resistance-profile for K103N. The mutant enzyme was tested with three NNRTIs: Loviride R90385 (α-Anilinophenylacetamide, α-APA), HBY 097 (a quinoxaline derivative), and CZ-1 as shown in Figure 27. HBY097 was the smallest and most flexible of the three inhibitors. CZ-1 was the largest and most rigid due to the naphthalene rings in its structure. With the exception of CZ-1, they share a common binding pocket (137). Mechanism of inhibition by each inhibitor was investigated to obtain quantitative evidence for functional characterization of the K103N mutant. Correlation of data obtained from kinetic measurements with X-ray crystal structures provided a deeper level of understanding of drug resistance mechanism of HIV-1 RT. The results of these experiments can be applied towards future design of drugs to counteract emerging resistance mutations.

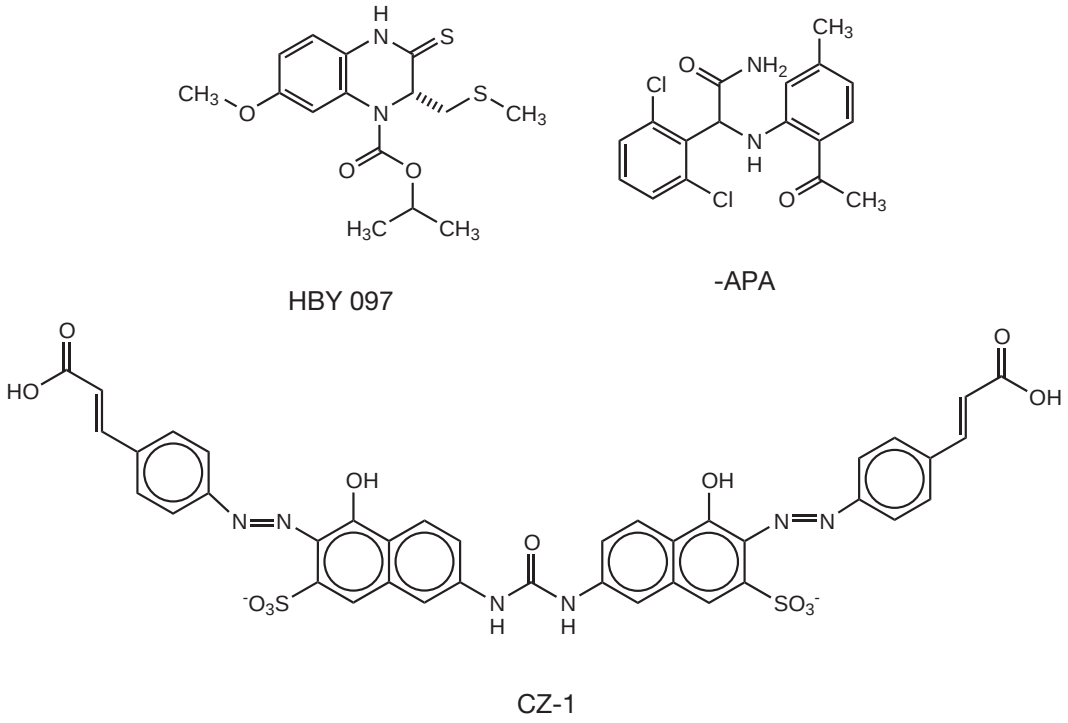


Figure 27. Structural formulas of a-APA, HBY 097, and CZ-1.

## 2. RESULTS

Crystal structures suggested that the K103N mutation reduces the NNRTI binding rate (104). I hypothesized that the shape of the NNRTI, i.e., size and flexibility, attribute to the binding affinity. In order to explore the functional significance of a single amino acid substitution at the NNRTI binding site on

HIV-1 RT, I performed pre-steady state kinetic analysis of polymerization by wild type and K103N in presence of α-APA, HBY 097, and CZ-1. Effects of different NNRTIs on single nucleotide incorporation by wild type and K103N mutant HIV-1 RT were compared by the following quantitative measurements: rates of burst and steady-state phase during the first turnover, apparent equilibrium dissociation constants for E•D complexes, apparent equilibrium dissociation constants for the NNRTIs to HIV-1 RT (i.e. $K_{d,\ APA}$, $K_{d,\ HBY}$, $K_{d,CZ}$), observed binding rates for the NNRTIs to RT, and the apparent equilibrium dissociation constants for dATP to active E•D complex ($K_{d,dATP}$).

## 2.1. DNA-directed dATP incorporation by K103N

Initial characterization of HIV-1 RT mutant, K103N, was carried out by single nucleotide incorporation experiments using the same substrate, 25/45-mer primer/template DNA duplex (Fig. 13). Mutant E•D complex was rapidly mixed with a saturating concentration of dATP, the next correct nucleotide for the 45mer template. Each reaction was quenched with 0.5 M EDTA, pH 8.0. Similar to wild type enzyme, the time course of 26-mer DNA product from catalysis by K103N showed a burst phase followed by a slow linear phase. The burst phase corresponded to the first turnover of the enzyme. The slope of the slow linear phase divided by the active enzyme concentration provided the rate constant for

release of the primer/template from enzyme after nucleotide incorporation (62,146). Results from the initial assay indicated that although K103N catalyzed the reaction at slightly faster burst rate, both the burst and steady state rates of catalysis by K103N were similar to catalysis by wild type HIV-1 RT (Table 3).

### 2.2. Active site titration of K103N with 25/45-mer DNA.

Both K103N and wild type HIV-1 RT catalyzed the nucleotide incorporation in a biphasic pattern, suggesting faster catalysis than release of product from the enzyme. Under these conditions, the amplitude of the burst phase in a single nucleotide incorporation reaction corresponds to the concentration of active E•D complexes. Accordingly, the amplitude renders an estimate of active enzyme and can be used to determine the equilibrium dissociation constant of DNA from K103N (Fig. 28) by titration of HIV-1 RT with DNA. Single nucleotide incorporation experiments were performed where a fixed concentration of K103N was pre-incubated with $^{32}$P- 25/45-mer DNA over a range of concentrations. The solution of E•D complex was mixed with an equal volume of dATP. Figure 28 shows the DNA concentration dependence of the burst amplitude. Data were fit to obtain a $K_d$ value of 6 ± 1 nM which is not substantially different from that seen for wild type RT (3 ± 1 nM from my observation and 5 nM observed by Kati et al. (62)). These results suggest that

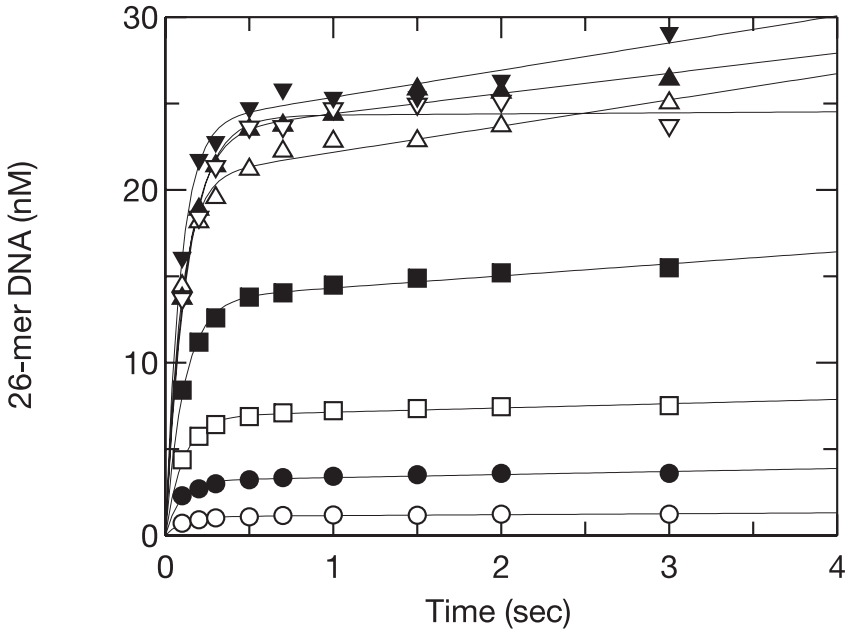
26-mer DNA (nM)
30
20
10
0
0
1
2
3
4
Time (sec)

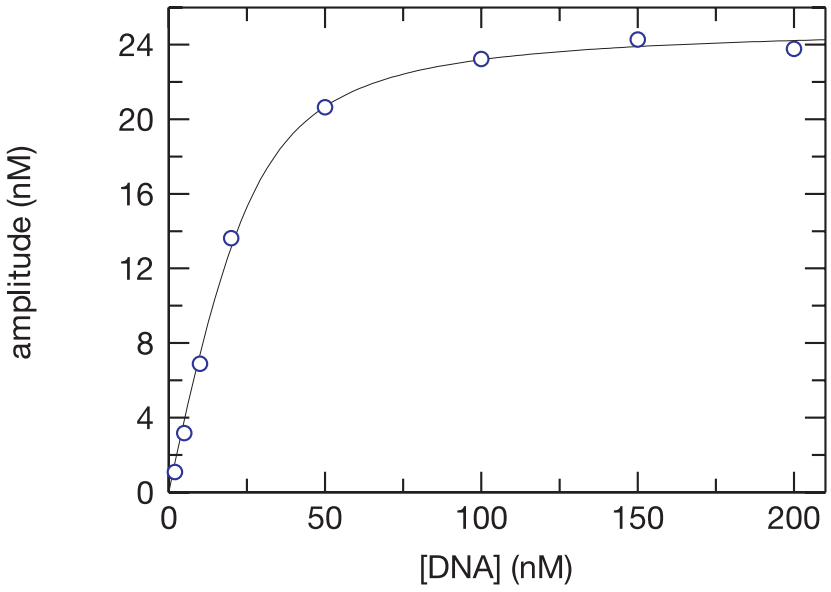
amplitude (nM)
24
20
16
12
8
4
0
0
50
100
150
200
[DNA] (nM)

Figure 28. Active site titration of K103N with DNA duplex. K103N (37.5 nM as determined by UV absorbance measurements at 280 nm) and eight different concentrations of 5'-$^{32}$P-25d/45d were incubated for 5 minutes at 37$^{o}$C in reaction buffer. The E•D complex was then rapidly mixed with saturating concentrations of $Mg^{2+}$•dATP (100 μM). The reaction was quenched with 0.5 M EDTA after indicated times. Upper panel: time courses of product formation at 5 (○), 10(●), 20(□), 50(■), 100(△), 200(▲), 500(▽), and 800 (▼) nM DNA were fit to the burst equation to obtain the amplitude of the burst phase. The average of the eight burst rates was 9.55 $s^{-1}$. Lower panel: The amplitudes were plotted as a function of the 25d/45d concentration. Data was fit to the quadratic equation (Chapter 2) rendering a $K_d$ value for the E•D complex of 6.2 ± 0.8 nM. The maximum amplitude, 25.1 ± 0.4 nM, indicated that approximately 67% of the enzyme in solution is active. K103N concentrations indicated for all other experiments are active site concentrations.

amino acid substitution at position 103 does not affect DNA binding.

### 2.3. Incorporation of the next correct nucleotide, dATP.

In order to determine whether the affinity of the incoming nucleotide for E•D complex was affected by the K103N mutation, single turnover experiments were executed in which a fixed concentration of pre-incubated E•D complex was rapidly mixed with dATP over a range of concentrations. Each time course was fit to the burst equation to obtain the burst rate at each nucleotide concentration. Figure 29 shows the dATP concentration dependence of the burst rate of the E•D complex. Comparison of $K_{d,dATP}$ values showed that K103N mutation weakened the nucleotide interaction by 2-3 fold, which is the same magnitude of change as observed for Y181C mutant (147). Therefore, K103N affects incoming nucleotide interactions with HIV-1 RT to the same extent as Y181C. In contrast to the change in $K_{d,dATP}$, the maximum incorporation rate was increased by 2-3 times in K103N RT.

Kinetic parameters governing DNA binding and nucleotide incorporation have been measured for K103N. The parameters for K103N were essentially identical to wild type RT, indicating that K103N does not change the general mechanism for single nucleotide incorporation. As shown above, K103N did not significantly alter DNA binding and dissociation but rather slightly altered the nucleotide interaction with the E•D complex. The mutation decreased the affinity

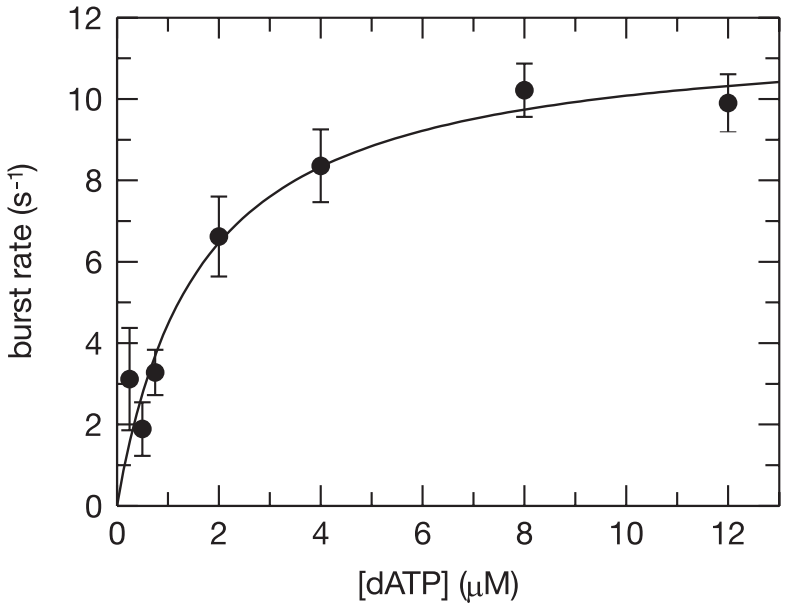


Figure 29. Pre-steady state burst rate dependence on dATP concentration. K103N (100 nM) and 5'-$^{32}$P-labeled 25/45-mer (200 nM) were pre-incubated in reaction buffer for 5 minutes at 37$^{o}$C. The reaction was initiated by mixing increase concentrations of $Mg^{2+}$•dATP and terminated by EDTA. Each burst curve was fit to the burst equation to obtain burst rates, which were in turn plotted as a function of dATP concentration. A hyperbolic fit defined a $K_{d,dATP}$ of 1.6 ± 0.4 μM and a maximum incorporation rate of 12 ± 1 $s^{-1}$.

nucleotide interactions with the E•D complex. The mutation decreased the affinity for the initial ground-state binding of dATP to E•D complex by 2 to 3-fold yet slightly increased the maximum incorporation rate by 2 to 3-fold. The overall specificity ($\frac{k_{pol}}{K_d}$) for dATP incorporation remained the same. Nevertheless, the observed changes are small enough to imply that overall mechanism of nucleotide incorporation catalyzed by K103N is the same as that of wild type RT.

## 2.4. BINDING AFFINITIES OF NNRTIS TO K103N RT.

Data presented in Chapter 3 supported the theory of slow equilibrium between E•D complex and CZ-1-bound or nevirpaine-bound E•D complex (21). Titrating the E•D complex with increasing amounts of inhibitor before initiation of dATP incorporation resulted in a correspondent decrease in burst amplitude. Since burst amplitude represents the amount of uninhibited E•D complex available for nucleotide incorporation in the first turnover, the decrease in amplitude with a constant burst rate means that the inhibitor dissociates from I•E•D complex slowly relative to the rate of polymerization. I performed analogous experiments with K103N in presence of CZ-1, HBY 097, and α-APA (Fig. 30-32) to inspect the effect of the mutation on the equilibrium between E•D complex and each inhibitor.

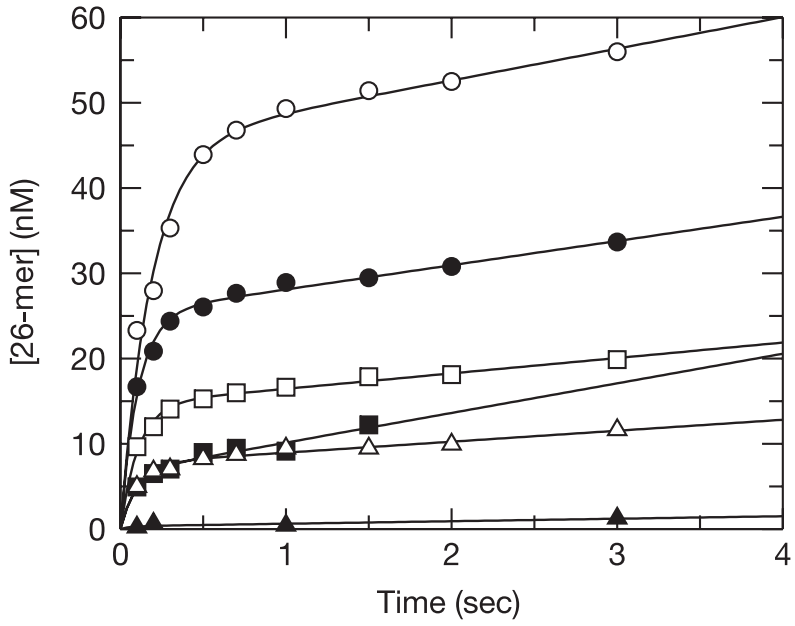
60
50
40
30
20
10
0
[26-mer] (nM)
0
1
2
3
4
Time (sec)

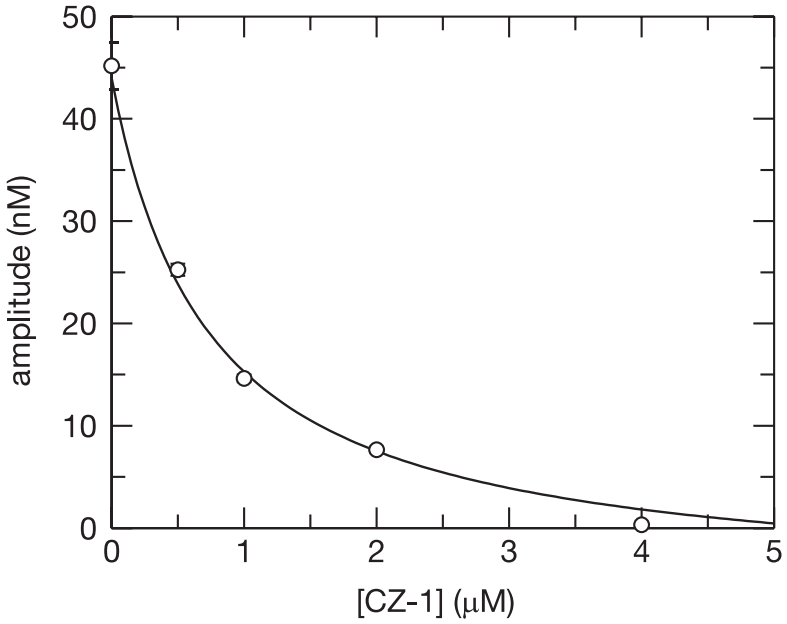
50
40
30
20
10
0
amplitude (nM)
0
1
2
3
4
5
[CZ-1] (μM)

Figure 30. Apparent equilibrium dissociation constant of CZ-1 to K103N RT. Upper panel: K103N RT (50 nM), 5'-$^{32}$P-25/45-mer DNA (100nM), and 0 (○), 0.5 (●), 1(□), 1.5(■), 2(△), or 4(▲) μM of CZ-1 were pre-incubated for 15-20 min at 37°C in reaction buffer, where the equilibrium between E•D and E•D•I complexes was established. The E•D complex was two-fold diluted by an equal volume of 150 μM dATP in buffer with 4 mM Magnesium Acetate. The reactions were allowed to react for 0.01 to 3 sec before quenching with EDTA. Each curve was fit to the burst equation, $y = A \cdot (1 - e^{-k \cdot t}) + m \cdot t$, to yield the maximum burst amplitude at each CZ-1 concentration. Lower panel: The function of burst amplitude vs. CZ-1 concentration was fit to a hyperbolic equation, $y = E - \frac{E \cdot I}{K_d + I} + B$, that defined an apparent $K_d$ of 0.74 ± 0.04 μM.

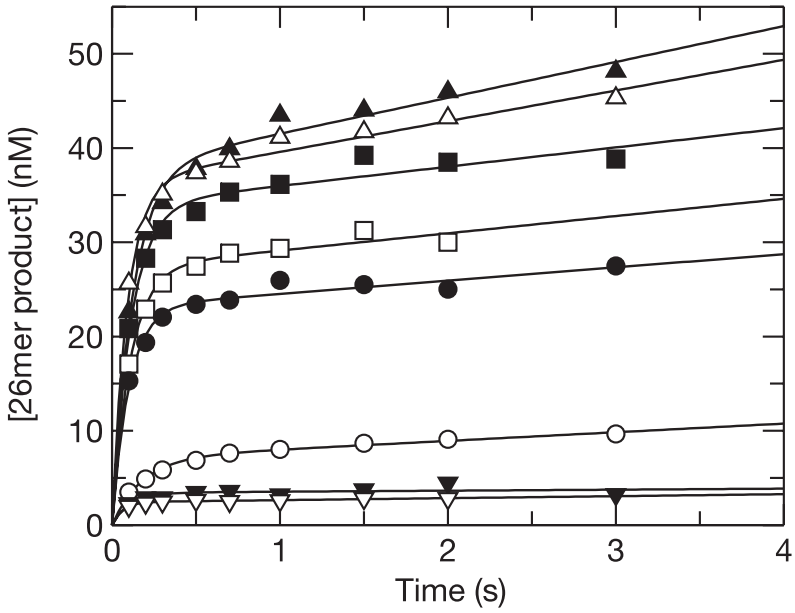
[26mer product] (nM)
Time (s)
0
10
20
30
40
50
0
1
2
3
4

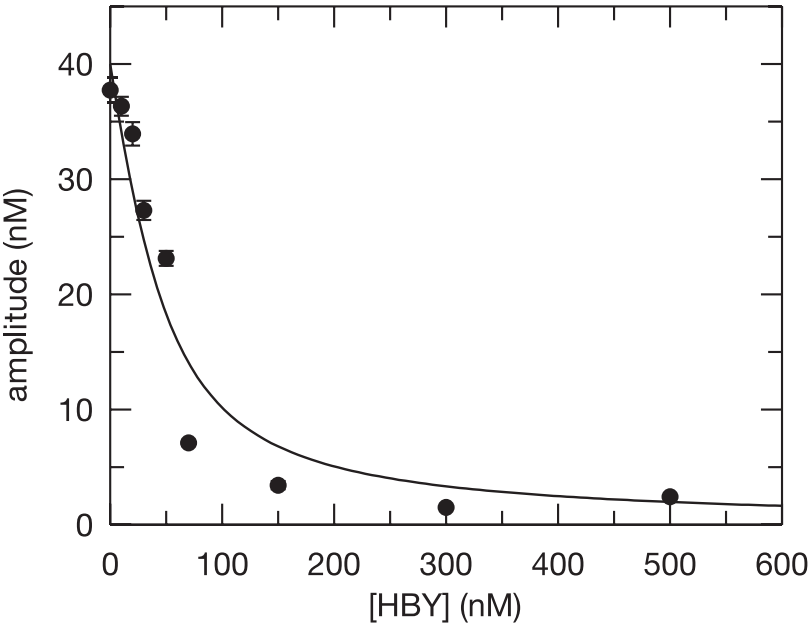
amplitude (nM)
[HBY] (nM)
0
10
20
30
40
0
100
200
300
400
500
600

Figure 31. Apparent equilibrium dissociation constant of HBY 097 to K103N RT. Upper panel: K103N RT (50 nM), 5'-$^{32}$P-25/45-mer DNA (100 nM), and 0 (▲), 0.01 (△), 0.02(■), 0.03(□), 0.05(●), 0.07 (○), 0.15 (▼) or 0.2 (▽) μM of HBY 097 were pre-incubated for 15-20 min at 37°C in reaction buffer, where the equilibrium between E•D and E•D•I complexes was established. The E•D complex was two-fold diluted by an equal volume of 150 μM dATP in buffer with 4 mM magnesium acetate. The reactions were allowed to react for 0.01 to 3 seconds before quenching with EDTA. Each curve was fit to the burst equation, $y = A \cdot (1 - e^{-k \cdot t}) + m \cdot t$, to yield the maximum burst amplitude at each CZ-1 concentration. Lower panel: The function of burst amplitude vs. CZ-1 concentration was fit to a hyperbolic equation, $y = E - \frac{E \cdot I}{K_d + I} + B$, to yield an apparent $K_d$ of 24 ± 7 nM.

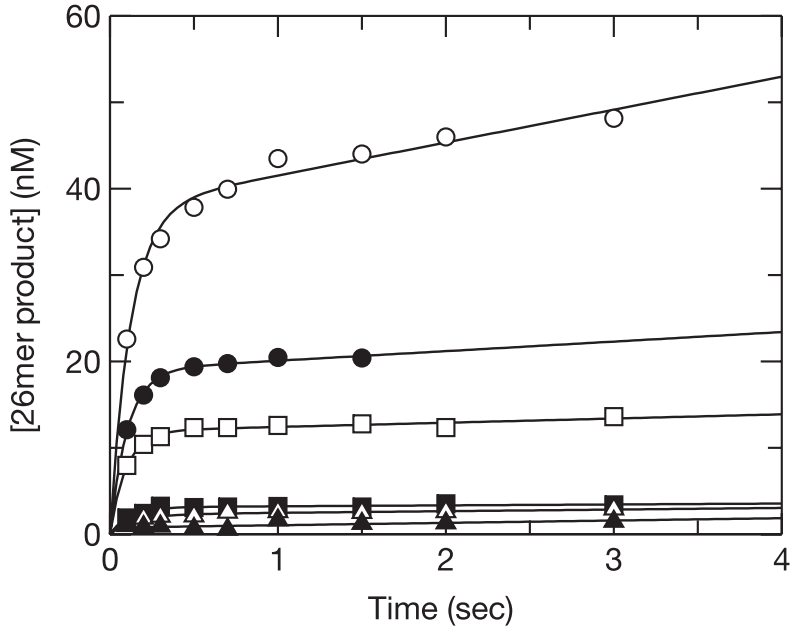
60
40
20
0
[26mer product] (nM)
0
1
2
3
4
Time (sec)

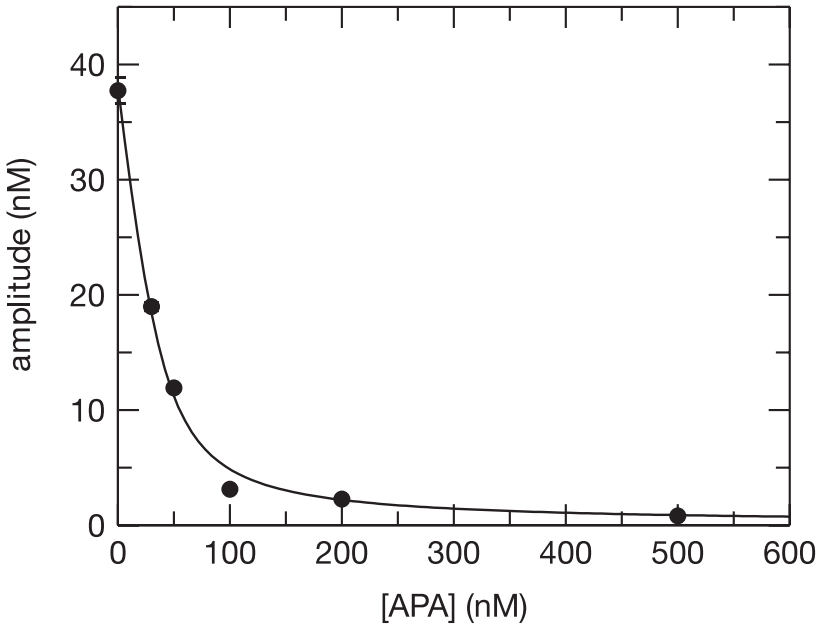
40
30
20
10
0
amplitude (nM)
0
100
200
300
400
500
600
[APA] (nM)

Figure 32. Apparent equilibrium dissociation constant of Loviride to K103N RT. Upper panel: K103N RT (50 nM), 5'-$^{32}$P-25/45-mer DNA (100nM), and 0(○), 0.03(●), 0.05(□), 0.1(■), 0.2(△), or 0.5(▲) μM of α-APA were pre-incubated for 15-20 min at 37°C in reaction buffer, where the equilibrium between E•D and E•D•I complexes was established. The E•D complex was two-fold diluted by an equal volume of 150 μM dATP in buffer with 4 mM magnesium acetate. The reactions were allowed to react for 0.01 to 3 sec before quenching with EDTA. Each curve was fit to the burst equation, $y = A \cdot (1 - e^{-k \cdot t}) + m \cdot t$, to yield the maximum burst amplitude at each CZ-1 concentration. Lower panel: The function of burst amplitude vs. CZ-1 concentration was fit to a hyperbolic equation, $y = E - \frac{E \cdot I}{K_d + I} + B$, that defined an apparent $K_d$ value of 9.5 ± 1.4 nM.

E•D was titrated with increasing concentrations of each inhibitor prior to rapid mixing with dATP for indicated times, followed by quench with EDTA (Fig. 30-32). The consistent burst rate for reaction with each inhibitor was evidence to affirm that the fast rate of incorporation was due to the first turnover of uninhibited E•D complex. Hence the decrease in burst amplitude in correspondence with the increase in inhibitor concentration was a result of formation of I•E•D complexes, which affords a direct measurement of the concentration of I•E•D complex. The relationship between amplitude and inhibitor concentration determined the apparent equilibrium dissociation constant of the inhibitor from I•E•D complex (Fig. 30-32 and Table 3). With respect to wild type HIV-1 RT, the affinity of CZ-1, HBY 097, and a-APA to K103N RT increased 1.8, 2.4, and 3.5-fold, respectively. This slight enhancement in inhibitor binding affinity is the opposite of what was expected of this mutation. The hydrogen bond that K103N adds at the entrance of the NNRTI binding pocket (104) did not seem to deter inhibitor binding after all.

### 2.5. Association and dissociation rate constants of NNRTIs with K103N RT-DNA complex.

Further investigation into the effect of K103N mutation on equilibrium dissociation constant of the three inhibitors was achieved by determining the association ($k_{on}$) and dissociation ($k_{off}$) rates of the inhibitors. K103N was pre-

incubated with $^{32}$P-25/45-mer DNA. The E•D complex was mixed with an equal volume of inhibitor (at 5, 10, 15, or 20 μM after mixing) for specified times (Fig. 33-35 upper panels). Next, I•E•D complex was mixed with dATP for 0.2 second to allow the completion of a single turnover of uninhibited active E•D complex. Finally, the reaction was quenched with 0.5 M EDTA, pH 8.0.

The product from the 0.2 second reaction is due to catalysis by uninhibited E•D complex because the dissociation of inhibitor from I•E•D complex is slow with respect to the rate of uninhibited polymerization. For the same reason, the observed decrease in product concentration is due to the inhibitor binding to and inactivating the E•D complex. Data of normalized product as a function of time was fit to a single exponential decay equation (Chapter 2) to obtain the observed binding rate ($k_{obs}$) for each inhibitor. The association ($k_{on}$) and dissociation ($k_{off}$) rates of inhibitor with E•D complex were defined by the equation, $k_{obs} = k_{on} * [I] + k_{off}$, which was used together with $K_d = \frac{k_{off}}{k_{on}}$ so that $k_{off}$ is consistent with previously determined $K_d$ of each inhibitor. The observed binding rates increased linearly with inhibitor concentration in reactions catalyzed by either the wild type or K103N RT (Fig. 33-35 lower panels). HBY 097 and α-APA showed 3 to 4-times slower dissociation rates from K103N than wild type RT. CZ-1 and α-APA showed a faster association rate to K103N. The bulkiest

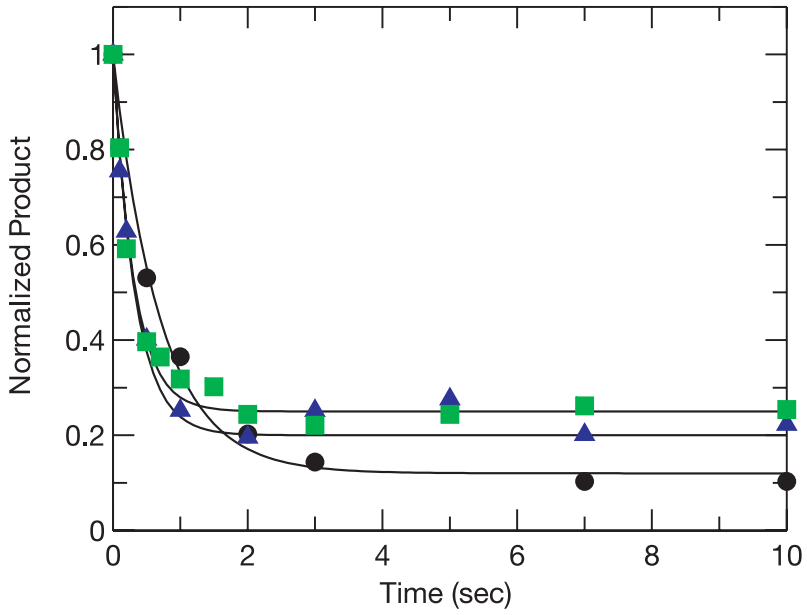
Normalized Product
Time (sec)
0
0.2
0.4
0.6
0.8
1
0
2
4
6
8
10

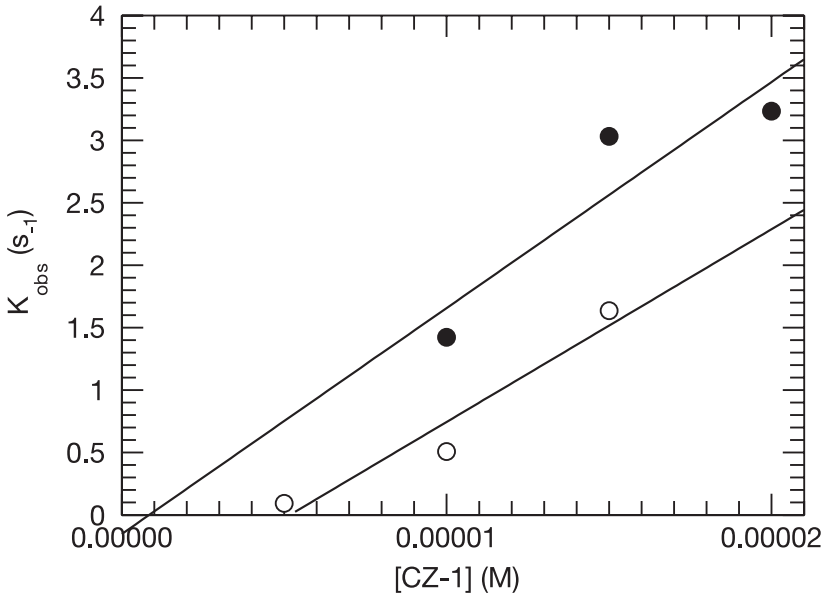
K obs (s-1)
[CZ-1] (M)
0
0.5
1
1.5
2
2.5
3
3.5
4
0.00000
0.00001
0.00002

Figure 33. Apparent binding rate of CZ-1 to wild type and K103N RT. RT (100 nM) was pre-incubated with [5'-$^{32}$P]-labeled DNA duplex (100 nM). The E·DNA solution was two-fold diluted when mixed with CZ-1 for the indicated times. Next, the E·D·I solution was mixed with an equal volume of dATP (100 μM) for 200 ms. Upper panel: fitting the curves to single exponential decays rendered apparent binding rates of 1.42 ± 0.11, 3.03 ± 0.22, and 3.23 ± 0.20 $s^{-1}$ for 10 (●), 15 (■), and 20 (▲) μM CZ-1 to $RT^{K103N}$-DNA complex. (B) ○were obtained by analysis of the CZ-1 concentration dependence of the observed binding rate constant. Due to large errors in the extrapolated intercept, binding rates were calculated by fitting data to the equations, $K_d = \frac{k_{off}}{k_{on}}$ and $k_{obs} = k_{on} * ([I] + K_d)$, such that $k_{off}$ was constrained to agree with both $K_d$ and $k_{obs}$ values. A linear fit rendered a slope of 0.18 ± 0.08 for $RT^{K103N}$ (○)and 0.04 ± 0.01 for $RT^{WT}$(●), so the $k_{on}$ rate was (18 ± 8) x $10^4$ $M^{-1}s^{-1}$ for K103N and (4.4 ± 0.9) x $10^4$ for WT, and $k_{off}$ rate was 0.13 ± 0.06 $s^{-1}$ for K103N and 0.06 ± 0.01 $s^{-1}$ for WT.

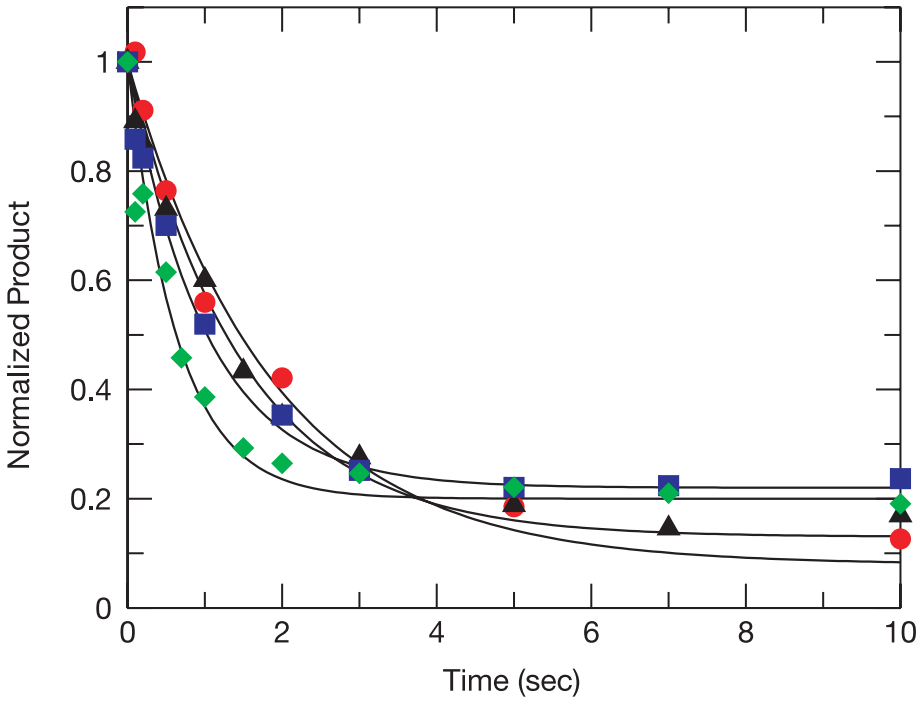
Normalized Product
1
0.8
0.6
0.4
0.2
0
0
2
4
6
8
10
Time (sec)

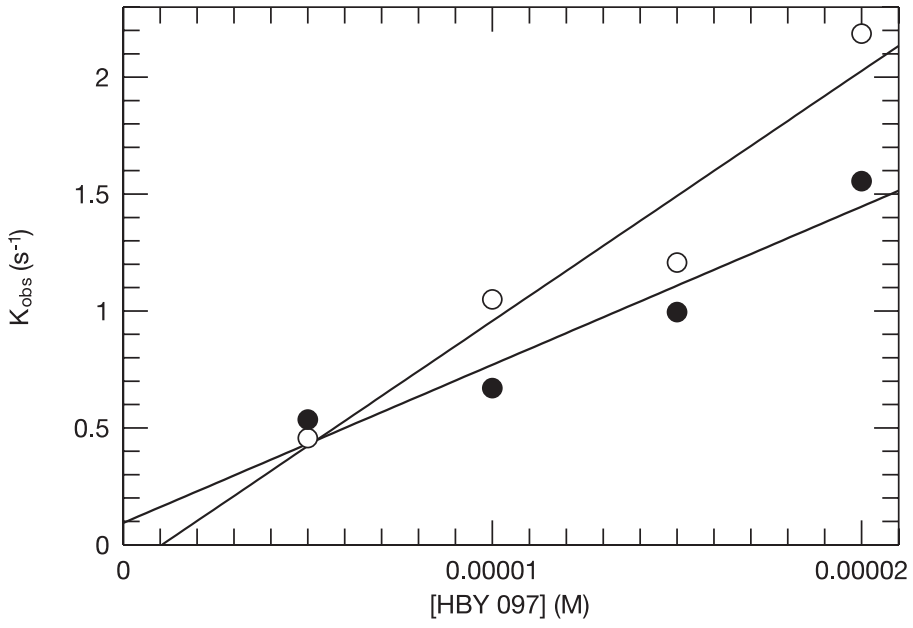
$K_{obs}$ ($s^{-1}$)
2
1.5
1
0.5
0
0
0.00001
0.00002
[HBY 097] (M)

Figure 34. Apparent binding rate of HBY 097 to wild type and K103N RT. RT (100 nM) was pre-incubated with [5'-$^{32}$P]-labeled DNA duplex (100 nM). The E·DNA solution was two-fold diluted when mixed with 5 (●), 10 (▲), 15 (■), or 20 (◆) μM of HBY for the indicated times. Next, the E·D·I solution was mixed with an equal volume of dATP (100 μM) for 200 ms. Upperpanel: fitting the curves to single exponential decays rendered apparent binding rates of 0.54 ± 0.04, 0.67 ± 0.03, 1.00 ± 0.06, and 1.56 ± 0.15 $s^{-1}$ for 5, 10, 15, and 20 μM HBY to $RT^{K103N}$-DNA complex. (B) Association and dissociation rate constants for formation of the E•D•I complex were obtained by analysis of the HBY concentration dependence of the observed binding rate constant. Due to large errors in the extrapolated intercept, binding rates were calculated by fitting data to the equations, $K_d = \frac{k_{off}}{k_{on}}$ and $k_{obs} = k_{on} * ([I] + K_d)$, such that $k_{off}$ was constrained to agree with both $K_d$ and $k_{obs}$ values. A linear fit rendered a slope of 0.11 ± 0.02 for $RT^{K103N}$ (●) and 0.07 ± 0.01 for $RT^{WT}$(○), so the $k_{on}$ rate was (11 ± 2) x $10^4$ $M^{-1}s^{-1}$ for WT and (6.8 ± 1.4) x $10^4$ for K103N, and $k_{off}$ rate was 0.002 ± 0.001 $s^{-1}$ for K103N and 0.006 ± 0.002 $s^{-1}$ for WT.

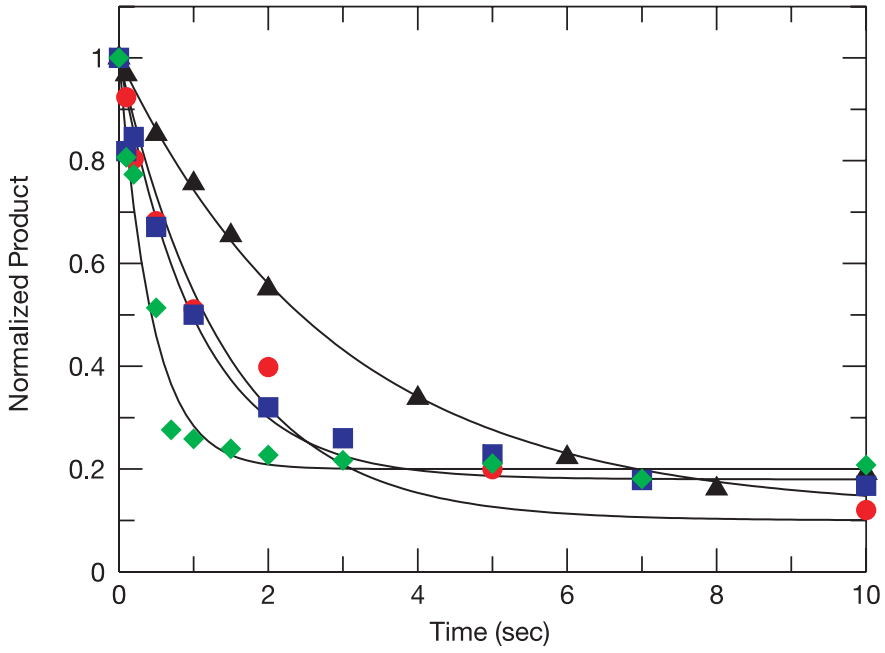
Normalized Product
Time (sec)
0
0.2
0.4
0.6
0.8
1
0
2
4
6
8
10

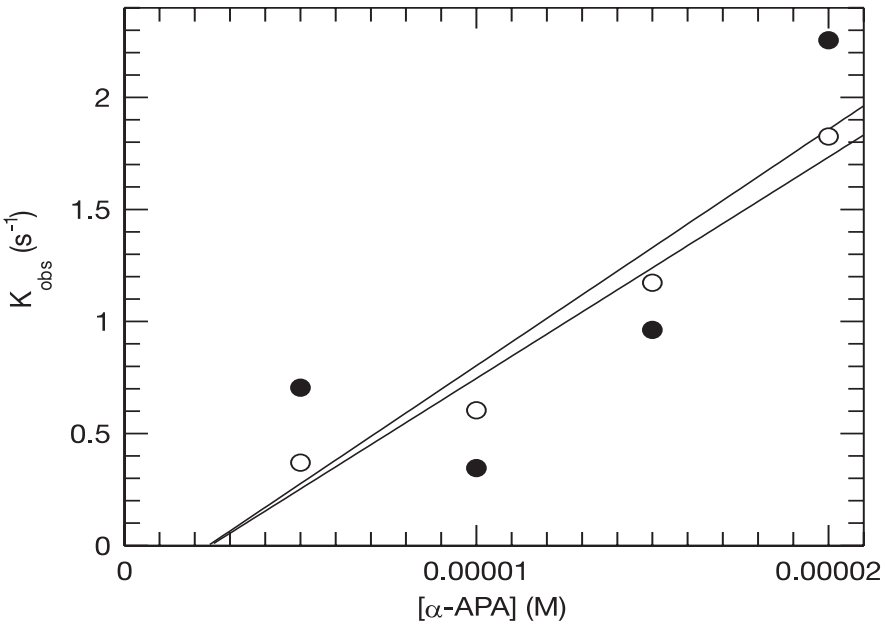
K obs (s-1)
[α-APA] (M)
0
0.5
1
1.5
2
0
0.00001
0.00002

Figure 35. Observed binding rate of α-APA to wild type and K103N RT. RT (100 nM) was pre-incubated with [5'-$^{32}$P]-labeled DNA duplex (100 nM). The E·DNA solution was two-fold diluted when mixed with 5 (●), 10 (▲), 15 (■), or 20 (◆) μM of α-APA for the indicated times. Next, the E·D·I solution was mixed with an equal volume of dATP (100 μM) for 0.2 second. Upperpanel: fitting the curves to single exponential decays rendered apparent binding rates of 0.35 ± 0.01, 0.70 ± 0.06, 0.96 ± 0.07, and 2.3 ± 0.2 $s^{-1}$ for 5, 10, 15, and 20 μM α-APA to $RT^{K103N}$-DNA complex. (B) Association and dissociation rate constants for formation of the E•D•I complex were obtained by analysis of the α-APA concentration dependence of the observed binding rate constant. Binding rates were calculated by fitting data to the equations, $K_d = \frac{k_{off}}{k_{on}}$ and $k_{obs} = k_{on} * ([I] + K_d)$, such that $k_{off}$ was constrained to agree with both the $K_d$ and $k_{obs}$ value due to large errors in the extrapolated intercept. A linear fit rendered a slope of 0.11 ± 0.05 for $RT^{K103N}$ (●) and 0.10 ± 0.01 for $RT^{WT}$(○), so the $k_{on}$ rate was (11 ± 5) x $10^4$ $M^{-1}s^{-1}$ for K103N and (9.9 ± 1.4) x $10^4$ $M^{-1}s^{-1}$ for WT, and $k_{off}$ rate was 0.001 ± 0.001 $s^{-1}$ for K103N and 0.003 ± 0.001 $s^{-1}$ for WT.

Table 2: Observed binding rates of inhibitors at various concentrations to $RT^{WT}$ and $RT^{K103N}$.

| Inhibitor | Concentration (μM) | WT $k_{obs}$ ($s^{-1}$) | K103N $k_{obs}$ ($s^{-1}$) |
|---|---|---|---|
| CZ-1 | 5 | 0.093 ± 0.009 | - |
| | 10 | 0.51 ± 0.02 | 1.42 ± 0.11 |
| | 15 | 1.64 ± 0.18 | 3.03 ± 0.22 |
| | 20 | 1.71 ± 0.13 | 3.23 ± 0.20 |
| HBY | 5 | 0.46 ± 0.03 | 0.54 ± 0.04 |
| | 10 | 1.05 ± 0.05 | 0.67 ± 0.03 |
| | 15 | 1.21 ± 0.11 | 1.00 ± 0.06 |
| | 20 | 2.19 ± 0.22 | 1.56 ± 0.15 |
| α-APA | 5 | 0.37 ± 0.05 | 0.35 ± 0.01 |
| | 10 | 0.60 ± 0.06 | 0.70 ± 0.06 |
| | 15 | 1.17 ± 0.13 | 0.96 ± 0.07 |
| | 20 | 1.83 ± 0.15 | 2.25 ± 0.17 |

Table 3: Kinetic properties of $RT^{WT}$ and $RT^{K103N}$.

| | wild type | K103N |
|---|---|---|
| $K_{d,DNA}$ (nM) | 3 ± 1 | 6.2 ± 0.8 |
| $k_{max}$ ($s^{-1}$) | 7.4 ± 0.5 | 12 ± 1.0 |
| $K_{d,dATP}$ (μM) | 0.53 ± 0.18 | 1.6 ± 0.4 |
| Burst rate ($s^{-1}$) | 7.0 ± 0.3 | 12 ± 1 |
| Steady State rate ($s^{-1}$) | 0.20 ± 0.02 | 0.23 ± 0.01 |
| $K_{d,CZ-1}$ (μM) | 1.3 ± 0.3 | 0.74 ± 0.04 |
| $k_{on,CZ-1}$ ($M^{-1}s^{-1}$) | (4.4 ± 0.9) x $10^4$ | (18 ± 8) x $10^4$ |
| $k_{off,CZ-1}$ ($s^{-1}$) | 0.06 ± 0.01 | 0.13 ± 0.06 |
| $K_{d,HBY}$ (μM) | 0.058 ± 0.013 | 0.024 ± 0.007 |
| $k_{on,HBY}$ ($M^{-1}s^{-1}$) | (11 ± 2) x $10^4$ | (6.8 ± 1.4) x $10^4$ |
| $k_{off,HBY}$ ($s^{-1}$) | 0.0062 ± 0.0018 | 0.0016 ± 0.0006 |
| $K_{d,APA}$ (μM) | 0.032 ± 0.007 | 0.0095 ± 0.0014 |
| $k_{on,APA}$ ($M^{-1}s^{-1}$) | (9.9 ± 1.4) x $10^4$ | (11 ± 5) x $10^4$ |
| $k_{off,APA}$ ($s^{-1}$) | 0.0032 ± 0.0008 | 0.0010 ± 0.0005 |

and most rigid CZ-1 associated with K103N at the fastest rate while the smallest HBY 097 bound with the slowest rate. Hydrophobic interaction of binding pocket residues with the aromatic rings of the inhibitor seemed to play an important role in the K103N mutant enzyme.

## 3. DISCUSSION

K103N changed incoming nucleotide interactions with HIV-1 RT by approximately 2 to 3 fold but did not affect the specificity of nucleotide incorporation, analogous to Y181C (147). These similar subtle effects by the two mutations might be due to the fact that the side chain of the residue was shortened in both mutations. On the other hand, the slightly faster burst exhibited by K103N attests to the evolutionary ability of HIV-1 RT to its advantage in replication.

The results presented here did not seem to support my hypothesis based on structures. HBY 097 showed slower association rate towards K103N, whereas α-APA bound to wild type and K103N mutant enzyme with comparable association rates, and CZ-1 associated with K103N at a slightly faster rate than with wild type. The size and flexibility of the inhibitor did not seem to affect binding affinity. The smallest inhibitor, HBY 097, did not display higher binding affinity than the other two inhibitors. In contrast, the bulkiest inhibitor, CZ-1, exhibited

the higher binding rate with K103N than with wild type HIV RT. K103N seemed to favor hydrophobic interaction with the aromatic rings in the inhibitor more than wild type RT.

While both HBY 097 and α-APA dissociated from K103N with a three to four-fold slower rate than from wild type, CZ-1 dissociated from K103N with a rate twice as fast as from wild type. These differences in association and dissociation rates were inconsequential when I compared the apparent equilibrium dissociation constants, for all three inhibitors displayed two- to three-fold smaller $K_d$ values for dissociation from K103N-DNA complexes than from WT-DNA complexes. Smaller $K_d$ value represents tighter binding. Increased inhibitor binding affinity in K103N was the opposite of my hypothesis. However, the values for each kinetic parameter were in such a small range that the changes were rather minimal. Apparently the data presented in this chapter cannot complete the characterization of the K103N mutant. More single nucleotide incorporation experiments in presence of other NNRTIs, especially nevirapine, delavirdine, and efavirenz, are needed to elucidate the resistance mechanism of this mutant HIV-1 RT.

Novel inhibitors with improved activity against NNRTI-resistant HIV have been designed based on predictions by computational methods such as Monte Carlo or molecular docking. The kinetic method I have presented in this dissertation is an efficient *in vitro* evaluation of novel drug compounds to

complement *in vivo* studies. More inhibitors under clinical trials should be tested against other recently discovered resistance mutants to get a complete picture of the relationship between specific mutations and development of drug resistance.

# CHAPTER 5: RNA-directed DNA polymerization by HIV-1 Reverse Transcriptase in Presence of Non-nucleoside Inhibitors

## 1. INTRODUCTION

Chapter 3 and 4 described studies performed with a duplex DNA substrate derived from the template for plus-strand DNA synthesis during the process of reverse transcription. However, the first step *in vivo* is minus-strand DNA synthesis utilizing a viral RNA template (Chapter 1). According to the established inhibition mechanism of CZ-1 (Chapter 3), this inhibitor should hinder the minus-strand DNA synthesis before the plus-strand DNA synthesis takes place. In order to test this theory, I carried out RNA-directed single nucleotide incorporation assays under identical reaction conditions to those for DNA-directed dATP incorporation experiments. This chapter describes the results of RNA-directed DNA polymerization in the presence and absence of CZ-1.

## 2. RESULTS

I compared RNA-directed dATP incorporation by wild type HIV-1 RT in the presence and absence of CZ-1 to the previous DNA-directed dATP incorporation by $RT^{WT}$ under identical reaction conditions. For these RNA-

directed DNA polymerization experiments, a 45-mer RNA template with the same sequence (Fig. 13B) as the previously used DNA template was synthesized by *in vitro* transcription with T7 RNA polymerase (Chapter 2).

## 2.1. RNA-directed dATP incorporation catalyzed by K103N and wild type RT.

Initial single nucleotide incorporation experiments with wild type and K103N mutant RT, using 25d/45r primer/template substrate (Fig. 36), were performed to compare the kinetics of both enzymes when accommodating an RNA or DNA template. Pre-steady state kinetic analysis for incorporation of dATP was conducted under conditions where the DNA concentration was in slight excess relative to the enzyme concentration. The reaction was carried out by rapidly mixing a pre-incubated solution of RT (either wild type or K103N mutant, 100 nM) and 5'-$^{32}$P-25d/45r (200 nM) with a solution of $Mg^{2+}$ (2 mM) and saturating concentrations of dATP ( 100 μM) (final concentrations) to initiate the polymerization. Reactions were quenched with 0.5 M EDTA at time intervals ranging from 0.01 to 2 second.

Plotting the concentration of 5'-$^{32}$P-26-mer DNA product against time (Fig. 36) revealed a pre-steady-state burst of nucleotide incorporation representing

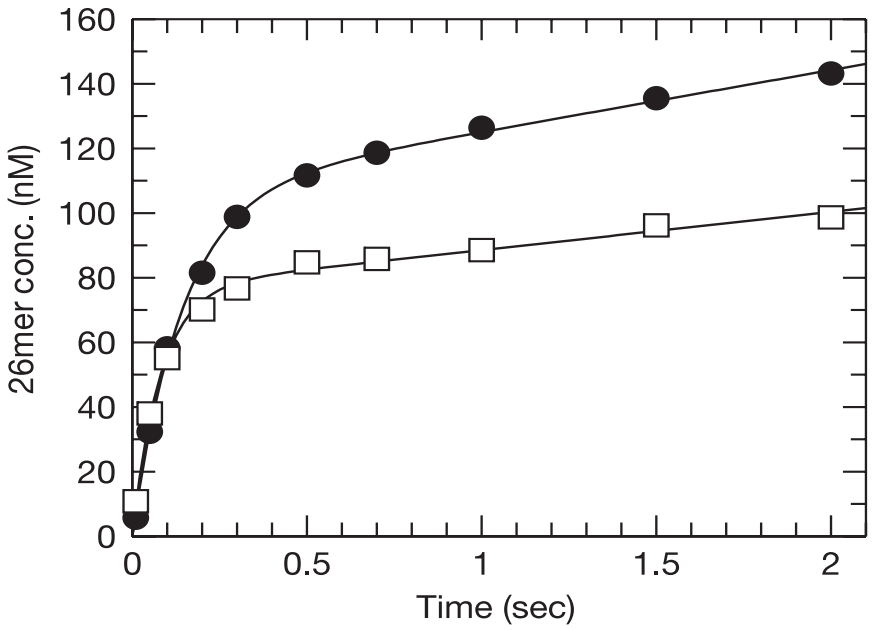


Figure 36. Single nucleotide incorporation by wild type RT using a 25d/45r primer/template. $RT^{WT}$ (●) or $RT^{K103N}$ (□) (100 nM) was pre-incubated with 5'-$^{32}$P-25d/45r (200 nM) for 10 minutes. Equal volumes of this E•D/R solution and 200 μM dATP in reaction buffer containing 4 mM $Mg^{2+}$ were rapidly mixed for indicated times. Reactions were quenched with EDTA. The 26-mer product concentration was plotted versus reaction time. Data were fit to the burst equation (Chapter 2). The burst rate from the exponential phase was 7.0 ± 0.3 $s^{-1}$ for wild type and 9.1 ± 0.3 $s^{-1}$ for K103N mutant. The steady state rate constants, 0.16 ± 0.02 $s^{-1}$ for wild type HIV-1 RT and 0.11 ± 0.02 $s^{-1}$ for K103N, were obtained by dividing the slope of the linear phase by the active enzyme concentration.

the first turnover of the enzyme followed by a linear phase corresponding to the slower steady state release of the product (62,148). This biphasic behavior indicates that the overall rate-limiting step during incorporation of a single correct nucleotide is the product release after the chemistry step (62). Fitting the time courses to the burst equation rendered a burst rate of 7.0 ± 0.3 $s^{-1}$ for $RT^{WT}$ with DNA template, 9.1 ± 0.3 $s^{-1}$ for $RT^{WT}$ with RNA template, 12 ± 1 $s^{-1}$ for $RT^{K103N}$ with DNA template, and 17 ± 2 $s^{-1}$ for $RT^{K103N}$ with DNA template. Data fit also yielded the steady state rates: 0.20 $s^{-1}$ for $RT^{WT}$ with DNA template and 0.16 $s^{-1}$ for $RT^{WT}$ with RNA template, 0.23 $s^{-1}$ for $RT^{K103N}$ with DNA template, and 0.11 $s^{-1}$ for $RT^{K103N}$ with RNA template. The kinetic parameters of polymerization with the two templates by both enzymes are summarized in Table 4. Similar to previous observations (62), $RT^{WT}$ and $RT^{K103N}$ both exhibited slightly faster polymerization rates in experiments employing an RNA template, relative to experiments using a DNA template. On the other hand, $RT^{K103N}$ showed a slower steady state rate with RNA template than with DNA template, while $RT^{WT}$ exhibited the same steady state rate with both templates. These results are similar to what have been observed previously in our lab. The biphasic shape of the product formation curve implied that the incorporation of dATP catalyzed by either the mutant or wild type RT, using either 25d/45d or 25d/45r substrate, maintained a similar reaction mechanism as established previously (62). The initial characterization demonstrated that the wild type enzyme used in my

experiments possessed the same kinetic properties as previously reported (21,62). Like the Y181C mutant (147), the pathway for single nucleotide incorporation catalyzed by K103N is similar to that determined for wild type RT.

## 2.2. Measurement of kinetics for dATP incorporation using RNA template.

K103N mutation seemed to increase the maximum incorporation rate as well as the apparent equilibrium dissociation constant for dATP during DNA-directed polymerization (Chapter 3). It would be necessary to further characterize this mutant by inspecting its effect on RNA-directed correct nucleotide incorporation. I wanted to determine if K103N exhibited the same template specificity as wild type RT. The $K_d$ for dATP binding to the enzyme with an RNA template was determined in an analogous manner as that for dATP binding to the enzyme with a DNA template, by reacting a pre-incubated solutions of RT (100 nM) and primer/template (200 nM) with varying $Mg^{2+}$•dATP concentrations and recording product formation with time. As shown in the upper panel of Figure 37, the burst or single-turnover rates for formation of 26/45-mer product increased with higher concentrations of dATP. The dependence of the burst rate of $RT^{K103N}$ on dATP concentration is shown in the lower panel of Figure 37, with

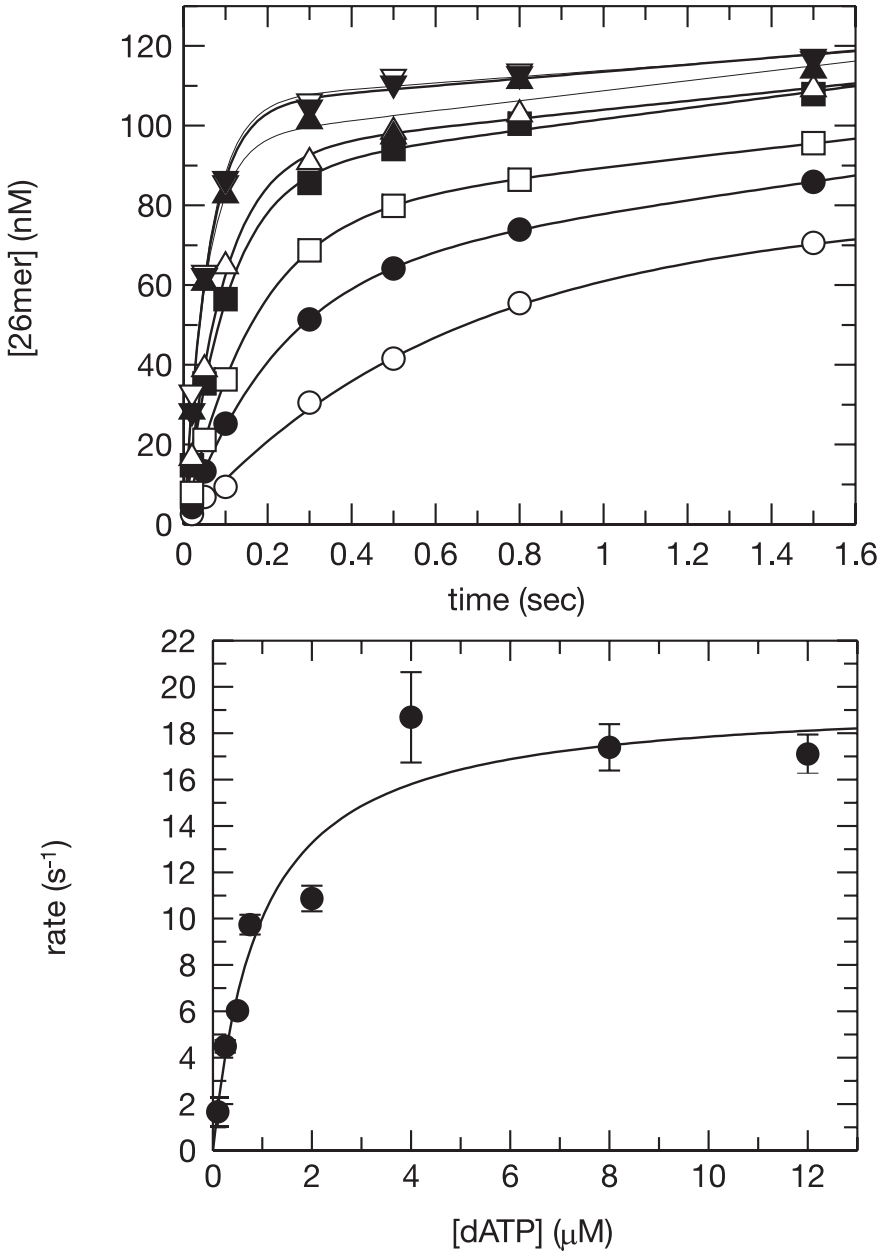
[26mer] (nM)
120
100
80
60
40
20
0
0
0.2
0.4
0.6
0.8
1
1.2
1.4
1.6
time (sec)
rate ($s^{-1}$)
22
20
18
16
14
12
10
8
6
4
2
0
0
2
4
6
8
10
12
[dATP] (μM)

Figure 37. Pre-steady state rate dependence of dATP concentration in RNA-directed incorporation by $RT^{K103N}$. K103N (100 nM) and 5'-$^{32}$P-25d/45r (200 nM) were incubated in reaction buffer for 5 minutes. The polymerization reaction was initiated by the addition of increasing concentrations of $Mg^{2+}$•dATP and quenched with EDTA after specified times. Upper panel: Time courses were fit to the burst equation to calculate the apparent first turnover rate of the burst phase. Lower panel: hyperbolic function of burst rate vs. dATP concentration yielded a $K_{d,dATP}$ of 0.95 ± 0.26 μM and maximum rate of 19 ± 2 $s^{-1}$.

the data fit to a hyperbola, defining a $K_d$ of 1.0 ± 0.3 μM for RNA template (as compared to 1.6 ± 0.4 μM for DNA template), and a maximum rate of incorporation of 19 ± 2 $s^{-1}$ for RNA template (as compared to 12 ± 1 $s^{-1}$ for DNA template) (Table 4). The specificity of nucleotide incorporation was defined as $\frac{k_{pol}}{K_d}$. The specificity constant remained at approximately 8 $s^{-1}\mu M^{-1}$ for $RT^{WT}$, irrespective of template. However, in the case of $RT^{K103N}$, the specificity for an RNA template was 2.5 fold greater than for a DNA template (7.5 to 19 $s^{-1}\mu M^{-1}$). The kinetic data suggest that while $RT^{WT}$ shows little preference for one template over the other, $RT^{K103N}$ favors an RNA template over a DNA template for polymerization.

### 2.3. RNA-directed DNA polymerization in presence of CZ-1

I also wanted to determine if CZ-1 exhibited the same inhibition mechanism for 25d/45r substrate as for 25d/45d substrate. Therefore I quantitated the apparent equilibrium dissociation constant of CZ-1 and HIV-1 RT with a 25d/45r substrate using pre-steady state kinetic analysis. In chapter 3, I have reported a reduction in the amplitude of the burst phase of polymerization upon titration of the wild type E•D complex with CZ-1. The burst amplitude is a

quantitative representation of uninhibited E•D complex continuing on to polymerization (Chapter 1).

I examined the effect of RNA-directed single nucleotide incorporation catalyzed by the wild type enzyme in presence of the novel drug compound, CZ-1. Increasing concentrations of CZ-1 were incubated with $RT^{WT}$ and 25d/45r before rapid mixing with dATP. Reactions were stopped after various times with EDTA. The burst amplitudes were obtained by fitting the time course at each CZ-1 concentration to the burst equation. There was a pronounced decrease in the burst amplitude as the CZ-1 concentration was increased. However, there was no substantial change in the burst rate of RNA-directed polymerization accompanying the decreasing amplitude. Therefore, polymerization could only occur in actively bound E•D/R complexes. The fast burst rate of incorporation was a result of the first turnover of uninhibited enzyme. Therefore, the reduction in the burst amplitude of RNA-directed dATP incorporation (Fig. 38) was due to a lack of polymerization activity in inhibited E•D/R complex, which allowed us to quantitate the equilibrium dissociation constant of CZ-1 with the enzyme complex. Figure 38 shows the inverse relationship between the amplitude of the burst phase and the concentration of CZ-1 in the reaction. Fitting the data to a quadratic equation (Chapter 2) yielded a $K_d$ value of 3.1 ± 1.3 μM. CZ-1 binding affinity to RT-25d/45r was increased by two fold, as compared to that of RT-25d/45d complex (1.3 ± 0.2 μM). The RNA template did not seem to

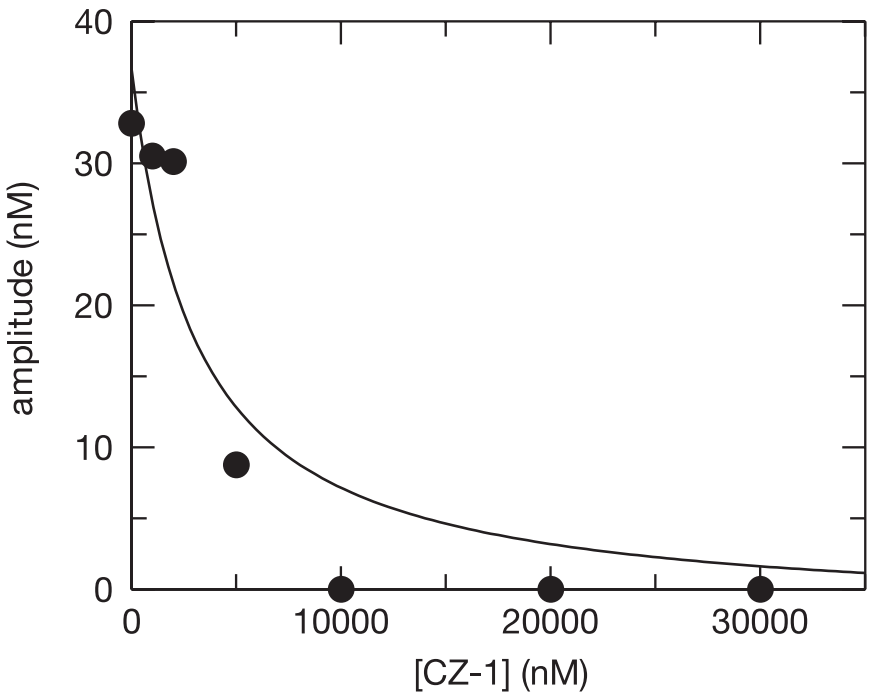


Figure 38. Apparent equilibrium dissociation constant of CZ-1 from RNA/DNA-$RT^{WT}$ complex. Wild type RT (50 nM) was pre-incubated with 5'-$^{32}$P-labeled 25d/45r (100 nM, two-fold excess over enzyme) for 5 minutes at 37$^{o}$C in reaction buffer. Increasing concentrations of CZ-1 were added to the E•D/R solution and incubated for 10 minutes. The partially saturated enzyme complex was then rapidly mixed with saturating concentrations of $Mg^{2+}$•dATP for 0.01 to 1 second. Reactions were quenched with 0.5 M EDTA. Individual time courses were fit to the burst equation. Burst amplitudes (●) were plotted against CZ-1 concentration. Data were fit to a quadratic equation that defined an apparent $K_d$ of 3.1 ± 1.3 μM.

Table 4: Kinetic difference between DNA vs. RNA-directed polymerization catalyzed by wild type and K103N RT.

| | wt-D/D | wt-D/R | K103N-D/D | K103N-D/R |
|---|---|---|---|---|
| $k_{pol}$ ($s^{-1}$) | 7.4 ± 0.5 | 19 ± 2 | 12 ± 1 | 19 ± 2 |
| $K_{d,dATP}$ (μM) | 0.74 ± 0.19 | 2.5 ± 0.6 | 1.6 ± 0.4 | 1.0 ± 0.3 |
| Burst rate ($s^{-1}$) | 7.0 ± 0.3 | 17 ± 2 | 12 ± 1 | 17 ± 2 |
| Steady State rate ($s^{-1}$) | 0.20 ± 0.02 | 0.16 ± 0.02 | 0.23 ± 0.01 | 0.11 ± 0.02 |
| $K_{d,CZ-1}$ (μM) | 1.3 ± 0.2 | 3.1 ± 1.3 | 0.74 ± 0.04 | - |
| $K_{d,CZ-1,Triton}$ (μM) | 5.2 ± 1.4 | 13 ± 3 | - | - |

significantly affect the binding of CZ-1 to HIV-1 RT in this experiment.

## 3. DISCUSSION

Chapter 3 and 4 described the mechanism of HIV-1 RT inhibition by non-nucleoside inhibitors, where a DNA duplex was used as a substrate by the HIV-1 RT, in order to simulate plus-strand synthesis in the process of reverse transcription (see Chapter 1). During the first stage of reverse transcription *in vivo*, RT uses a viral RNA template in minus-strand synthesis primed by a cellular tRNA molecule. Previous transient-state kinetic measurements demonstrated the difference in dNTP binding affinity, maximum polymerization rate, and fidelity between a RNA/DNA and DNA/DNA primer/template (62,73). The affinity of primer/template remained the same for D443N RT (an RNase H deficient mutant), as previously demonstrated through active site titration experiments by Rebecca Spence. Here I have measured the elementary steps in RNA-directed polymerization pathway using both the wild type and K103N mutant.

Initial single turnover experiments with the mutant $RT^{K103N}$-25d/45r complex revealed the same biphasic pattern of product formation as the wild type HIV-1 RT, indicating a fast incorporation of nucleotide followed by slower steady state release of the primer/template. The burst rate of wild type and K103N using an DNA/RNA duplex, 25d/45r, as a primer/template was increased slightly compared to the identical reaction with a DNA duplex, 25d/45d, substrate. Previous studies showed that the burst behavior of polymerization is the result of

a conformational change of the enzyme immediately preceding the chemistry step (21,62,68,72,149,150), thereby directing the incoming nucleotide in the proper orientation for effective catalysis. Here the results suggest that DNA/RNA duplex is the preferred substrate, as it contributes to a slight increase in the rate of conformational change of HIV-1 RT.

As a validation for the observation that the first turnover catalyzed by either wild type or K103N RT with an RNA template was fast relative to catalysis with a DNA template, it was necessary to determine if the affinity of the next correct nucleotide, dATP, has been changed by the RNA template accordingly. The apparent equilibrium dissociation constant of the incoming nucleotide showed that the affinity of dATP was indeed increased for polymerization by the wild type enzyme, but not for the reaction catalyzed by K103N mutant. The result here is inconclusive.

I investigated the effect of RNA template on the potency of the novel inhibitor, CZ-1. The RNA-directed single nucleotide incorporation experiments in presence of CZ-1 were performed identically as DNA-directed experiments (Chapter 3). Likewise, an equilibrium dissociation constant for CZ-1 with the wild type enzyme and RNA/DNA complex was derived based on the correlation between the reduction in the burst amplitude and the amount of I•E•D/R complex. The $K_d$ value was 3.1 μM for CZ-1 and the E•D/R complex, representing an approximately two-fold weaker affinity of CZ-1 for the E•D/R complex.

The pre-steady state measurements of the RNA-directed DNA polymerization by wild type and K103N mutant HIV-1 RT described in this chapter indicated that HIV-1 RT utilizes an RNA template with an analogous overall mechanism as that of a DNA template (62). The apparent affinity of CZ-1 for HIV-1 RT was 2 fold lower in presence of an RNA template, relative to that of a DNA template. This might imply that RNA competes with CZ-1 better than DNA for HIV-1 RT. The extremely slow turnover of the HIV-1 RT in the presence of saturating amounts of CZ-1 proves the hindrance of the chemical step of the RNA-directed nucleotide polymerization when CZ-1 is bound to the enzyme, similar to DNA-directed nucleotide incorporation.

The results discussed in this chapter expand my previous conclusions of the inhibition mechanism of CZ-1 to include not only DNA-directed but RNA-directed DNA polymerization. As RNA is the viral template in minus-strand DNA synthesis, the RNA-directed polymerization experiment enhances my understanding of the inhibition by CZ-1 *in vivo*.

# CHAPTER 6: SUMMARY

CZ-1 (2-naphthalenesulfonic acid, 4-hydroxy-7-[[[[5-hyroxy-6-[(4-cinnamylphenyl)azo]-7-sulfo-2-naphthalenyl]amino]carbonyl]amino]-3-[(4-cinnamylphenyl)]azo), disodium salt) is a novel non-nucleoside inhibitor that was designed to bind at an unconventional site on human immunodeficiency virus (HIV) type 1 reverse transcriptase (RT) (1). We have investigated the mechanism by which CZ-1 inhibits wild-type HIV-1 RT. Using pre-steady state kinetic methods, we examined the effect of CZ-1 on the parameters governing the single nucleotide polymerization catalyzed by RT. Analysis of the pre-steady-state burst phase of deoxyadenosine triphosphate (dATP) incorporation showed that CZ-1 decreased the amplitude of the reaction as previously shown for other NNRTIs due to the slow equilibration of the inhibitor with RT (21). However CZ-1 also weakened the apparent DNA binding affinity. Wild-type RT binds a 25/45-mer DNA duplex with an apparent $K_d$ of 3 nM, which was increased to 388 nM, 336 nM, and 933 nM in the presence of 2, 5, and 10 μM of CZ-1, respectively. Likewise, the $K_d$ of CZ-1 binding to RT increased at higher DNA concentration, from 1.3 μM to 3.4 μM. In contrast, the $K_d$ and the maximum incorporation rate of the incoming nucleotide did not depend on the concentration of CZ-1. We therefore conclude that CZ-1 represents a new class of non-nucleoside RT inhibitors (NNRTIs) distinct from Nevirapine and related NNRTIs. CZ-1 can

bind to RT in both the absence and presence of DNA. In the ternary enzyme-DNA-CZ-1 complex (E•DNA•I), the binding of DNA is weakened and incorporation of the next nucleotide onto the primer is inhibited. A possible mode of inhibition for CZ-1 is the distortion of RT conformation and the consequent misalignment of DNA at the active site.

CZ-1 inhibits HIV-1 RT activity similarly as conventional NNRTIs based on the measured kinetic parameters. In presence of CZ-1, binding of the incoming nucleotide, dATP, remained tight. Moreover, CZ-1 neither affected the burst (turnover) rate of RT nor the apparent equilibrium dissociation constant for dATP. The data agreed with the proposed mechanism of inhibition that non-nucleoside inhibitors hamper the chemical step for correct incorporation, whereas in uninhibited polymerization pathway, the conformational change ensuing nucleotide binding is the rate-limiting step and controls the fast rate of incorporation for the uninhibited enzyme.

Previous studies showed that non-nucleoside inhibitors such as nevirapine and TIBO could be released slowly from the I•E•D complex relative to the rate of polymerization of the uninhibited enzyme, resulting in residual polymerization activity in E•D complex with saturating concentrations of the inhibitors (21). CZ-1 is distinct from the conventional NNRTIs because it did not allow any residual polymerization when it was bound to E•D complex at a saturating amount.

Novel inhibitors with improved activity against NNRTI-resistant HIV have been designed based on predictions by computational methods such as Monte Carlo or molecular docking. The kinetic method I have presented in this dissertation is an efficient *in vitro* evaluation of novel drug compounds to complement *in vivo* studies. More inhibitors under clinical trials should be tested against other recently discovered resistance mutants to get a complete picture of the relationship between specific mutations and development of drug resistance.

Kinetic measurements of polymerization by the viral enzymes in the presence of each specific drug compound can be used to examine drug potency and efficacy. This approach will have a profound biological application in drug design for other viral diseases such as hepatitis C, influenza, etc. because it is applicable towards evaluation of drugs selected through random screening for other diseases.

References


1. Skillman, A. G.; Maurer, K. W.; Roe, D. C.; Stauber, M. J.; Eargle, D.; Ewing, T. J.; Muscate, A.; Davioud-Charvet, E.; Medaglia, M. V.; Fisher, R. J.; Arnold, E.; Gao, H. Q.; Buckheit, R.; Boyer, P. L.; Hughes, S. H.; Kuntz, I. D.; Kenyon, G. L. *Bioorg.Chem* **2002,** *30*(6), 443-458.

2. Barre-Sinoussi, F.; Chermann, J. C.; Rey, F.; Nugeyre, M. T.; Chamaret, S.; Gruest, J.; Dauguet, C.; Axler-Blin, C.; Vezinet-Brun, F.; Rouzioux, C.; Rozenbaum, W.; Montagnier, L. *Science* **1983,** *220*(4599), 868-871.

3. Baltimore, D. *Faseb Journal* **1995,** *9*(15), 1660-1663.

4. Temin, H. M.; Mizutani, S. *Reviews in Medical Virology* **1998,** *8*(1), 6-8.

5. Gray, H.; Wong, T. W. *Journal of Biological Chemistry* **1992,** *267*(9), 5835-5841.

6. Blattner, W.; Gallo, R. C.; Temin, H. M. *Science* **1988,** *241*(4865), 515.

7. Chermann, J. C.; Barre-Sinoussi, F.; Dauguet, C.; Brun-Vezinet, F.; Rouzioux, C.; Rozenbaum, W.; Montagnier, L. *Antibiot.Chemother.* **1983,** *32* 48-53.

8. Gallo, R. C.; Salahuddin, S. Z.; Popovic, M.; Shearer, G. M.; Kaplan, M.; Haynes, B. F.; Palker, T. J.; Redfield, R.; Oleske, J.; Safai, B.; . *Science* **1984,** *224*(4648), 500-503.

9. Aoki, T.; Miyakoshi, H.; Usuda, Y.; Chermann, J. C.; Barre-Sinoussi, F.; Ting, R. C.; Gallo, R. C. *Lancet* **1984,** *2*(8408), 936-937.

10. Wellink, J.; van Kammen, A. *Arch.Virol.* **1988,** *98*(1-2), 1-26.

11. Pathak, V. K.; Temin, H. M. *Proceedings of the National Academy of Sciences of the United States of America* **1990,** *87*(16), 6019-6023.

12. Preston, B. D. *Science* **1997,** *275*(5297), 228-229.

13. Wain-Hobson, S. *AIDS* **1989,** *3 Supplement 1* S13-S18.

14. Wain-Hobson, S. *Trends Microbiology* **1996,** *4* 135-141.

15. Mansky, L. M.; Temin, H. M. *Journal of Virology* **1995,** *69*(8), 5087-5094.

16. Fischer, M.; Hafner, R.; Schneider, C.; Trkola, A.; Joos, B.; Joller, H.; Hirschel, B.; Weber, R.; Gunthard, H. F. *AIDS* **2003,** *17*(2), 195-199.

17. Kohlstaedt, L. A.; Wang, J.; Friedman, J. M.; Rice, P. A.; Steitz, T. A. *Science* **1992,** *256*(5065), 1783-1790.

18. Jacobomolina, A.; Ding, J. P.; Nanni, R. G.; Clark, A. D.; Lu, X. D.; Tantillo, C.; Williams, R. L.; Kamer, G.; Ferris, A. L.; Clark, P.; Hizi, A.; Hughes, S. H.; Arnold, E. *Proceedings of the National Academy of Sciences of the United States of America* **1993,** *90*(13), 6320-6324.

19. Hsiou, Y.; Ding, J.; Das, K.; Clark, A. D., Jr.; Hughes, S. H.; Arnold, E. *Structure* **1996,** *4*(7), 853-860.

20. Sarafianos, S. G.; Das, K.; Tantillo, C.; Clark, A. D.; Ding, J.; Whitcomb, J. M.; Boyer, P. L.; Hughes, S. H.; Arnold, E. *Embo Journal* **2001,** *20*(6), 1449-1461.

21. Spence, R. A.; Kati, W. M.; Anderson, K. S.; Johnson, K. A. *Science* **1995,** *267*(5200), 988-993.

22. Cristofaro, J. V.; Rausch, J. W.; Le Grice, S. F. J.; DeStefano, J. J. *Biochemistry* **2002,** *41*(36), 10968-10975.

23. Lightfoote, M. M.; Coligan, J. E.; Folks, T. M.; Fauci, A. S.; Martin, M. A.; Venkatesan, S. *Journal of Virology* **1986,** *60*(2), 771-775.

24. Legrice, S. F. J.; Naas, T.; Wohlgensinger, B.; Schatz, O. *Embo Journal* **1991,** *10*(12), 3905-3911.

25. Morris, M. C.; Berducou, C.; Mery, J.; Heitz, F.; Divita, G. *Biochemistry* **1999,** *38*(46), 15097-15103.

26. Arts, E. J.; Le Grice, S. F. *Prog.Nucleic Acid Res.Mol.Biol.* **1998,** *58* 339-393.

27. Kvaratskhelia, M.; Miller, J. T.; Budihas, S. R.; Pannell, L. K.; Le Grice, S. F. *Proc.Natl.Acad.Sci.U.S A* **2002,** *99*(25), 15988-15993.

28. Huang, H. F.; Chopra, R.; Verdine, G. L.; Harrison, S. C. *Science* **1998,** *282*(5394), 1669-1675.

29. Madrid, M.; Lukin, J. A.; Madura, J. D.; Ding, J.; Arnold, E. *Proteins* **2001,** *45*(3), 176-182.

30. Rodgers, D. W.; Gamblin, S. J.; Harris, B. A.; Ray, S.; Culp, J. S.; Hellmig, B.; Woolf, D. J.; Debouck, C.; Harrison, S. C. *Proceedings of the National Academy of Sciences of the United States of America* **1995,** *92*(4), 1222-1226.

31. Ding, J.; Das, K.; Hsiou, Y.; Sarafianos, S. G.; Clark, A. D., Jr.; Jacobo-Molina, A.; Tantillo, C.; Hughes, S. H.; Arnold, E. *J.Mol.Biol.* **1998,** *284*(4), 1095-1111.

32. Beard, W. A.; Bebenek, K.; Darden, T. A.; Li, L.; Prasad, R.; Kunkel, T. A.; Wilson, S. H. *Journal of Biological Chemistry* **1998,** *273*(46), 30435-30442.

33. Sarafianos, S. G.; Das, K.; Ding, J. P.; Boyer, P. L.; Hughes, S. H.; Arnold, E. *Chemistry & Biology* **1999,** *6*(5), R137-R146.

34. Sawaya, M. R.; Prasad, R.; Wilson, S. H.; Kraut, J.; Pelletier, H. *Biochemistry* **1997,** *36*(37), 11205-11215.

35. Brautigam, C. A.; Steitz, T. A. *Curr.Opin.Struct.Biol.* **1998,** *8*(1), 54-63.

36. Doublie, S.; Tabor, S.; Long, A. M.; Richardson, C. C.; Ellenberger, T. *Nature* **1998,** *391*(6664), 251-258.

37. Sarafianos, S. G.; Clark, A. D.; Das, K.; Tuske, S.; Birktoft, J. J.; Ilankumaran, P.; Ramesha, A. R.; Sayer, J. M.; Jerina, D. M.; Boyer, P. L.; Hughes, S. H.; Arnold, E. *Embo Journal* **2002,** *21*(23), 6614-6624.

38. Rey, M. A.; Spire, B.; Dormont, D.; Barre-Sinoussi, F.; Montagnier, L.; Chermann, J. C. *Biochem.Biophys.Res.Commun.* **1984,** *121*(1), 126-133.

39. Le Grice, S. F.; Cameron, C. E.; Benkovic, S. J. *Methods Enzymol.* **1995,** *262* 130-144.

40. Watson, K. F.; Schendel, P. L.; Rosok, M. J.; Ramsey, L. R. *Biochemistry* **1979,** *18*(15), 3210-3219.

41. Goff, S. P. *Journal of Acquired Immune Deficiency Syndromes and Human Retrovirology* **1990,** *3*(8), 817-831.

42. Huber, H. E.; Mccoy, J. M.; Seehra, J. S.; Richardson, C. C. *Journal of Biological Chemistry* **1989,** *264*(8), 4669-4678.

43. Varmus, H.; Swanstrom, R. in *RNA tumor viruses*, Weiss, R.; Teich, N.; Varmus, H.; Coffin, J., editors; Cold Spring Harbor Laboratory Publications: New York, 1984; pp. 369-512.

44. Hottiger, M.; Hubscher, U. *Biol.Chem Hoppe Seyler* **1996,** *377*(2), 97-120.

45. You, J. C.; McHenry, C. S. *J.Biol.Chem* **1993,** *268*(22), 16519-16527.

46. You, J. C.; McHenry, C. S. *J.Biol.Chem* **1994,** *269*(50), 31491-31495.

47. Telesnitsky, A.; Goody, R. S. Strong-stop strand transfer during reverse transcription., in *Reverse Transcriptase*, Skalka, A. M.; Goff, S. P., editors; Cold Spring Harbor Laboratory Publications: New York, 1993; pp. 49-83.

48. Grandgenett, D. P.; Vora, A. C.; Schiff, R. D. *Virology* **1978,** *89*(1), 119-132.

49. Suo, Z. C.; Johnson, K. A. *Biochemistry* **1997,** *36*(41), 12468-12476.

50. Ding, J.; Jacobomolina, A.; Nanni, R. G.; Lu, X.; Williams, R. L.; Clark, A. D.; Hughes, S. H.; Arnold, E. *Biophysical Journal* **1993,** *64*(2), A350.

51. Hermann, T.; Meier, T.; Gotte, M.; Heumann, H. *Nucleic Acids Res.* **1994,** *22*(22), 4625-4633.

52. Divita, G.; Baillon, J. G.; Rittinger, K.; Chermann, J. C.; Goody, R. S. *Journal of Biological Chemistry* **1995,** *270*(48), 28642-28646.

53. Wohrl, B. M.; Tantillo, C.; Arnold, E.; Le Grice, S. F. *Biochemistry* **1995,** *34*(16), 5343-5356.

54. Molling, K.; Bolognesi, D.; Bauer, H.; Busen, W.; Plassmann, H.; Hausen, P. *Nat.New Biol.* **71 A.D.,** *234*(51), 240-243.

55. Smith, C. M.; Smith, J. S.; Roth, M. J. *Journal of Virology* **1999,** *73*(8), 6573-6581.

56. Smith, C. M.; Potts, W. B.; Smith, J. S.; Roth, M. J. *Virology* **1997,** *229*(2), 437-446.

57. Champoux, J. J. Roles of Ribonuclease H in Reverse Transcription, in *Reverse Transcriptase*, Skalka, A. M.; Goff, S. P., editors; Cold Spring Harbor Labratory Publications: New York, 1993; pp. 103-177.

58. Kvaratskhelia, M.; Budihas, S. R.; Le Grice, S. F. J. *Journal of Biological Chemistry* **2002,** *277*(19), 16689-16696.

59. Gao, H. Q.; Boyer, P. L.; Arnold, E.; Hughes, S. H. *Journal of Molecular Biology* **1998,** *277*(3), 559-572.

60. Rausch, J. W.; Lener, D.; Miller, J. T.; Julias, J. G.; Hughes, S. H.; Le Grice, S. F. J. *Biochemistry* **2002,** *41*(15), 4856-4865.

61. Powell, M. D.; Beard, W. A.; Bebenek, K.; Howard, K. J.; Le Grice, S. F. J.; Darden, T. A.; Kunkel, T. A.; Wilson, S. H.; Levin, J. G. *Journal of Biological Chemistry* **1999,** *274*(28), 19885-19893.

62. Kati, W. M.; Johnson, K. A.; Jerva, L. F.; Anderson, K. S. *J.Biol.Chem.* **1992,** *267*(36), 25988-25997.

63. Johnson, K. A. Transient-State Kinetic Analysis of Enzyme Reaction Pathways. [XX], 1-61. 1992. Academic Press, Inc. THE ENZYMES.

64. Divita, G.; Muller, B.; Immendorfer, U.; Gautel, M.; Rittinger, K.; Restle, T.; Goody, R. S. *Biochemistry* **1993,** *32*(31), 7966-7971.

65. Kruhoffer, M.; Urbanke, C.; Grosse, F. *Nucleic Acids Research* **1993,** *21*(17), 3943-3949.

66. Reardon, J. E. *Biochemistry* **1992,** *31*(18), 4473-4479.

67. Reardon, J. E. *Journal of Biological Chemistry* **1993,** *268*(12), 8743-8751.

68. Hsieh, J. C.; Zinnen, S.; Modrich, P. *Journal of Biological Chemistry* **1993,** *268*(33), 24607-24613.

69. Suo, Z. C.; Johnson, K. A. *Journal of Biological Chemistry* **1998,** *273*(42), 27259-27267.

70. Wohrl, B. M.; Krebs, R.; Goody, R. S.; Restle, T. *Journal of Molecular Biology* **1999,** *292*(2), 333-344.

71. Rothwell, P. J.; Berger, S.; Kensch, O.; Felekyan, S.; Antonik, M.; Wohrl, B. M.; Restle, T.; Goody, R. S.; Seidel, C. A. M. *Proceedings of the National Academy of Sciences of the United States of America* **2003,** *100*(4), 1655-1660.

72. Rittinger, K.; Divita, G.; Goody, R. S. *Proc.Natl.Acad.Sci.U.S.A* **1995,** *92*(17), 8046-8049.

73. Kerr, S. G.; Anderson, K. S. *Biochemistry* **1997,** *36*(46), 14056-14063.

74. Johnson, K. A. *Philos.Trans.R.Soc.Lond B Biol.Sci.* **1992,** *336*(1276), 107-112.

75. Boyer, J. C.; Bebenek, K.; Kunkel, T. A. *Proceedings of the National Academy of Sciences of the United States of America* **1992,** *89*(15), 6919-6923.

76. Fedoroff, O. Y.; Salazar, M.; Reid, B. R. *Journal of Molecular Biology* **1993,** *233*(3), 509-523.

77. Sugimoto, N.; Nakano, S.; Katoh, M.; Matsumura, A.; Nakamuta, H.; Ohmichi, T.; Yoneyama, M.; Sasaki, M. *Biochemistry* **1995,** *34*(35), 11211-11216.

78. Suo, Z. C.; Johnson, K. A. *Biochemistry* **1997,** *36*(41), 12459-12467.

79. Suo, Z. C.; Johnson, K. A. *Biochemistry* **1997,** *36*(48), 14778-14785.

80. Suo, Z. C.; Johnson, K. A. *Biochemistry* **1996,** *35*(28), 9.

81. Johnson, A. A.; Ray, A. S.; Hanes, J.; Suo, Z.; Colacino, J. M.; Anderson, K. S.; Johnson, K. A. *J.Biol.Chem.* **2001,** *276*(44), 40847-40857.

82. Esnouf, R.; Ren, J.; Ross, C.; Jones, Y.; Stammers, D.; Stuart, D. *Nat.Struct.Biol.* **1995,** *2*(4), 303-308.

83. Merluzzi, V. J.; Hargrave, K. D.; Labadia, M.; Grozinger, K.; Skoog, M.; Wu, J. C.; Shih, C. K.; Eckner, K.; Hattox, S.; Adams, J.; . *Science* **1990,** *250*(4986), 1411-1413.

84. Romero, D. L.; Busso, M.; Tan, C. K.; Reusser, F.; Palmer, J. R.; Poppe, S. M.; Aristoff, P. A.; Downey, K. M.; So, A. G.; Resnick, L.; . *Proc.Natl.Acad.Sci.U.S A* **1991,** *88*(19), 8806-8810.

85. Young, S. D.; Britcher, S. F.; Tran, L. O.; Payne, L. S.; Lumma, W. C.; Lyle, T. A.; Huff, J. R.; Anderson, P. S.; Olsen, D. B.; Carroll, S. S.; . *Antimicrob.Agents Chemother.* **1995,** *39*(12), 2602-2605.

86. Manfredi, R.; Calza, L.; Chiodo, F. *J.Acquir.Immune Defic.Syndr.* **2004,** *35*(5), 492-502.

87. Temiz, N. A.; Bahar, I. *Proteins* **2002,** *49*(1), 61-70.

88. Esnouf, R.; Ren, J.; Ross, C.; Jones, Y.; Stammers, D.; Stuart, D. *Nat.Struct.Biol.* **1995,** *2*(4), 303-308.

89. Palaniappan, C.; Fay, P. J.; Bambara, R. A. *J.Biol.Chem* **1995,** *270*(9), 4861-4869.

90. Richman, D. D. *Annu.Rev.Pharmacol.Toxicol.* **1993,** *33* 149-164.

91. Balzarini, J.; Karlsson, A.; Perez-Perez, M. J.; Vrang, L.; Walbers, J.; Zhang, H.; Oberg, B.; Vandamme, A. M.; Camarasa, M. J.; De Clercq, E. *Virology* **1993,** *192*(1), 246-253.

92. Balzarini, J.; Karlsson, A.; Vandamme, A. M.; Perez-Perez, M. J.; Zhang, H.; Vrang, L.; Oberg, B.; Backbro, K.; Unge, T.; San Felix, A.; . *Proc.Natl.Acad.Sci.U.S.A* **1993,** *90*(15), 6952-6956.

93. Saag, M. S.; Emini, E. A.; Laskin, O. L.; Douglas, J.; Lapidus, W. I.; Schleif, W. A.; Whitley, R. J.; Hildebrand, C.; Byrnes, V. W.; Kappes, J. C.; . *N.Engl.J.Med.* **1993,** *329*(15), 1065-1072.

94. Byrnes, V. W.; Sardana, V. V.; Schleif, W. A.; Condra, J. H.; Waterbury, J. A.; Wolfgang, J. A.; Long, W. J.; Schneider, C. L.; Schlabach, A. J.; Wolanski, B. S.; . *Antimicrob.Agents Chemother.* **1993,** *37*(8), 1576-1579.

95. Balzarini, J.; Weeger, M.; Camarasa, M. J.; De Clercq, E.; Uberla, K. *Biochem.Biophys.Res.Commun.* **1995,** *211*(3), 850-856.

96. Balzarini, J.; Perez-Perez, M. J.; Velazquez, S.; San Felix, A.; Camarasa, M. J.; De Clercq, E.; Karlsson, A. *Proc.Natl.Acad.Sci.U.S.A* **1995,** *92*(12), 5470-5474.

97. Balzarini, J.; De ClercQ, E. *Methods Enzymol.* **1996,** *275* 472-502.

98. Buckheit, R. W., Jr.; Kinjerski, T. L.; Fliakas-Boltz, V.; Russell, J. D.; Stup, T. L.; Pallansch, L. A.; Brouwer, W. G.; Dao, D. C.; Harrison, W. A.; Schultz, R. J.; . *Antimicrob.Agents Chemother.* **1995,** *39*(12), 2718-2727.

99. Buckheit, R. W., Jr.; Fliakas-Boltz, V.; Yeagy-Bargo, S.; Weislow, O.; Mayers, D. L.; Boyer, P. L.; Hughes, S. H.; Pan, B. C.; Chu, S. H.; Bader, J. P. *Virology* **1995,** *210*(1), 186-193.

100. Buckheit, R. W., Jr.; Fliakas-Boltz, V.; Decker, W. D.; Roberson, J. L.; Stup, T. L.; Pyle, C. A.; White, E. L.; McMahon, J. B.; Currens, M. J.; Boyd, M. R.; . *Antiviral Res.* **1995,** *26*(2), 117-132.

101. Pelemans, H.; Esnouf, R.; Dunkler, A.; Parniak, M. A.; Vandamme, A. M.; Karlsson, A.; De Clercq, E.; Kleim, J. P.; Balzarini, J. *J.Virol.* **1997,** *71*(11), 8195-8203.

102. Ren, J.; Milton, J.; Weaver, K. L.; Short, S. A.; Stuart, D. I.; Stammers, D. K. *Structure.Fold.Des* **2000,** *8*(10), 1089-1094.

103. Lindberg, J.; Sigurdsson, S.; Lowgren, S.; Andersson, H. O.; Sahlberg, C.; Noreen, R.; Fridborg, K.; Zhang, H.; Unge, T. *Eur.J.Biochem.* **2002,** *269*(6), 1670-1677.

104. Hsiou, Y.; Ding, J. P.; Das, K.; Clark, A. D.; Boyer, P. L.; Lewi, P.; Janssen, P. A. J.; Kleim, J. P.; Rosner, M.; Hughes, S. H.; Arnold, E. *Journal of Molecular Biology* **2001,** *309*(2), 437-445.

105. Maass, G.; Immendoerfer, U.; Koenig, B.; Leser, U.; Mueller, B.; Goody, R.; Pfaff, E. *Antimicrob.Agents Chemother.* **1993,** *37*(12), 2612-2617.

106. Stahlhut, M.; Li, Y.; Condra, J. H.; Fu, J.; Gotlib, L.; Graham, D. J.; Olsen, D. B. *Protein Expr.Purif.* **1994,** *5*(6), 614-621.

107. Johnson, K. A. *Methods Enzymol.* **1986,** *134* 677-705.

108. Lakowicz, J. R. *Principles of Fluorescence Spectroscopy;* Plenum Press: New York, 1983.

109. Palella, F. J., Jr.; Delaney, K. M.; Moorman, A. C.; Loveless, M. O.; Fuhrer, J.; Satten, G. A.; Aschman, D. J.; Holmberg, S. D. *N.Engl.J.Med.* **1998,** *338*(13), 853-860.

110. Piot, P. *Science* **1998,** *280*(5371), 1844-1845.

111. Dykes, C.; Najjar, J.; Bosch, R. J.; Wantman, M.; Furtado, M.; Hart, S.; Hammer, S. M.; Demeter, L. M. *J Infect.Dis.* **2004,** *189*(6), 1091-1096.

112. Mitsuya, H.; Weinhold, K. J.; Furman, P. A.; St Clair, M. H.; Lehrman, S. N.; Gallo, R. C.; Bolognesi, D.; Barry, D. W.; Broder, S. *Proc.Natl.Acad.Sci.U.S A* **1985,** *82*(20), 7096-7100.

113. Mitsuya, H.; Broder, S. *Proc.Natl.Acad.Sci.U.S A* **1986,** *83*(6), 1911-1915.

114. Johnson, A. A.; Ray, A. S.; Hanes, J.; Suo, Z.; Colacino, J. M.; Anderson, K. S.; Johnson, K. A. *J.Biol.Chem.* **2001,** *276*(44), 40847-40857.

115. Johnson, A. A.; Ray, A. S.; Hanes, J.; Suo, Z.; Colacino, J. M.; Anderson, K. S.; Johnson, K. A. *J.Biol.Chem.* **2001,** *276*(44), 40847-40857.

116. Lee, H.; Hanes, J.; Johnson, K. A. *Biochemistry* **2003,** *42*(50), 14711-14719.

117. De Clercq, E. *Med.Res.Rev.* **1993,** *13*(3), 229-258.

118. Esnouf, R.; Ren, J.; Ross, C.; Jones, Y.; Stammers, D.; Stuart, D. *Nat.Struct.Biol.* **1995,** *2*(4), 303-308.

119. Esnouf, R.; Ren, J.; Ross, C.; Jones, Y.; Stammers, D.; Stuart, D. *Nat.Struct.Biol.* **1995,** *2*(4), 303-308.

120. De Clercq, E. *Farmaco* **1999,** *54*(1-2), 26-45.

121. Tramontano, E.; Piras, G.; Mellors, J. W.; Putzolu, M.; Bazmi, H. Z.; La Colla, P. *Biochem.Pharmacol.* **1998,** *56*(12), 1583-1589.

122. Ren, J.; Nichols, C.; Bird, L.; Chamberlain, P.; Weaver, K.; Short, S.; Stuart, D. I.; Stammers, D. K. *J.Mol.Biol.* **2001,** *312*(4), 795-805.

123. Perach, M.; Rubinek, T.; Hughes, S. H.; Hizi, A. *J.Mol.Biol.* **1997,** *268*(3), 648-654.

124. Sarafianos, S. G.; Das, K.; Clark, A. D.; Ding, J. P.; Boyer, P. L.; Hughes, S. H.; Arnold, E. *Proceedings of the National Academy of Sciences of the United States of America* **1999,** *96*(18), 10027-10032.

125. Boyer, P. L.; Sarafianos, S. G.; Arnold, E.; Hughes, S. H. *Journal of Virology* **2002,** *76*(7), 3248-3256.

126. Roberts, J. D.; Bebenek, K.; Kunkel, T. A. *Science* **1988,** *242*(4882), 1171-1173.

127. Sebastian, J.; Faruki, H. *Med.Res.Rev.* **2004,** *24*(1), 115-125.

128. Sturmer, M.; Doerr, H. W.; Staszewski, S.; Preiser, W. *Antivir Ther.* **2003,** *8*(3), 239-244.

129. Mansky, L. M.; Pearl, D. K.; Gajary, L. C. *J.Virol.* **2002,** *76*(18), 9253-9259.

130. Mansky, L. M. *Virology* **2003,** *307*(1), 116-121.

131. Johnson, K. A. *Annu.Rev.Biochem.* **1993,** *62* 685-713.

132. McGovern, S. L.; Helfand, B. T.; Feng, B.; Shoichet, B. K. *J.Med.Chem* **2003,** *46*(20), 4265-4272.

133. McGovern, S. L.; Caselli, E.; Grigorieff, N.; Shoichet, B. K. *J.Med.Chem* **2002,** *45*(8), 1712-1722.

134. Shoichet, B. K.; McGovern, S. L.; Wei, B.; Irwin, J. J. *Curr.Opin.Chem Biol.* **2002,** *6*(4), 439-446.

135. Seidler, J.; McGovern, S. L.; Doman, T. N.; Shoichet, B. K. *J.Med.Chem* **2003,** *46*(21), 4477-4486.

136. Shih, C. K.; Rose, J. M.; Hansen, G. L.; Wu, J. C.; Bacolla, A.; Griffin, J. A. *Proc.Natl.Acad.Sci.U.S A* **1991,** *88*(21), 9878-9882.

137. Bacolla, A.; Shih, C. K.; Rose, J. M.; Piras, G.; Warren, T. C.; Grygon, C. A.; Ingraham, R. H.; Cousins, R. C.; Greenwood, D. J.; Richman, D.; . *J.Biol.Chem* **1993,** *268*(22), 16571-16577.

138. Hsiou, Y.; Das, K.; Ding, J.; Clark, A. D., Jr.; Kleim, J. P.; Rosner, M.; Winkler, I.; Riess, G.; Hughes, S. H.; Arnold, E. *J.Mol.Biol.* **1998,** *284*(2), 313-323.

139. Bacheler, L. T.; Anton, E. D.; Kudish, P.; Baker, D.; Bunville, J.; Krakowski, K.; Bolling, L.; Aujay, M.; Wang, X. V.; Ellis, D.; Becker, M. F.; Lasut, A. L.; George, H. J.; Spalding, D. R.; Hollis, G.; Abremski, K. *Antimicrob.Agents Chemother.* **2000,** *44*(9), 2475-2484.

140. Miller, V.; de Bethune, M. P.; Kober, A.; Sturmer, M.; Hertogs, K.; Pauwels, R.; Stoffels, P.; Staszewski, S. *Antimicrob.Agents Chemother.* **1998,** *42*(12), 3123-3129.

141. Bacheler, L.; Jeffrey, S.; Hanna, G.; D'Aquila, R.; Wallace, L.; Logue, K.; Cordova, B.; Hertogs, K.; Larder, B.; Buckery, R.; Baker, D.; Gallagher, K.; Scarnati, H.; Tritch, R.; Rizzo, C. *J.Virol.* **2001,** *75*(11), 4999-5008.

142. Kleim, J. P.; Winters, M.; Dunkler, A.; Suarez, J. R.; Riess, G.; Winkler, I.; Balzarini, J.; Oette, D.; Merigan, T. C. *J.Infect.Dis.* **1999,** *179*(3), 709-713.

143. Jackson, J. B.; Becker-Pergola, G.; Guay, L. A.; Musoke, P.; Mracna, M.; Fowler, M. G.; Mofenson, L. M.; Mirochnick, M.; Mmiro, F.; Eshleman, S. H. *AIDS* **2000,** *14*(11), F111-F115.

144. Das, K.; Ding, J.; Hsiou, Y.; Clark, A. D., Jr.; Moereels, H.; Koymans, L.; Andries, K.; Pauwels, R.; Janssen, P. A.; Boyer, P. L.; Clark, P.; Smith, R. H., Jr.; Kroeger Smith, M. B.; Michejda, C. J.; Hughes, S. H.; Arnold, E. *J.Mol.Biol.* **1996,** *264*(5), 1085-1100.

145. Kroeger Smith, M. B.; Rouzer, C. A.; Taneyhill, L. A.; Smith, N. A.; Hughes, S. H.; Boyer, P. L.; Janssen, P. A.; Moereels, H.; Koymans, L.; Arnold, E.; . *Protein Sci.* **1995,** *4*(10), 2203-2222.

146. Reardon, J. E.; Miller, W. H. *J Biol.Chem* **1990,** *265*(33), 20302-20307.

147. Spence, R. A.; Anderson, K. S.; Johnson, K. A. *Biochemistry* **1996,** *35*(3), 1054-1063.

148. Patel, S. S.; Wong, I.; Johnson, K. A. *Biochemistry* **1991,** *30*(2), 511-525.

149. Patel, S. S.; Wong, I.; Johnson, K. A. *Biochemistry* **1991,** *30*(2), 511-525.

150. Patel, P. H.; Jacobo-Molina, A.; Ding, J.; Tantillo, C.; Clark, A. D., Jr.; Raag, R.; Nanni, R. G.; Hughes, S. H.; Arnold, E. *Biochemistry* **1995,** *34*(16), 5351-5363.

# Vita

Louise Zhiying Wang was born in Shanghai, China on October 28, 1973, the daughter of Raymond Wang and Ludy Zhu. The family moved to United States in 1988. After completing her study at Quincy High School, Quincy, Massachusetts in 1992, she attended Brandeis University in Waltham, Massachusetts. She received the degree of Bachelor of Arts in Biochemistry in May, 1996. In August, 1998 she entered graduate school at University of Texas at Austin. She joined her thesis advisor's lab in July, 1999.

Permanent address: 208 Falls Blvd., Quincy, MA 02169

This dissertation was typed by the author.